

Double-Network Hydrogels for Intraoral Ultrasound Imaging

By

Jiaqiang Yi

A thesis submitted in partial fulfillment of the requirements for the degree of

Master of Science

In

CHEMICAL ENGINEERING

Department of Chemical and Materials Engineering

University of Alberta

© Jiaqiang Yi, 2020

Abstract

Ultrasound imaging has great potential in intraoral diagnosis, due to its portability, low cost, and low safety risks. A couplant is normally placed between transducers and tissues for better ultrasound image quality. If applied intraorally, the couplants should possess good stability in water, robust mechanical properties, as well as good affinity to transducers and tissues. However, commercial couplants, such as Aquaflex (AF), are designed for external use and cannot fulfill these requirements. With great similarity to the extracellular structure, excellent mechanical properties, and numerous commercialized biomedical applications, double-network tough hydrogels could act as the potential candidate for couplants. In this thesis, a review of the ultrasound process and the defects of commercial couplants, biomedical applications of hydrogels, and mechanisms to synthesize tough hydrogels are presented first. Methods to quantify mechanical properties, friction properties, adhesion properties, ultrasound properties, and biocompatibility are explained next. Then, two types of double-network (DN) hydrogels and their application in intraoral ultrasound imaging are explored.

In the first theme, Polyacrylamide/Alginate (PAM/Alginate) double-network hydrogels were evaluated for intraoral ultrasound imaging via a comprehensive comparison of physical, mechanical, frictional and ultrasound properties to AF. The

PAM/Alginate DN hydrogel not only possesses better stability in water as well as improved mechanical properties and higher coefficients of friction than AF but also can provide similar ultrasound image quality as AF does. Moreover, the PAM/Alginate DN hydrogel shows lower cytotoxicity to both cancer (Hela) and fibroblast cells (MRC-5). With all these significant features, PAM/Alginate DN hydrogels serve as a proof-of-concept ultrasound couplant with great potential in intraoral ultrasound imaging.

In the second theme, inspired by the mussel adhesion mechanism, we explored a poly(vinyl alcohol)-polyacrylamide-polydopamine (PVA-PAM-PDA) hydrogel synthesized by incorporating PDA into the PAM-PVA double-network for intraoral ultrasound imaging. The hydrogel not only maintains good stability in water and superior mechanical properties but also can adhere to different substrates (metal, glass, and porcine skin) without losing the original adhesiveness after multiple adhesion–strip cycles. Besides, when applied to image porcine mandibular incisor, it could provide a similar ultrasound image quality as AF does. With these features, such hydrogel can serve as the candidate for ultrasound couplant in intraoral ultrasound imaging.

This work has explored the application of double-network hydrogels to intraoral ultrasound imaging and provided useful insights into the development of

multifunctional hydrogel-based interfaces between human tissues and medical devices for health monitoring and disease diagnosis applications. Via a comprehensive comparison of the above-mentioned properties to AF, we have expanded the application of double-network hydrogels to intraoral ultrasound imaging as the candidates for couplants.

Keywords: Intraoral diagnosis, Double-network hydrogel, Ultrasound imaging, Frictional properties, Adhesion

Preface

This thesis is the original work conducted by Jiaqiang Yi under the supervision of Dr. Hongbo Zeng, presented in manuscript format.

Chapter 1 of this thesis is the introduction

Chapter 2 of this thesis explains the main experimental techniques and methods involved in this thesis.

Chapter 3 of this thesis has been published as Jiaqiang Yi, Kim-Cuong T. Nguyen, Wenda Wang, Wenshuai Yang, Mingfei Pan, Edmond Lou, Paul W. Major, Lawrence H. Le, and Hongbo Zeng, “Polyacrylamide/Alginate double-network tough hydrogels for intraoral ultrasound imaging”, the *Journal of Colloid and Interface Science*, **2020**, 578, 598-607. I was responsible for data collection, analysis, and manuscript composition. Kim-Cuong T. Nguyen helped with the ultrasound experiment and the composition of the manuscript for the ultrasound part. Wenda Wang conducted the cell cytotoxicity test and helped the manuscript revision. Wenshuai Yang conducted the SEM measurement and contributed to the manuscript revision. Mingfei Pan also contributed to the manuscript revision and experiment design. Dr. Paul W. Major and Dr. Edmond Lou were involved in the conceptualization. Dr. Hongbo Zeng and Dr. Lawrence H. Le were the

corresponding authors and were involved in the experimental design and manuscript revision.

Chapter 4 of this thesis has been submitted as Jiaqiang Yi, Kim-Cuong T. Nguyen, Wenda Wang, Wenshuai Yang, Mingfei Pan, Edmond Lou, Paul W. Major, Lawrence H. Le, and Hongbo Zeng, “Mussel-inspired adhesive double-network hydrogel for intraoral ultrasound imaging”, *ACS Applied Bio Materials*. I was responsible for data collection, analysis, and manuscript composition. Kim-Cuong T. Nguyen helped the ultrasound experiments and composed the manuscript for the ultrasound part. Wenda Wang, Wenshuai Yang, and Mingfei Pan provided helpful discussions and contributed to the manuscript revision. Dr. Paul W. Major and Dr. Edmond Lou were involved in the conceptualization. Dr. Hongbo Zeng and Dr. Lawrence H. Le were involved in the experimental design and manuscript revision.

The overall conclusion and future work are summarized in Chapter 5.

Acknowledgement

First and foremost, I would like to express my sincere gratitude to Dr. Hongbo Zeng, for his patient guidance, encouragement, and advice during my master's study at the University of Alberta. Dr. Zeng is an experienced and professional scholar who taught me how to think and solve problems in a scientific and systematic method. I appreciate his invaluable guidance during my graduate study.

I am also grateful to Dr. Lawrence H. Le and Kim-Cuong T. Nguyen for their support and suggestions in this work. They have helped me conduct the ultrasound experiment, compose the manuscript for the ultrasound part, and contributed to the manuscript revision. Their precise and rigorous attitude to research has influenced me in my research work and my personality.

Additionally, I must express my gratitude to Wenda Wang, a Ph.D. candidate in our research group, for his constructive advice on my experimental design, result discussion, manuscript revision, and guidance during my dark day. Besides, I appreciate the help of Dr. Linbo Han when I first came to Canada. Moreover, I would also like to thank my fellows, Wenshuai Yang and Mingfei Pan, for their help and support during my master's study. Also, I am thankful to Dr. Lu Gong, Dr. Jingsi Chen, Dr. Wenjihao Hu, Meng Wu, Li Xiang, Qiongyao Peng and other group members for their helpful discussion and support during my research.

The financial supports from the Natural Sciences and Engineering Research Council of Canada (NSERC), Canada Foundation for Innovation (CFI) and the Canada Research Chairs Program (H.Zeng) are highly acknowledged.

Finally, I would like to thank my parents and my sister for their continuous support and unconditional love. Without their full support and understanding, I would not be where I am today. I also want to thank Diane Fereig and Dhruv Sharma for their guidance in the exploration of the spiritual world.

Table of Contents

Abstract	ii
Preface.....	v
Acknowledgement	vii
Table of Contents	ix
List of Figures	xv
List of Tables	xxi
List of abbreviations.....	xxii
1. Introduction.....	1
1.1. Ultrasound imaging	1
1.1.1. Ultrasound imaging process.....	1
1.1.2. The applications of ultrasound imaging and the status of commercially available couplants.....	1
1.2. A brief introduction of hydrogels.....	2
1.3. The biomedical applications of hydrogels	3
1.4. Existing challenges of conventional hydrogels.....	3
1.5. Tough hydrogels.....	4

1.5.1. Methods to synthesize tough hydrogels	4
1.5.1.1. Homogenous tough hydrogels	5
1.5.1.2. Double-network tough hydrogels	6
1.5.1.3. Nanocomposite tough hydrogels	9
1.5.2. The application of tough hydrogels	11
1.5.3. Polymers for double-network tough hydrogel	11
1.5.3.1. Alginate.....	12
1.5.3.2. PAM.....	12
1.5.3.3. PVA.....	13
1.5.3.4. PDA.....	13
1.6. Objectives	14
1.7. Thesis structure.....	15
2. Experimental techniques.....	16
2.1. Mechanical properties	16
2.1.1. Stress-strain curve	16
2.1.2. Toughness	17
2.1.3. Fracture energy.....	18

2.1.4. Compression strength.....	19
2.1.5. Viscoelasticity.....	20
2.2. Friction properties	21
2.3. Adhesion properties.....	21
2.4. Biocompatibility	22
2.5. Ultrasound properties	23
2.6. Ultrasound imaging	25
3. Polyacrylamide/Alginate double-network tough hydrogel for intraoral ultrasound imaging.....	27
3.1. Introduction	27
3.2. Materials and Methods	29
3.2.1. Materials.....	29
3.2.2. Synthesis of PAM/Alginate hydrogels.....	29
3.2.3. FTIR and microstructure characterization	29
3.2.4. Swelling test.....	30
3.2.5. Mechanical properties	31
3.2.6. Friction tests	32

3.2.7. Ultrasonic characterization	32
3.2.8. Ultrasonic imaging.....	35
3.2.9. Cell cytotoxicity	35
3.3. Results and Discussion.....	36
3.3.1. Fabrication of PAM/Alginate hydrogels.....	36
3.3.2. Mechanical properties	40
3.3.3. Frictional properties	43
3.3.4. Ultrasonic properties	45
3.3.5. Biocompatibility.....	48
3.4. Conclusions	49
4. Mussel inspired adhesive double-network hydrogel for intraoral ultrasound imaging.....	51
4.2. Introduction	51
4.3. Materials and Methods	52
4.3.1. Materials.....	52
4.3.2. Hydrogel preparation	53
4.3.3. Characterization	54

4.3.4. Swelling test.....	54
4.3.5. Mechanical tests.....	55
4.3.6. Adhesion test.....	56
4.3.7. Ultrasound characterization.....	57
4.3.8. Ultrasound imaging.....	58
4.4. Results and Discussion.....	59
4.4.1. Fabrication and characterization of the PVA-PAM-PDA hydrogels ...	59
4.4.2. Mechanical properties.....	62
4.4.3. Adhesion ability.....	67
4.4.4. Ultrasound properties.....	70
4.4.5. Ultrasound imaging.....	71
4.5. Conclusions.....	72
5. Conclusions and Future Work.....	74
5.2. Major Conclusions and Contributions.....	74
5.3. Future Work.....	75
Bibliography.....	76
Appendices.....	88

Appendix A Supporting Information for Chapter 3	88
Appendix B Supporting Information for Chapter 4.....	91

List of Figures

Figure 1.1 Typical strategies for synthesizing tough hydrogels. (A) Tetra-PEG hydrogel (Homogenous hydrogel). (B) Double-network hydrogel (DN hydrogel). (C) Nanocomposite hydrogel (NC hydrogel). [36] <i>Image was reproduced from [36]</i>	5
Figure 1.2 (A) Within the alginate- Ca^{2+} hydrogels, the G blocks on different alginate polymer chains form ionic crosslinks with Ca^{2+} . (B) In the PAM hydrogels, the PAM polymer chains form covalent crosslinks through N, N-methylenebisacrylamide (MBAA; green squares). (C) In the alginate-PAM DN hydrogels, the two types of polymer networks (alginate- Ca^{2+} and PAM) are intertwined and joined by covalent crosslinks (blue triangles) between amine groups on PAM chains and carboxyl groups on alginate chains. [38] <i>Image was reproduced from [38]</i>	8
Figure 1.3 Schematic illustrations of the preparation of PVA/PAM hydrogels. (A) The control hydrogel. (B) The F-T (freeze-thawing) hydrogel. (C) The A-S (anneal-swelling) hydrogel. [40] <i>Image was reproduced from [40]</i>	9
Figure 1.4 Schematic illustration of the gelation process of PDA-Clay-PAM hydrogel. [42] <i>Image was reproduced from [42]</i>	10
Figure 1.5 The application areas for tough hydrogels with specific fields. [46] <i>Image was reproduced from [46]</i>	11
Figure 1.6 Chemical structure of alginic acid.....	12
Figure 2.1 Stress-strain curve showing typical yield behavior.....	17
Figure 2.2 The typical curve to calculate the toughness of materials.....	18

Figure 2.3 (A) Sample shape ($w = 5$ mm, $L = 50$ mm, $d = 7.5$ mm, the length of the initial notch is 20 mm). (B) The tearing method to measure fracture energy. F_t is the tearing force, V_p is the pulling velocity and V is the crack velocity. [63] *Image was reproduced from [63]* 19

Figure 2.4 Common adhesion test methods. 22

Figure 2.5 The ultrasound signals: (A) a water pulse; (B) a sample signal; (C) the amplitude spectrum of the water pulse; (D) the amplitude spectrum of the sample signal. [10] *Image was reproduced from [10]* 24

Figure 2.6 The schematic illustration of the experimental setup for the pulse transmission method. [67] *Image was reproduced from [67]*..... 25

Figure 2.7 Ultrasound experiment: (A) The touch-screen SonixTablet ultrasound phased array system. (B) The 128-element L40-8/12 transducer (Analogic, Vancouver, Canada) is positioned to scan the LCI. [68] *Image was reproduced from [68]* 26

Figure 3.1 Schematic illustration of the gelation process of PAM/Alginate hydrogels 37

Figure 3.2 (A) The FTIR spectra of Acrylamide (AM), Alginate and H-2 (PAM/Alginate hydrogel). (B) The SEM image of H-2 (PAM/Alginate hydrogel). (C) The element mapping site of H-2. (D). The calcium element mapping in H-2..... 38

Figure 3.3 (A) The water content of the as-prepared PAM/Alginate hydrogels and AF. (B) The equilibrium swelling ratio of the as-prepared PAM/Alginate hydrogels. (C) Frozen-dry H-2 and AF swelling in deionized water for 12 hours and 24 hours respectively. (D) The relative weight of the as-prepared PAM/Alginate hydrogels and AF versus immersion time. 40

Figure 3.4 (A) H-3 at the initial and three times stretching states. (B) The nominal stress curves. (C) The true stress curves. (D) The toughness from the nominal stress curves. (E) The sample

shape (Left, $L = 50$ mm, $w = 5$ mm, $h = 6.5$ mm, notch = 20 mm) and schematic illustration of the tearing experiment (Right, F_t is the tearing force, and V is the pulling velocity). (F) The corresponding fracture energy. 42

Figure 3.5 Frictional properties. (A) The dependences of the friction force on the normal force. (B) The dependences of the coefficient of friction (CF) on the normal force. 45

Figure 3.6 Ultrasonic characterization of potential couplants. (A) The transmission-through experimental setup. (B) A couplant mounted in a holder. (C) The reference pulse (Red, water) and sample pulse (Black, H-2.5). (D) The phase velocities versus frequency. (E) The attenuation coefficient versus frequency. 46

Figure 3.7 Ultrasonic imaging of the dento-periodontium: (A) The imaged incisor. (B) A schematic illustration of oral structure. (C) The ultrasound image with AF as the couplant. (D) The ultrasound image with H-2.5 as the couplant. 48

Figure 3.8 Cell viability of HeLa cancer cells and MRC-5 fibroblast cells after 3 hours incubation with the extracts. 49

Figure 4.1 Schematic illustration of the fabrication of PVA-PAM-PDA hydrogels. (A) The formation of the PVA-PDA complex. (B) The formation of 1st chemically crosslinked PAM network in the PVA-PDA mixture. (C) The formation of 2nd physically crosslinked PVA network. (D) The PVA-PAM-PDA hydrogel was applied as the couplant for intraoral ultrasound imaging. 60

Figure 4.2 (A) The FTIR spectra of DA (dopamine hydrochloride), Hd-2, H-2, PVA, and AM (acrylamide). (B) The SEM image of Hd-2 (PVA-PAM-PDA hydrogel). (C) The SEM image of H-2 (PVA-PAM hydrogel). 61

Figure 4.3 (A) The water percentage of the PVA-PAM-PDA hydrogels, PVA-PAM hydrogels, and AF. (B) The equilibrium swelling ratio of PVA-PAM-PDA hydrogels at different time intervals..... 62

Figure 4.4 (A) The stress-strain curves of the PVA-PAM-PDA hydrogels and AF. (B) The toughness and Young’s modulus of the PVA-PAM-PDA hydrogels and AF. Successive loading-unloading tensile test cycles of (C) Hd-2 and (D) AF. 64

Figure 4.5 (A) Images of AF (upper) and Hd-2 (lower) undergoing compression testing to 70% strain. Cyclic loading-unloading curves: (B) AF. (C) Hd-0.5. (D) Hd-1. (E) Hd-2. 66

Figure 4.6 (A) The photos of Hd-2 adhered to different substrates: (1) glass, (2) skin, (3) metal, (4) finger and metal at two sides, (5) the back of hand and metal at two sides, (6) bending arm upward, and (7) bending arm downward. (B) Schematic illustration of the tensile adhesion test process (Left: attachment, F_c , Compression force; Right: detachment, F_a , Adhesion force). (C) The adhesion strength of samples to glass, metal, and porcine skin. (D) Repeatable adhesion behavior of Hd-2 (PVA-PAM-PDA hydrogel) to different substrates (glass, metal, and porcine skin). 69

Figure 4.7 Ultrasound characterization of the potential couplants. (A) The transmission-through experimental setup. (B) The reference pulse (Black, water) and sample pulse (Red, Hd-2). (C) The phase velocities versus frequency. (D) The attenuation coefficient versus frequency. 71

Figure 4.8 Ultrasound scan of a porcine incisor: (A) A schematic illustration of the ultrasound scan of the tooth-periodontium structure where the couplant sits between the transducer and the tissues. (B) The ultrasound image with AF as the couplant. (C) The ultrasound image with H-2 as the couplant. (D) The ultrasound image with Hd-2 as the couplant. 72

Figure S3.1 The pictures of the as-prepared PAM/Alginate hydrogels and commercial gel pad. (A) H-1. (B) H-1.5. (C) H-2. (D) H-2.5. (E) H-3. (F) AF. 88

Figure S3.2 The densities of the as-prepared PAM/Alginate hydrogels and AF..... 88

Figure S3.3 The as-prepared PAM/Alginate hydrogel samples (H-1 – H-3, from left to right) swelling in water. (A) After 12h. (B) After 48h. 89

Figure S3.4 The friction coefficient curves of H-2.5 under different normal loads: (A) 1 mN (low load). (B) 10 mN (medium load). (C) 30 mN (high load). 89

Figure S4.1 The pictures of the as-prepared PVA-PAM-PDA hydrogels, PVA-PAM hydrogels, and commercial gel pad: (A) Hd-0.5. (B) Hd-1. (C) Hd-2. (D) H-0.5. (E) H-1. (F) H-2. (G) AF (Aquaflex ultrasound gel pad). 91

Figure S4.2 (A) The densities of the as-prepared PVA-PAM-PDA hydrogels, PVA-PAM hydrogels, and AF. (B) The equilibrium swelling ratio of PVA-PAM hydrogels at different time intervals..... 92

Figure S4.3 Frozen-dry AF and the as-prepared hydrogels immersed in distilled water. 12 h: (A) AF, (B) Hd-0.5, Hd-1, Hd-2, H-0.5, H-1, andH-2 (from left to right) ; 24 h: (C) AF, (D) Hd-0.5, Hd-1, Hd-2, H-0.5, H-1, andH-2 (from left to right). 92

Figure S4.4 (A) The stress-strain curves of the PVA-PAM hydrogels and AF. (B) The toughness and Young’s modulus of the PVA-PAM hydrogels and AF. (C) The successive loading-unloading tensile test cycles of H-2. 93

Figure S4.5 Images of the samples undergoing the stretching-releasing process. (A) Hd-2. (B) AF. (C) H-2. 94

Figure S4.6 (A) Images of Hd-2 undergoing compression testing to 70% strain. The cyclic loading-unloading curves of PVA-PAM hydrogels: (B) H-0.5, (C) H-1, (D) H-2..... 95

Figure S4.7 Dynamic rheology of the samples on frequency: (A) PVA-PAM-PDA hydrogels, (B) AF. Dynamic rheology of the samples on strain: (C) PVA-PAM-PDA hydrogels, (D) AF. 96

Figure S4.8 (A) The phase velocities of PVA-PAM hydrogels and AF versus frequency. (B) The attenuation coefficient of PVA-PAM hydrogel and AF versus frequency 97

List of Tables

Table 1.1 Some examples of commercialized hydrogels for wound dressings. [21, 29] <i>Table was reproduced from [21, 29]</i>	3
Table 4.1 The compositions of the PVA-PAM-PDA (Hd) hydrogels and PVA-PAM (H) hydrogels (Hydrogels are denoted by their PAM/PVA ratios).....	54
Table S3.1 Group velocities, dispersion, and nBUA of hydrogels. († The attenuation coefficients, α are determined at 17 MHz, the dominant frequencies of the spectra.)	90
Table S4.1 Group velocities, dispersion, and nBUA of AF and the as-prepared hydrogels. († The attenuation coefficients, α are determined at 19.5 MHz, the dominant frequencies of the spectra.)	97

List of abbreviations

3D	Three-dimensional
AF	Aquaflex gel pad
AM	Acrylamide
APS	Ammonium persulfate
A-S	Anneal-swelling
CBNP	Carbon-black nanoparticle
CF	Coefficient of friction
CT	Computed tomography
DMEM	Dulbecco's Modified Eagle Medium
DN	Double-Network
ECM	Extracellular Matrix
EDS	Energy-dispersive X-ray spectroscopy
ESR	Equilibrium swelling ratio
FESEM	Field Emission Scanning Electron Microscope
FTIR	Fourier-transform infrared spectroscopy
F-T	Freeze-thawing
MBAA	N, N'-Methylenebisacrylamide
MTT	3-(4,5-dimethylthiazol-2-yl)-2,5-diphenyltetrazolium bromide
NC	Nanocomposite
PAM	Polyacrylamide
PAMPS	Poly (2-acrylamido-2-methylpropanesulfonic acid)
PBS	Phosphate buffered saline

PDA	Polydopamine
PMMA	Poly (methyl methacrylate)
PNIPAM	Poly-N-Isopropylacrylamide
PVA	Poly (vinyl alcohol)
QCT	Quantitative computed tomography
rGO	reduced graphene oxide
ROI	Regions of interest
SEM	Scanning electron microscope
TEMED	N, N, N', N'-Tetramethyl-ethylenediamine
Tetra-PEG	Tetra-polyethylene glycol

1. Introduction

1.1. Ultrasound imaging

1.1.1. Ultrasound imaging process

The ultrasound imaging process is mainly divided into two parts, ultrasound wave generation and echo detection and interpretation [1-3]. In the ultrasound generation, the ultrasound wave is normally produced by a piezoelectric transducer encased in a plastic housing. Phased array techniques are usually employed to enable the ultrasound machine to change the direction and depth of focus. Then, the ultrasound wave travels into the body and comes into focus at the desired depth. Materials on the surface of the transducer enhance the transmission of ultrasound into the body [4, 5]. Besides, a gel pad is put between the transducer and the patient's skin to delay signals for better signal differentiation. However, the ultrasound wave may be reflected where the acoustic impedance of media changes. In the echo detection and interpretation, the return ultrasound wave vibrates the transducer, and then the transducer turns the vibrations into electrical pulses which are detected by the ultrasound scanner and interpreted into ultrasound images. Therefore, to form an image, the ultrasound scanner needs to determine how long it takes echoes to be received and how strong the signal is.

1.1.2. The applications of ultrasound imaging and the status of commercially available couplants

Medical ultrasound is a diagnosis technique developed from ultrasound imaging. It can be utilized to image internal body structures such as tendons, muscles, joints, blood vessels, and internal organs [6, 7]. Moreover, it is also applied to help guide biopsies, diagnose heart conditions,

and assess damage after a heart attack. Compared to Computed Tomography (CT) or X-Ray, ultrasound diagnosis has several advantages [8]. First, it is portable as well as financially affordable and can provide real-time images. Second, it is non-invasive and extremely safe, without risks of ionizing radiation. Besides, ultrasound images can demonstrate medical images of soft tissues with better clarity than X-ray. Additionally, there is not any report about the harmful effects on humans from the standard diagnostic ultrasound.

During the ultrasound imaging process, gel pads are used as couplants to delay ultrasound signals away from the initial trigger signals for better signal discrimination and to keep the ultrasound beam in the focal zone [9, 10]. However, commercially available couplants, such as AF, are designated for external use. If applied intraorally, AF may face challenges, including low stability in water, poor mechanical properties, low affinity to transducer and tissues, etc.

1.2.A brief introduction of hydrogels

Hydrogels are three-dimensional (3D) crosslinked polymer networks with high water content and great similarity to the extracellular matrix (ECM) [11]. Their cross-linking interactions can be intermolecular bondings (e.g. hydrogen bonding), ionic bonding, and covalent bonding [12]. With different structures and polymer compositions, hydrogels can possess a variety of properties such as self-healing, temperature-sensitive, pH-sensitive, adhesive, conductive, anti-bacterial, and biocompatible properties. After the discovery of the first synthetic hydrogel by Wichterle and Lim in 1954 [13, 14], hydrogels have been widely utilized in the agriculture sector [15, 16], industrial process [17], diagnostics [18], and bioengineering [19, 20]. Due to their similarities to the ECM, their applications as biomaterials are also comprehensively explored [21-25].

1.3. The biomedical applications of hydrogels

Different hydrogels with tuned properties were developed for tissue engineering [26], wound dressing [27], controlled drug delivery systems [28]. A list of commercialized synthetic products from modified natural polymers are presented in **Table 1.1**. Therefore, hydrogels could potentially act as the couplants for intraoral ultrasound imaging.

Product	Major Components	Main Properties
Granugel® (ConvaTec)	Pectin, carboxymethyl-cellulose, propylene glycol, and water	A transparent and viscous hydrogel for the management of partial and full-thickness wounds. It may be used as a filler for dry cavity wounds to provide a moist healing environment
Intrasite Gel® (Smith & Nephew)	Modified carboxymethyl-cellulose (2.3%), propylene glycol (20%), and water	Amorphous sterile hydrogel used in dressing shallow and deep open wounds
Purilon Gel® (Coloplast)	Sodium carboxymethyl-cellulose and water (90%)	Indicated in conjunction with a secondary dressing for necrotic and sloughy wounds as well as first and second degrees burns
Aquaflo™ (Covidien)	Polyethylene glycol, propylene glycol, and water	It has a disc-shape that maximizes wound coverage and helps fill shallow cavities. The translucent gel allows wound visualization
Woundtab® (First Water)	Sulphonated copolymer, carboxymethyl-cellulose, glycerol, and water	The dressing contains a superabsorbent hydrogel that can absorb bacteria and retain them in its structure.

Table 1.1 Some examples of commercialized hydrogels for wound dressings. [21, 29] *Table was reproduced from [21, 29]*

1.4. Existing challenges of conventional hydrogels

Although conventional hydrogels have already been widely used in biomedical applications, they still face huge challenges for biomedical applications, due to their poor mechanical properties [30]. Conventional hydrogels are mechanically weak, which could lead to their fracture and tearing during biomedical applications [31]. Two factors could lead to the brittleness of conventional

hydrogels. First, conventional hydrogels are normally synthesized from monomers and cross-linkers via free radical polymerization. Due to the potential difference in reactivity at different sites, hydrogels are generally heterogeneously cross-linked. When the hydrogels are applied with external loading, the heterogeneity in crosslinkers leads to the uneven distribution of stress [32]. Besides, when experiencing force loadings, conventional hydrogels do not have energy dissipation mechanisms, which would lead to the fracture of the hydrogel structure [33]. Therefore, poor mechanical properties of conventional hydrogels limit their biomedical applications.

1.5. Tough hydrogels

To address the poor mechanical properties of conventional hydrogels, tough hydrogels were first introduced by Gong et al in 2003 [34]. Tough hydrogels are hydrogels with tensile stress between 0.1 MPa and 1 MPa and fracture energy between 100 J/m² and 1000 J/m². Due to their excellent mechanical properties, they have been proposed for artificial cartilage, wound dressing, cornea repair material, contact lenses [31, 35].

1.5.1. Methods to synthesize tough hydrogels

As shown in **Figure 1.1**, to address the aforementioned problems of conventional hydrogels, different methods are developed to synthesize tough hydrogels, such as increasing the homogeneity of hydrogels, incorporating the double-network (DN) into hydrogels, and integrating nanocomposite (NC) inside hydrogels.

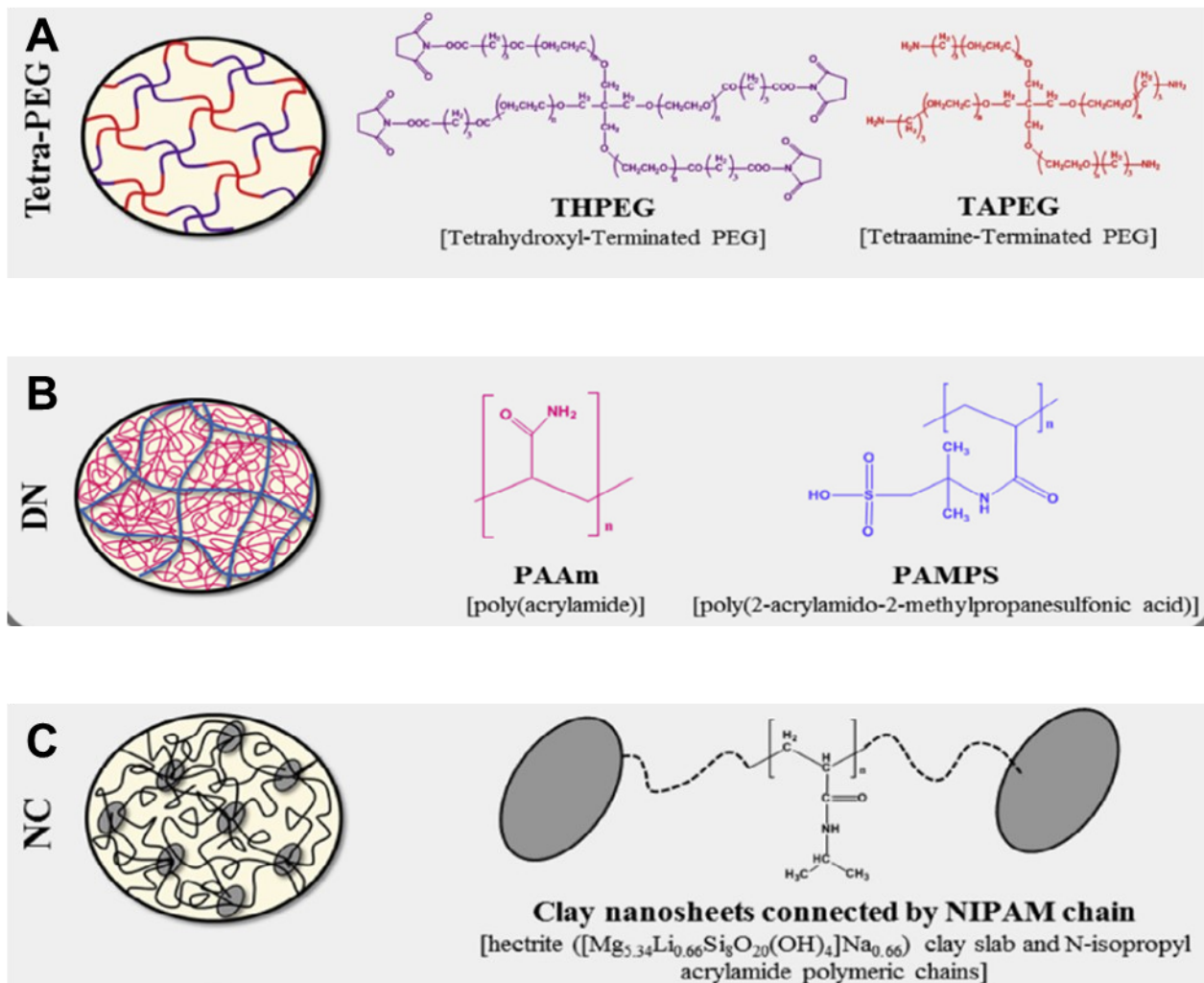


Figure 1.1 Typical strategies for synthesizing tough hydrogels. (A) Tetra-PEG hydrogel (Homogenous hydrogel). (B) Double-network hydrogel (DN hydrogel). (C) Nanocomposite hydrogel (NC hydrogel). [36] *Image was reproduced from [36]*

1.5.1.1. Homogenous tough hydrogels

Homogenous tough hydrogels are synthesized by increasing the homogeneity of polymerization. Tetra-PEG (Tetra-poly ethylene glycol) is a general example of homogeneous hydrogels, introduced by Sakai et al [37]. Each macromonomer is derived from PEG (polyethylene glycol) with a tetrahedron-like structure different in terminal functional groups, either an amine or

succinimidyl ester. By controlling the unitary molar ratio of two macromonomers, the uniform 3D-crosslinked structure can be obtained via the formation of the amide bond between their terminal groups (**Figure 1.1A**). Although it exhibits the advantages of excellent mechanical properties, in-situ gel formation, and biocompatibility, it is confined to monomers with the tetrahedron-like structure.

1.5.1.2. Double-network tough hydrogels

By incorporating two polymer networks with different physical properties into the hydrogel, the first double-network hydrogel, PAMPS/PAM (poly (2-acrylamido-2-methylpropanesulfonic acid)/polyacrylamide) hydrogel (**Figure 1.1B**), was introduced by Gong et al [34]. Due to the synergistic effect in double-network, DN hydrogels show much better mechanical properties than two independent structures. To possess good mechanical properties, the first network is typically designed to be densely crosslinked, acting as the framework, while the second network is usually loosely crosslinked, employing the energy dissipation mechanism. Therefore, their double-network structure is normally synthesized via a two-step process: (1) the formation of the framework of rigid gels via the polymerization and crosslinking in the first step; (2) the formation of the loosely crosslinked network within the first network in the second step.

Although PAMPS/PAM tough hydrogel has a fracture stress 20 times higher than that of either PAMPS hydrogel or PAM hydrogel, the PAMPS network is irreversibly crosslinked, and the fracture of the PAMPS network is unrecoverable. In the stretching process, the PAMPS network dissipates energy by the fracture of the PAMPS network. Once the energy dissipation layer is damaged, this type of double-network hydrogel will lose its toughness and function. To enhance the recoverability of tough hydrogels after fracture, different double-network tough hydrogels

were synthesized via reversibly crosslinked bonding. Suo et al. reported an alginate–polyacrylamide hydrogels with covalently crosslinked polyacrylamide network and ionically crosslinked Ca^{2+} -Alginate network in **Figure 1.2** [38, 39]. The polyacrylamide network serves as the framework for the hydrogel, while the Ca^{2+} -Alginate network is reversibly crosslinked and utilized to employ the energy dissipation mechanism. This hydrogel can possess extraordinary mechanical properties while retaining its toughness after repeated loadings. Moreover, He et al. have also developed PVA/PAM (poly (vinyl alcohol)/polyacrylamide) double-network hydrogels via the freeze-thawing or anneal-swelling methods in **Figure 1.3** [40]. PVA/PAM double-network hydrogels are composed of the physically crosslinked PVA network and covalently crosslinked PAM network. The PVA network enhances the toughness via the energy-dissipation mechanism, while the PAM network retains the high stretchability and water content via its long hydrophilic chains.

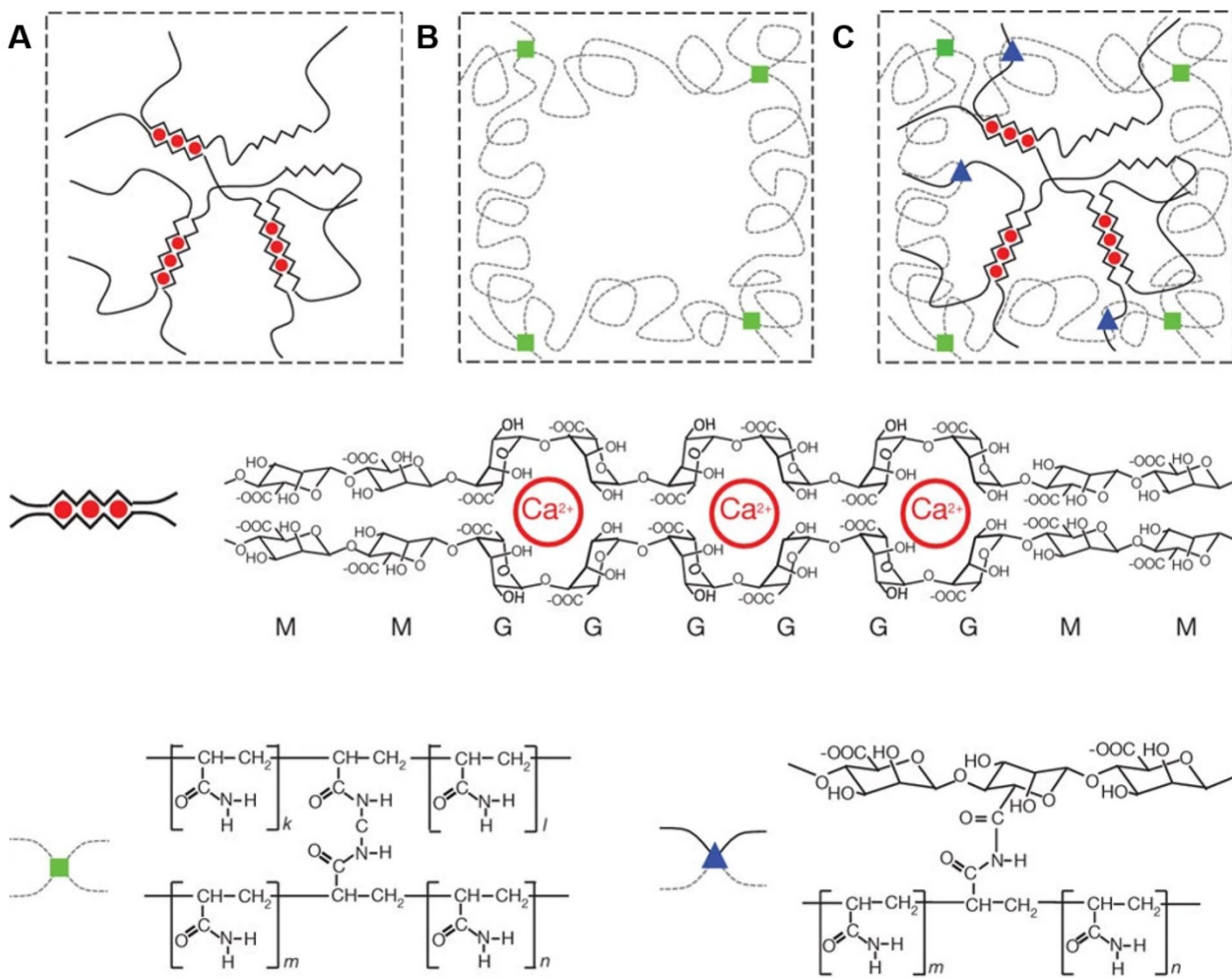


Figure 1.2 (A) Within the alginate-Ca²⁺ hydrogels, the G blocks on different alginate polymer chains form ionic crosslinks with Ca²⁺. (B) In the PAM hydrogels, the PAM polymer chains form covalent crosslinks through N, N-methylenebisacrylamide (MBAA; green squares). (C) In the alginate-PAM DN hydrogels, the two types of polymer networks (alginate-Ca²⁺ and PAM) are intertwined and joined by covalent crosslinks (blue triangles) between amine groups on PAM chains and carboxyl groups on alginate chains. [38] *Image was reproduced from [38]*

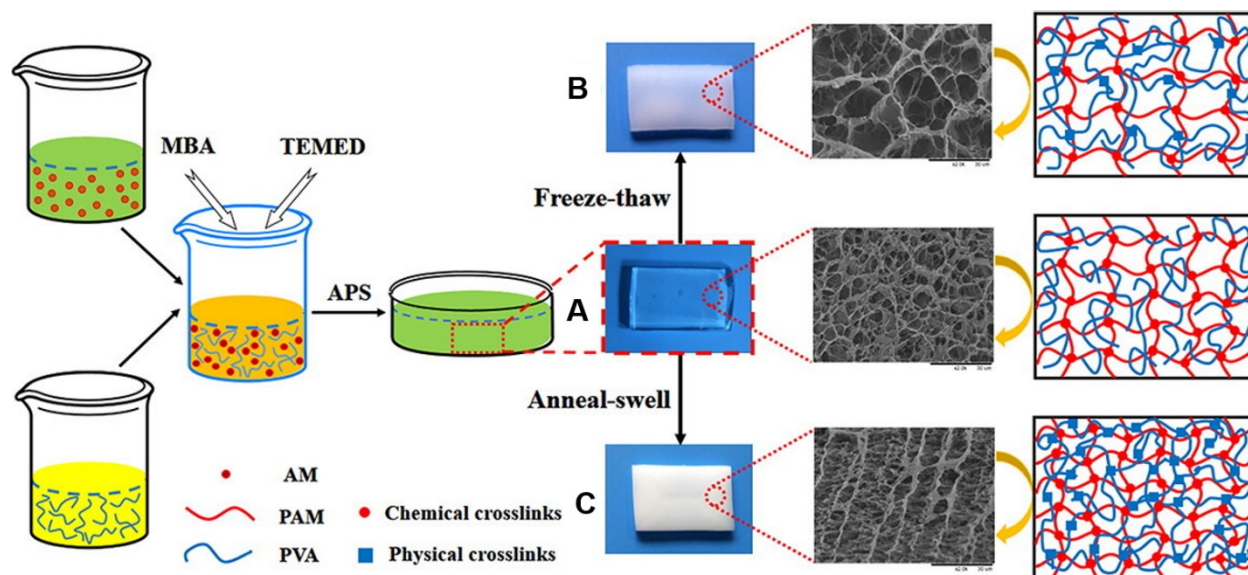


Figure 1.3 Schematic illustrations of the preparation of PVA/PAM hydrogels. (A) The control hydrogel. (B) The F-T (freeze-thawing) hydrogel. (C) The A-S (anneal-swelling) hydrogel. [40]

Image was reproduced from [40]

1.5.1.3. Nanocomposite tough hydrogels

Tough hydrogels can also be developed via incorporating nanocomposite (clay, natural mineral silicate, and nanoplatelets) into the hydrogel network. Nanocomposite tough hydrogels were first proposed by Haraguchi and Takehisa [41]. The hybrid structure is achieved via the in-situ free radical polymerization of specific monomers on the nanocomposite surface after the homogenous dispersion of nanocomposite in aqueous solutions. Due to the strong ionic and coordination interaction between the nanocomposite surface and the end groups of the polymer chain, nanocomposite can serve as multifunctional crosslinkers. In their work, the clay/PNIPAM (Poly-N-Isopropylacrylamide) Nanocomposite hydrogel (**Figure 1.1C**) was synthesized with the clay as the crosslinker. It can have a tensile strength of 0.1 MPa and elongation of over 1000%.

Besides, mussel-inspired adhesive and tough hydrogels, PDA-Clay-PAM (polydopamine-clay-polyacrylamide) hydrogels, were proposed by Lu et al. via the polymerization of nano-clay-confined dopamine and crosslinking of acrylamide for wound dressing [42]. As shown in **Figure 1.4**, with the incorporation of nano-clay, PDA-Clay-PAM hydrogel can have an elongation of over 4000%, the tensile stress of 0.25 MPa, and adhesion of 30 KPa. With the similar design strategies, reduced graphene oxide/polyacrylamide (rGO-PAM) tough hydrogels are developed for implantable electronics, and carbon-black nanoparticle/polyacrylamide (CBNP/PAM) tough hydrogels are synthesized for electricity conduction [43-45]. However, nanocomposites could lead to potential health risks and reduce the quality of ultrasound images.

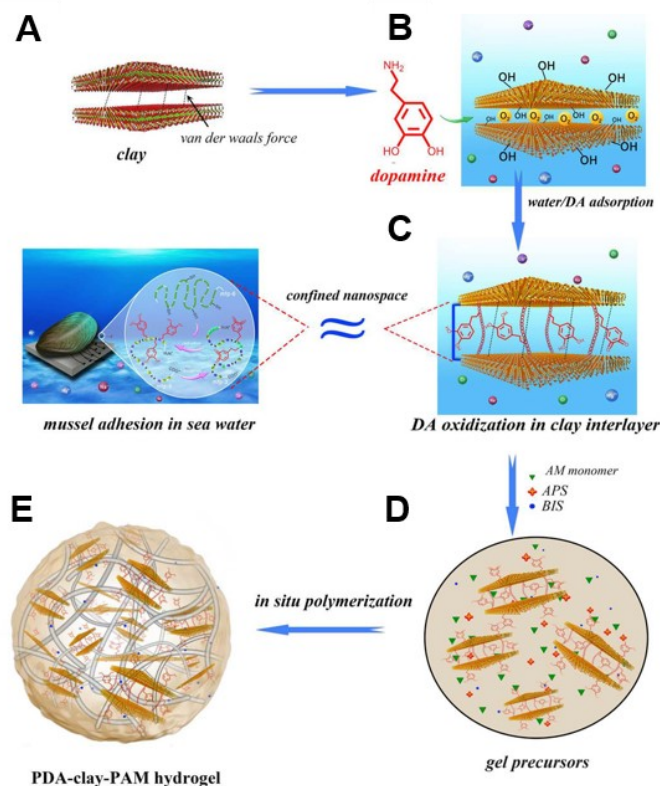


Figure 1.4 Schematic illustration of the gelation process of PDA-Clay-PAM hydrogel. [42] *Image was reproduced from [42]*

1.5.2. The application of tough hydrogels

The applications of tough hydrogels are extensively explored via the modification of their chemical structure. As illustrated in **Figure 1.5**, tough hydrogels can be utilized as biomaterials for tissue engineering and drug delivery [46]. Among them, PMMA (poly (methyl methacrylate)) and other tough hydrogels have been commercialized as contact lenses [47-49]. Besides, poly (2-acrylamide-2-methyl-propane sulfonic acid)/poly (N, N' -dimethyl acrylamide) DN hydrogel and similar hydrogels have been proposed as artificial cartilage [50, 51]. There is great potential to expand the biomedical application of tough hydrogels to intraoral diagnosis.

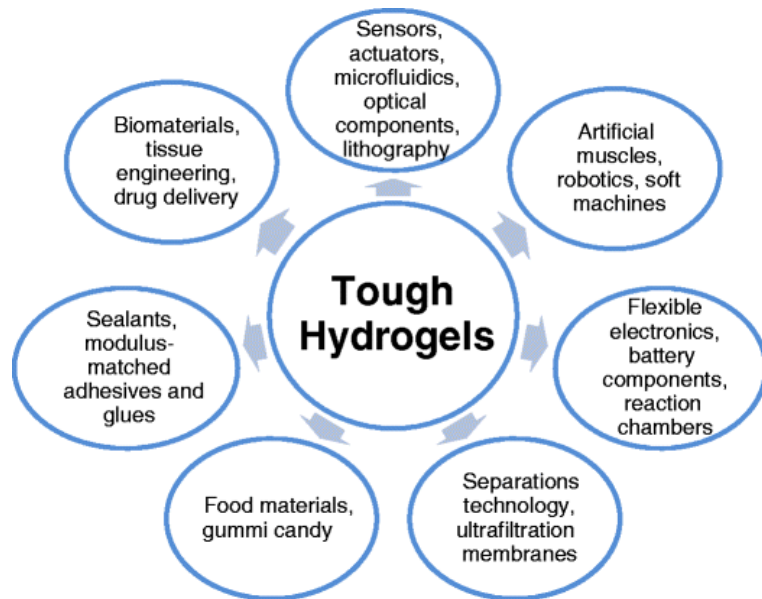


Figure 1.5 The application areas for tough hydrogels with specific fields. [46] *Image was reproduced from [46]*

1.5.3. Polymers for double network tough hydrogel

Double-network tough hydrogels are composed of two layers of crosslinked polymer networks. The polymers for each network have strong impacts on their properties. Among all the

polymers mentioned above, Alginate, PAM, PVA, and PDA are selected to form the crosslinked polymer networks for their unique structure and properties explained below.

1.5.3.1. Alginate

Sodium alginate (Alginate) is the salt of alginic acid, a natural polysaccharide distributed widely in the cell walls of brown algae. It is hydrophilic and can form viscous gums when it is hydrated. Alginic acid (**Figure 1.6**) is a copolymer of (1-4)-linked β -D-mannuronate and C-5 epimer α -L-guluronate in different sequences. When incorporated in hydrogels, alginate can enhance porosity, cell proliferation, mechanical properties. Hydrogels, composed of alginate, are widely used in wound dressing, tissue engineering, cell encapsulation, and so on [52, 53].

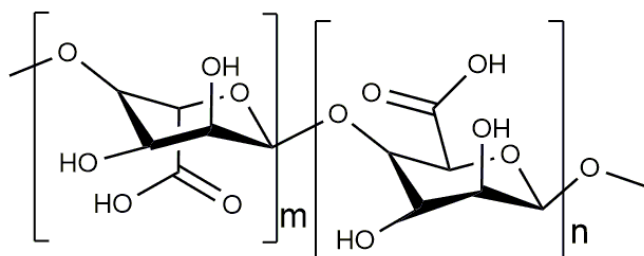


Figure 1.6 Chemical structure of alginic acid.

1.5.3.2. PAM

PAM (polyacrylamide) is a polymer formed from the polymerization of acrylamide. With amide groups, PAM is highly water-absorbent. PAM hydrogels can be formed with acrylamide as the monomer, N, N'-methylenebisacrylamide (MBAA) as the crosslinker. Via the copolymerization with other molecules, PAM-based hydrogels, due to their excellent mechanical properties, can be used to manufacture soft contact lenses and biomaterials for wound dressing. Although there are concerns about the release of acrylamide, a known neurotoxin and carcinogen,

numerous experiments have illustrated that PAM hydrogels still possess excellent biocompatibility [54-56].

1.5.3.3. PVA

PVA (poly (vinyl alcohol)), a water-soluble synthetic polymer, can form hydrogels via the freezing-thawing or annealing-swelling process. At first, PVA dissolves in water at 90 °C, forming homogenous solutions. In the freeze-thawing process, it is subject to the freezing and thawing cycle for 2 cycles to form the PVA hydrogels; in the anneal-swelling, it needs to experience a process of drying, annealing and subsequently immersing in water to form hydrogels [40]. Due to its well-known biocompatibility, low tendency to protein adhesion, and excellent mechanical properties, PVA-based hydrogels are widely utilized in cartilage replacements, contact lenses, and eye drops [57-59].

1.5.3.4. PDA

PDA (polydopamine) is the polymer of dopamine, with great similarity to the structures of mussel adhesive proteins, synthesized by the self-polymerization of dopamine. Inspired by mussel adhesion mechanism, PDA has been integrated into hydrogels to enhance their adhesion properties for numerous biomedical applications, such as DOPA-Fe³⁺ gelatine hydrogel for surgical operation, PDA-Clay-PAM hydrogel for skin regeneration, and PDA-pGO-PAM hydrogels for implantable bioelectronics [42, 43, 60-62]. Besides, dopamine acts both as a hormone and a neurotransmitter in the brain and body, which also illustrates PDA possess extraordinary biocompatibility.

1.6.Objectives

Although ultrasound imaging has been widely applied in medical diagnosis, there are few reports about the application of ultrasound to intraoral imaging. Compared to external ultrasound imaging, intraoral imaging is more complicated. It requires the couplant to have good stability in water, excellent mechanical properties to fit the intraoral structures, high affinity to tissues and transducers for the excellent transmission of the ultrasound wave, and biocompatibility. One of the main barriers is that the couplant (Aquaflex, AF), commercially available for ultrasound imaging, cannot meet these requirements. Double-network hydrogels, tuned with specific properties, have been widely used in biomedical applications, which could potentially act as good candidates for the ultrasound couplants.

The overall goal of this project is to expand the application of ultrasound imaging to the intraoral diagnosis via the introduction of double-network hydrogels as couplants and evaluate the feasibility of different DN hydrogels by a comprehensive comparison to the commercial gel pad (AF). The detailed objectives are listed as follow:

(1) To develop PAM-Alginate double-network hydrogels with different alginate contents, evaluating their feasibility as couplants through stability in water, mechanical properties, friction properties, biocompatibility, and ultrasound imaging.

(2) To develop PVA-PAM-PDA double-network hydrogel with different PAM/PVA ratios, evaluating their feasibility as couplants through stability in water, mechanical properties, adhesion properties, and ultrasound imaging.

1.7. Thesis structure

Chapter 1 gives a general introduction of ultrasound imaging, the barrier to intraoral ultrasound imaging, an overview of hydrogels and tough hydrogels followed by their biomedical applications as well as different fabrication strategies for tough hydrogels. Besides, the objectives of this work are briefly explained.

Chapter 2 presents several techniques and methods to evaluate their properties as ultrasound imaging couplants, including mechanical properties, frictional properties, adhesion properties, biocompatibility, and ultrasound properties.

Chapter 3 introduces the synthesis of PAM-Alginate double-network tough hydrogels and comprehensive characterization of their properties, compared to Aquaflex (AF). PAM/Alginate hydrogels with different alginate contents were synthesized with the covalent crosslinking of acrylamide and the ionic cross-linking of alginate. Their stability in water, mechanical properties, friction properties, biocompatibility, and ultrasound properties were demonstrated in comparison to AF.

Chapter 4 reports the fabrication of PVA-PAM-PDA double-network hydrogels and their properties. PVA-PAM-PDA hydrogels were synthesized via the incorporation of PDA into PVA-PAM double-network. Their stability in water, mechanical properties, adhesion properties, and ultrasound properties were evaluated regarding AF and PVA-PAM hydrogels to evaluate PVA-PAM-PDA hydrogels as the candidates for couplants of intraoral ultrasound imaging.

Chapter 5 lists the overall conclusions regarding our results and the suggestions for future work.

2. Experimental techniques

2.1. Mechanical properties

2.1.1. Stress-strain curve

As shown in **Figure 2.1**, the stress-strain curve is one of the unique properties of materials, measured by the amount of deformation (strain) under loadings (stress). The stress and strain can be normal or shear. They can also be uniaxial, biaxial, or multiaxial. The deformation can come from compression, stretching, torsion, and rotation. For the intraoral ultrasound application, only uniaxial stretching and compression are considered. The tensile strain (ε_t , **equation 1**) is calculated by the extended length ($L-L_0$) divided by the initial length (L_0). For engineering purposes, the cross-section area is assumed to be consistent as the initial cross-section area. The engineering tensile stress (S , also known as nominal stress, **equation 2**) is determined by normalizing the force (F) by the initial cross-section area (A_0). However, the actual cross-section area will decrease while samples undergo elastic or plastic deformation. Therefore, the true stress (σ) is also introduced for reference via multiplying engineering stress by the strain according to **equation 3**.

$$\varepsilon_t = \frac{L - L_0}{L_0} \quad (1)$$

$$S = \frac{F}{A_0} \quad (2)$$

$$\sigma = \varepsilon_t S \quad (3)$$

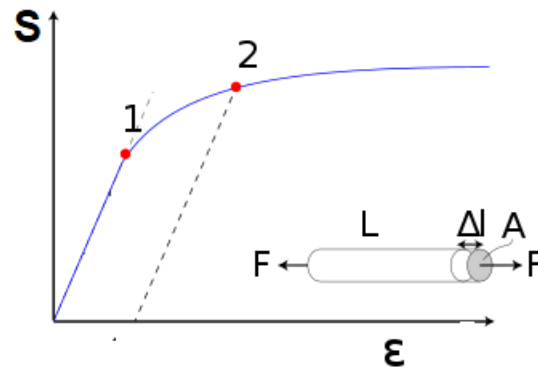


Figure 2.1 Stress-strain curve showing typical yield behavior.

Normally, the stress-strain curve has three regions (**Figure 2.1**). The first region is the linear elastic stage, and the stress is proportional to the strain and follows Hooke's law. Moreover, Young's modulus can be calculated from the slope of the stress-strain curve. In this region, materials only undergo elastic deformation. At the end of the first region, materials start experiencing plastic deformation. In the second region, the stress still increases as material elongates, except that the slope of the stress-strain curve is flat. In the third region, materials experience heterogeneous deformation and reinforce as the stress concentrates on the small cross-section. Based on the stress-strain curve, materials can be divided into two categories, brittle and ductile materials. When subjected to stress, brittle materials fracture with little elastic deformation and without significant plastic deformation while ductile materials can be plastically twisted without crack. The hydrogels studied here are ductile materials.

2.1.2. Toughness

Toughness describes the capacity of a material to absorb energy and plastically deform without fracturing. It can be quantified by the amount of energy per unit volume that a material

can absorb before rupturing (**Figure 2.2**). Toughness (U) can be calculated via the area under the stress-strain curve:

$$U = \int_0^{\epsilon_f} S d\epsilon_t \quad (4)$$

where ϵ_t is the strain, ϵ_f is the strain upon failure, and S is the nominal stress.

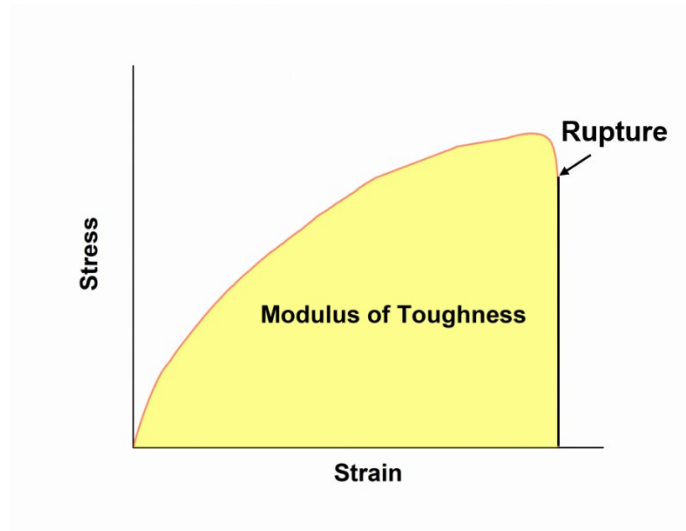


Figure 2.2 The typical curve to calculate the toughness of materials.

Brittle materials, like ceramics, could be strong but possess limited ductility. Therefore, they are not tough. In reverse, ductile materials with low fracture strain are not tough, either. Materials must be both strong and ductile to have high toughness. To have high toughness, materials should have both high stress and high fracture strain.

2.1.3. Fracture energy

Fracture energy is usually defined as the work needed to create a unit area of the fracture surface, normally used to quantify the intrinsic resistance of materials in fracture mechanics.

Fracture energy (G) could be influenced by the cross-linking density of the double-network. As is shown in **Figure 2.3**, it can be calculated from the average tearing force from the tearing test:

$$G = \frac{F_t}{w} \quad (5)$$

where F_t is the average tearing force and w is the width of the sample.

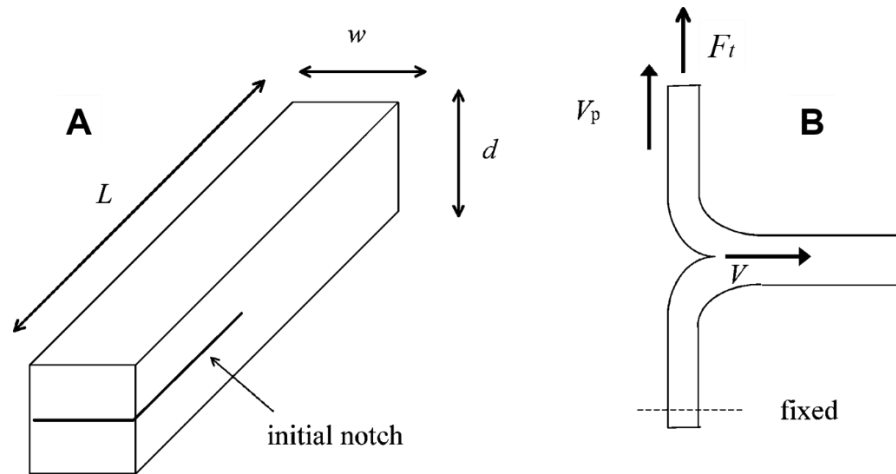


Figure 2.3 (A) Sample shape ($w = 5$ mm, $L = 50$ mm, $d = 7.5$ mm, the length of the initial notch is 20 mm). (B) The tearing method to measure fracture energy. F_t is the tearing force, V_p is the pulling velocity and V is the crack velocity. [63] *Image was reproduced from [63]*

2.1.4. Compression strength

Compression strength is the capacity of a material to withstand loads that reduce its size. While tensile strength resists tension, compression strength resists compression. When the compression strength exceeds the materials' compression strength limit, some may fracture while others might deform irreversibly. Like tensile stress, because the cross-section area changes in the compression, compression strength also has nominal stress (engineering stress) and the true stress. Normally,

nominal stress (σ_c) is considered, defined as the compression force (F_c) divided by the initial cross-section area (A_0), as shown in **equation 6**.

$$\sigma_c = \frac{F_c}{A_0} \quad (6)$$

2.1.5. Viscoelasticity

Viscoelasticity is part of the mechanical property of materials that possess both viscosity and elasticity when undergoing deformation. Viscous materials, such as water, resist strain linearly when the external load is applied. However, elastic materials, such as rubber, immediately return to their original state after external stress is removed. Viscoelasticity of materials can be studied with dynamic mechanical analysis, applying small oscillatory stress and measuring the resulting strain [64]. The dynamic modulus (G) can be applied to demonstrate the relationship between the oscillating stress and strain:

$$G = G' + iG'' \quad (7)$$

in this equation, $i^2 = -1$, G' and G'' are storage modulus and loss modulus, respectively,

$$G' = \frac{\sigma_0}{\varepsilon_0} \cos \delta \quad (8)$$

$$G'' = \frac{\sigma_0}{\varepsilon_0} \sin \delta \quad (9)$$

where σ_0 , ε_0 , and δ are the amplitudes of stress, the strain, and the phase shift between them, respectively.

2.2. Friction Properties

Friction is the force that resists the relative motion. It can happen between solid surfaces and fluid layers. Friction can be categorized into dry friction, fluid friction, and lubricated friction. Normally, friction between hydrogels and substrates depends on the normal load, the contact area, hydration, substrate, hydrogel structure, and sliding speed [65]. The Coefficient of Friction (μ , **equation 10**) is the ratio between friction force (f) and normal force (F_n).

$$\mu = \frac{f}{F_n} \quad (10)$$

Fluid, like water and oil, can act as a lubricant to reduce the wearing of two solid surfaces, which could decrease the friction coefficient accordingly. A tribometer is usually used to measure friction on the surface.

2.3. Adhesion Properties

Adhesion is the capacity of surfaces to cling to the other surface. Based on the mechanism, adhesion is proposed as mechanical adhesion, chemical adhesion, dispersive adhesion, electrostatic adhesion, and diffusive adhesion. Mechanical adhesion comes from the interlock of two surfaces. Chemical adhesion happens when two separate surfaces form ionic, covalent, or hydrogen bonds. Dispersive adhesion occurs when two surfaces are held together by Van der Waals forces. Electrostatic adhesion results from the electrostatic interaction between two surfaces. Diffusive adhesion derives from the diffusion of one end of molecules into the other material. Normally, adhesion between materials is a mixture of several adhesion mechanisms. Based on the different demands, numerous test methods are proposed to measure the adhesion in **Figure 2.4**,

shear, tensile (vertical), and 180° peel test. Here, the tensile adhesion test method is adopted to measure the adhesion of hydrogels to different substrates.

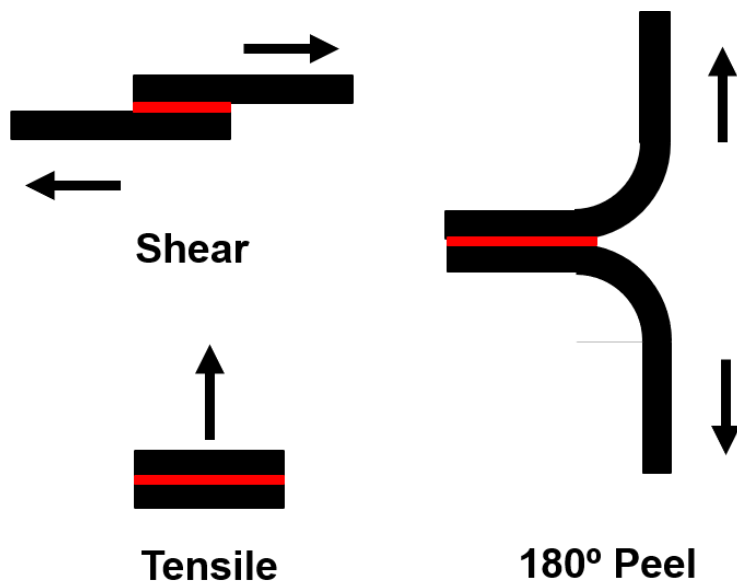


Figure 2.4 Common adhesion test methods.

2.4. Biocompatibility

Biocompatibility quantifies the extent of how the material is compatible with biological systems. It could be demonstrated by cell cytotoxicity, which quantifies its property of being toxic to cells. MTT assay, a colorimetric analysis, can be used to assess the cytotoxicity of materials [66]. In brief, under defined condition, NAD(P)H-dependent cellular oxidoreductase enzymes can reflect the number of viable cells. These enzymes can reduce the tetrazolium dye, MTT, to its insoluble formazan, a purple colour. Then, by comparing it to the blank group, the number of viable cells could be calculated from their color difference in colorimetric analysis.

2.5. Ultrasound properties

Group velocity, phase velocity, and attenuation coefficient are three important properties of the ultrasound wave. The ultrasound velocities may vary in different media. When ultrasound passes through different media, there would be energy loss in the interface and the interior [2, 4, 9]. As **Figure 2.5** shows, compared to water as the media, the decrease of amplitude, while the sample acts as the media, illustrates that the sample can cause energy loss. Besides, the energy loss could also be influenced by the frequency of ultrasound. The attenuation coefficients characterize the energy loss when a beam of ultrasound penetrates a volume of materials. The velocity and attenuation coefficient can be measured with the experiment setup in **Figure 2.6**. The speed of sound in water, V_{water} , was 1480 m/s measured from the water pulse, like the value determined by the expression:

$$V_{water} = 1402.9 + 4.835T - 0.047016T^2 + 0.00012725T^3 \quad (11)$$

at 19.5 °C. The speed of sound in the medium can be determined by the group velocity (V) via the substitution method:

$$V = \frac{h}{-\Delta t + \frac{h}{V_{water}}} \quad (12)$$

where Δt is the delay time between the arrival times of the reference points of the signals, and h is the sample thickness. The travelling speeds of the frequency components of the sample signal are given by the phase velocities ($c(\omega)$):

$$c(\omega) = \frac{\omega h}{-\Delta\phi(\omega) + \frac{\omega h}{V_{water}}} \quad (13)$$

where ω is the angular frequency, and $\Delta\phi(\omega)$ is the unwrapped phase difference between the water and sample spectra.

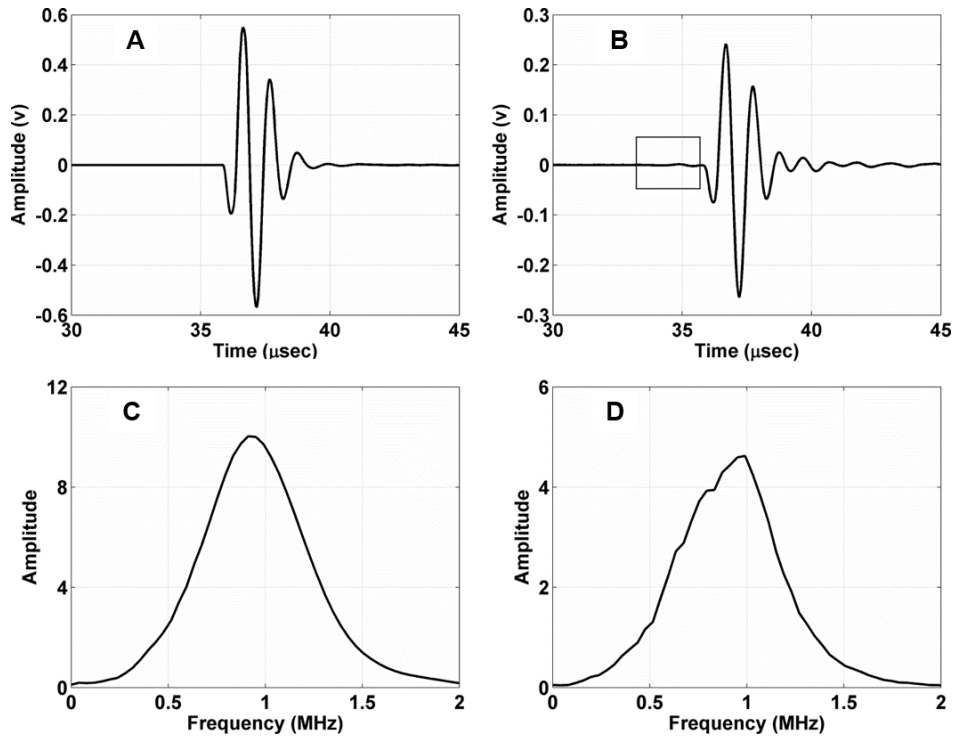


Figure 2.5 The ultrasound signals: (A) a water pulse; (B) a sample signal; (C) the amplitude spectrum of the water pulse; (D) the amplitude spectrum of the sample signal. [10] *Image was reproduced from [10]*

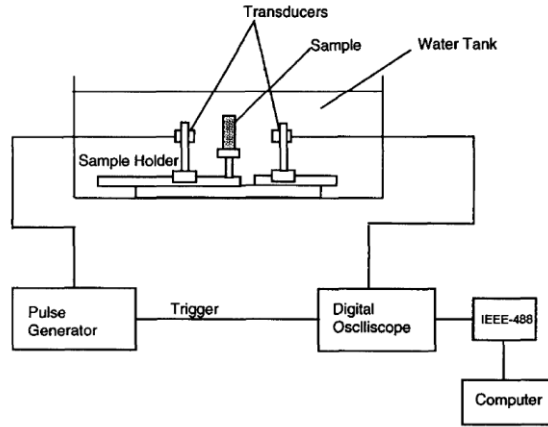


Figure 2.6 The schematic illustration of the experimental setup for the pulse transmission method.

[67] Image was reproduced from [67]

Ultrasonic energy loss due to scattering, absorption, and transmission is quantified by the attenuation coefficient, α (in dB/cm):

$$\alpha(\omega) = \frac{20}{h} \times \log_{10} \left[\frac{A_{ref}(\omega)}{A_{sample}(\omega)} \right] \quad (14)$$

where $A_{ref}(\omega)$ and $A_{sample}(\omega)$ are the amplitude spectra of the water and sample signals, as shown in **Figure 2.5**.

2.6. Ultrasound imaging

Different from the experimental setup for the pulse transmission method in **Figure 2.6**, ultrasound imaging is normally conducted with SonixTablet portable medical ultrasonic phased array system (**Figure 2.7A**, Analogic, Vancouver, Canada) with a 128-element array transducer (**Figure 2.7B**, L40-8/12, Analogic, Vancouver, Canada) at 20 MHz. Enamel, gingival, alveolar crest, and other oral structures can be clearly shown in ultrasound images.

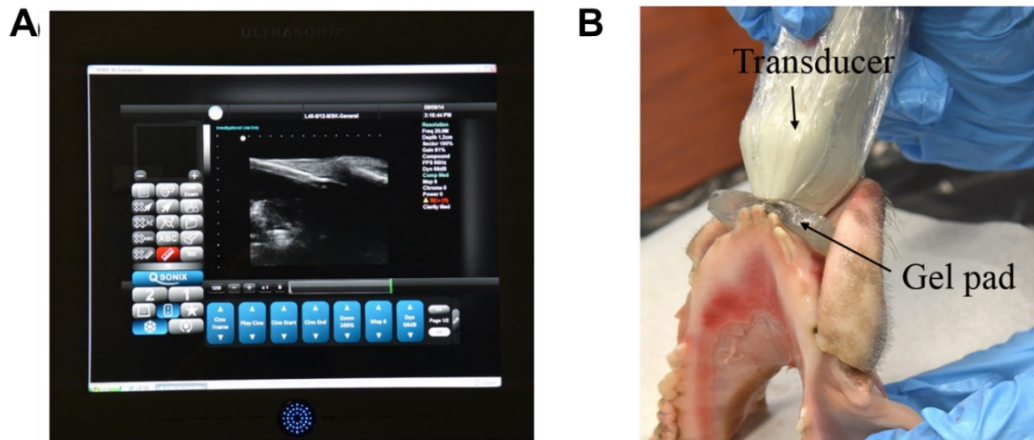


Figure 2.7 Ultrasound experiment: (A) The touch-screen SonixTablet ultrasound phased array system. (B) The 128-element L40-8/12 transducer (Analogic, Vancouver, Canada) is positioned to scan the LCI. [68] *Image was reproduced from [68]*

3. Polyacrylamide/Alginate double-network tough hydrogel for intraoral ultrasound imaging

3.1. Introduction

Ultrasound has been widely used in medical imaging, following the pioneering research of Wild and Reid in the 1950s [6, 8, 69, 70]. Compared to X-Ray and computed tomography, ultrasound imaging is portable, more cost-effective, and safer, without the risk of ionizing radiation [5, 7, 71, 72]. Considering these benefits, there are strong motivations to apply ultrasound to image dento-periodontal tissues and diagnose periodontal diseases. In ultrasound imaging, gel pads are often utilized as couplants for two main purposes: to delay ultrasound signals away from the initial trigger signals for better signal discrimination and to keep the ultrasound beam in the focal zone [1-4, 73]. However, currently available commercial gel pads, such as Aquaflex (AF), are limited to external applications. If applied intraorally, couplants should have the following properties: high stability in water, being resilient enough to conform to the surface of the gingiva (gum) without fracture, high coefficient of friction to maintain functional coupling with the tissues and transducer for excellent transmission of ultrasound, and biocompatibility. However, AF may not meet these requirements. Therefore, it is of utmost priority to develop a biomaterial with properties described above as the couplant for intraoral ultrasound imaging.

Hydrogels are three-dimensional (3D) crosslinked polymer networks with high water content and great similarities to the extracellular matrix (ECM) [52, 60, 61, 64, 74-80]. Therefore, hydrogels potentially serve as ideal candidates for ultrasound couplants. Nevertheless, being repeatedly stretched to conform to the contour and surface of the dental tissues, the conventional

hydrogels may lose their integrity and function in such applications due to their poor mechanical properties [31, 33, 81-85]. Different types of tough hydrogels with excellent mechanical properties, including interpenetrating (IPN) hydrogels, double-network (DN) hydrogels, and nanocomposite (NC) hydrogels have been reported [31, 38, 41, 86]. Considering their stability in water, outstanding mechanical properties, and excellent biocompatibility, they can be potentially applied as the couplants for intraoral ultrasound imaging. Among these, PAM/Alginate DN hydrogel is one type of well-studied tough hydrogels, which has been applied in numerous bioengineering applications [52, 55]. The unique DN structure not only limits the hydrogel to swell in water but also allows the fracture energy to be dissipated, which provides excellent stability in water and mechanical strength required in intraoral ultrasound imaging. However, both frictional and ultrasound properties of the PAM/Alginate hydrogel remain unknown. Besides, a comprehensive comparison of physical, mechanical, frictional and ultrasound properties to AF is required.

Here, we systematically studied the frictional and ultrasound properties of PAM/Alginate DN hydrogel and comprehensively compared all the essential properties required for intraoral ultrasound imaging between PAM/Alginate DN hydrogel and AF. The PAM/Alginate DN hydrogel not only displays better stability in water as well as superior mechanical properties and higher coefficients of friction to AF but also possesses similar ultrasound properties compared with AF. Besides, the developed hydrogel exhibits lower cytotoxicity to both cancer (HeLa) and normal fibroblast (MRC-5) cells. Given all the features, the PAM/Alginate DN hydrogel has been successfully demonstrated as the ultrasound couplant to image porcine mandibular incisor. The PAM/Alginate DN hydrogel may serve as the proof-of-concept ultrasound couplant for intraoral ultrasound imaging.

3.2. Materials and Methods

3.2.1. Materials

Phosphate buffered saline (PBS), alginic acid sodium salt from brown algae (Alginate, medium viscosity), acrylamide (AM, 99%), ammonium persulfate (APS, 98%), N, N'-Methylenebisacrylamide (MBAA, 99.5%), N, N, N', N'-Tetramethyl-ethylenediamine (TEMED, 99%), calcium chloride dihydrate (99%) were purchased from Sigma-Aldrich (USA) and used without further purification. Aquaflex Ultrasound gel pad (AF) was purchased from Parker Laboratories Inc (USA).

3.2.2. Synthesis of PAM/Alginate hydrogels

PAM/Alginate hydrogels were synthesized by the free radical polymerization of AM and ionic crosslinking of alginate [38, 87]. For a typical synthesis process, alginic acid sodium salt was dissolved in 40 mL PBS (pH = 7.4) to form the homogenous alginate solution. Then AM (4.8 g), MBAA (0.033 g), TEMED (36 μ L) and APS (0.012 g) were dissolved in the alginate solution. After stirring for a half-hour, the mixture was transported into a glass Petri dish followed by polymerization at 70 °C for 4 hours. Finally, the formed hydrogel was removed from the Petri dish and immersed in 3 M Calcium chloride solution for 24 hours. A series of hydrogels with 1, 1.5, 2, 2.5, and 3 w/v% of alginate were prepared, which were denoted as H-1, H-1.5, H-2, H-2.5, and H-3 respectively.

3.2.3. FTIR and microstructure characterization

Fourier transform infrared (FTIR) spectra of acrylamide, alginate and freeze-dried H-2 were obtained with the Nicolet iS50 FTIR Spectrometer (attenuated total reflectance, ATR mode) over

a wavenumber range of 500-4000 cm^{-1} with a resolution of 4 cm^{-1} . The microstructure and element distribution of H-2 were studied by Zeiss Sigma 300 VP Field Emission Scanning Electron Microscope (FESEM) with the Energy-dispersive X-ray spectroscopy (EDS) at 15 kV acceleration voltage. Samples were sectioned from the freeze-dried H-2 and sputter-coated with a thin layer of gold before SEM characterization.

3.2.4. Swelling test

The densities of all the as-prepared hydrogels and AF were determined by calculating their mass/volume ratios. Their water percentages (WP) were determined by their initial weights ($W_{initial}$) and their lyophilized weights (W_{dry}) according to **Equation 15**.

$$WP = \frac{(W_{initial} - W_{dry})}{W_{initial}} \quad (15)$$

The swelling test was used to determine the equilibrium swelling ratios and stability of the as-prepared hydrogels and AF. Lyophilized samples (the as-prepared hydrogels and AF) were immersed in 20 mL deionized water in sealed vials at room temperature. At the pre-set time interval, samples were taken out and excess water was removed with filter papers. Following that, samples were weighed, and their weights were recorded as W_{swell} . The test was not finished until W_{swell} kept constant. Then, the equilibrium swelling ratio (ESR) of each sample was determined using **Equation 16**.

$$ESR = \frac{(W_{swell} - W_{dry})}{W_{dry}} \quad (16)$$

To further demonstrate their stability in water, the degradation test of the as-prepared hydrogels and AF was performed by immersing them in deionized water. At designed time points, they were taken out, wiped with filter paper to remove excess water, and then weighted. Their stability in water was monitored by their relative weights (R_t):

$$R_t = \frac{W_t}{W_{initial}} \quad (17)$$

where $W_{initial}$ is their initial weights and W_t is their weights at t hour.

3.2.5. Mechanical properties

All mechanical tensile tests were conducted under room temperature via an AGS-X universal tensile test machine (Shimadzu, Japan) with a crosshead speed of 10 mm/min. All samples were prepared into stripes (50 mm in length \times 10 mm in width \times 6.5 mm in thickness). The nominal tensile stress (S) was calculated by the applied force divided by the initial cross-section area while the stretched/initial gauge length ratio gave the tensile strain. The true tensile stress was computed by multiplying the nominal tensile stress with the tensile strain [88, 89]. Besides, the toughness (U) of samples is defined by the area under the nominal stress-strain curve:

$$U = \int_0^{\varepsilon_f} S d\varepsilon_t \quad (18)$$

where ε_t is the strain, ε_f is the strain upon failure, and S is the nominal stress.

Fracture energy was measured by the tearing test with the same tensile equipment [63, 90, 91]. Regarding the standardized JIS-K 6252 1/2 sizes, samples were cut into 50mm \times 5mm \times 6.5mm cuboids with the initial notch of 20 mm. Two arms of each sample were clamped, and a constant

velocity of 10 mm/min was applied to pull the upper arm with the lower arm fixed. The tearing force was recorded to calculate the fracture energy (G) by the following equation:

$$G = \frac{F_t}{w} \quad (19)$$

where F_t is the average force during the tearing and w is the width of the hydrogel.

3.2.6. Friction tests

The frictional properties were evaluated by the ball-on-disc reciprocal tests on an NHR3 Nanotribo-meter Tester (Anton Paar) under room temperature (25 °C) [65, 92-96]. Samples were prepared as a disc of 10 mm × 10 mm × 3mm and fixed to the sample holder of the Nanotribo-meter. The ball-on-disc test was conducted by sliding against the titanium ball attached to the cantilever for a full amplitude of 4.00 mm and a frequency of 0.1 Hz. Each sample was tested for six consecutive periods with the normal force from 1 to 30 mN correspondingly. The average value of friction force was obtained from the friction curve. The coefficient of friction was computed by:

$$\mu = \frac{f}{F_n} \quad (20)$$

where μ is the coefficient of friction, f is the friction force, and F_n is the normal force.

3.2.7. Ultrasonic characterization

Three ultrasound properties, group velocity, phase velocity, and attenuation coefficient, were measured using the transmission-through technique in water [10, 67]. The samples were held in place by a gel pad holder. The water tank contained a pair of 6.35-mm-diameter 20-MHz unfocused transducers (Olympus NDT V312-N-SU and V317-N-SU, Waltham, MA) mounted

coaxially in the transducer holders. The two transducers, one as an emitter and the other as a receiver, were separated by 200 mm with the samples placed at 140 mm, further than the near field distance (136 mm) from the emitter. The sample holder was placed between two transducers and orientated so that the ultrasound beam was perpendicular to the surface of samples. Each sample was measured five times at five different regions of interest (ROI) with each ROI's location shifted 5 mm from the previous site while maintaining the same sample's distance from the emitter and the sample's surface perpendicular to the transducers. The transmitter was excited by an Olympus 5800 pulse-receiver (Panametrics, Waltham, MA) and the transmitted signals, intercepted by the receiver, were recorded and stored by a LeCroy WaveSuffer 422 digital oscilloscope (LeCroy, Chestnut Ridge, NY). The signals were sampled at 2 Gigasamples per second at 8-bit resolution, and the digitized waveform was continuously averaged over 256 times to increase the signal-to-noise-ratio.

Two signals were recorded without and with the sample in the beam path as a reference signal through water (water pulse) and a sample pulse. The speed of sound in water, V_{water} , was measured to be 1480 m/s from the water pulse and was similar to the value determined by the expression: [97]

$$V_{water} = 1402.9 + 4.835T - 0.047016T^2 + 0.00012725T^3 \quad (21)$$

at temperature, $T \sim 19.5^\circ\text{C}$. The speed of sound in the medium can be determined by the group velocity (V) via the substitution method [10]:

$$V = \frac{h}{-\Delta t + \frac{h}{V_{water}}} \quad (22)$$

where Δt is the delay time between the arrival times of the reference points of the signals, and h is the sample thickness. In this work, we used the arrival times of the envelope peaks to calculate the delay time [9]. The travelling speeds of the frequency components of the sample signal are given by the phase velocities ($c(\omega)$):

$$c(\omega) = \frac{\omega h}{-\Delta\varphi(\omega) + \frac{\omega h}{V_{water}}} \quad (23)$$

where ω is the angular frequency and $\Delta\varphi(\omega)$ is the unwrapped phase difference between the water and sample spectra. The useful frequency range, bounded between ± 6 dB, was determined. Dispersion is determined by the slope of the linear least-squares regression line fitted to the phase velocity versus frequency data within the same frequency range.

Ultrasonic energy loss due to scattering, absorption, and transmission is quantified by the attenuation coefficient, α (in dB/cm):

$$\alpha(\omega) = \frac{20}{h} \times \log_{10} \left[\frac{A_{ref}(\omega)}{A_{sample}(\omega)} \right] \quad (24)$$

where $A_{ref}(\omega)$ and $A_{sample}(\omega)$ are the amplitude spectra of the water and sample signals. The attenuation was not corrected for the transmission loss caused by the water-hydrogel interfaces. Similarly, when the attenuation is normalized by the relevant frequency band, we obtain the normalized broadband ultrasound attenuation (nBUA) in dB/MHz/cm.

3.2.8. Ultrasonic imaging

The H-2.5 and AF gel pads were used as couplants for an ex-vivo ultrasound experiment to compare the imaging clarity. A porcine center incisor was scanned using a SonixTablet portable medical ultrasonic phased array system (Analogic, Vancouver, Canada) with a 128-element array transducer (L40-8/12, Analogic, Vancouver, Canada) at 20 MHz. The transducer traversed the tooth and gingiva on the labial side so that the long axes of the probe and the tooth aligned [13]. A piece of about 5-mm thick gel pad (H-2.5 or AF) was placed between the contact areas to achieve good coupling and delay the pulse so that the enamel and gingiva were in the focal zone and their external surfaces could be imaged. Parker Aquasonic 100 ultrasound gel (Parker Laboratories Inc., USA) was used to fill in any void or gap between the transducer, gel pad and the porcine tissues. The system excited all 128 elements with electronic delays to generate an ultrasound beam that could focus at a desired focal depth and swept across the region of interest to create an image. A series of images were recorded with a frame rate of 54 Hz.

3.2.9. Cell cytotoxicity

The biocompatibility of H-2.5 and AF was tested by the MTT assay [66, 98, 99]. Briefly, the H-2.5 and AF were immersed in Dulbecco's Modified Eagle Medium (DMEM, cell cultivation medium) for 24 hours respectively. Fibroblast cells (MRC-5 cells) and cancer cells (HeLa cells) were seeded with a density of 6000 cells per well in 100 μ L of DMEM medium onto a 96-well plate for 24 hours. Then, the culture media were respectively replaced by 100 μ L of Fresh DMEM media, DMEM media containing the H-2.5 extracts, and DMEM media containing the AF extracts. After the cultivation of cells for 3 hours, the MTT solution was added into the mixture. Following 3 hours of cultivation, the media were removed, and dimethyl sulfoxide was put in to dissolve the

formazan crystals. The cell cytotoxicity was characterized by the optical density at 570 nm (OD_{570nm}) and calculated from the comparison of optical cell density under the condition with/without the extract. The culture medium and cell suspension (MRC-5 fibroblast cells and HeLa cells) without the hydrogel extract served as the blank and the control, respectively:

$$\text{Cell viability (\%)} = \frac{OD_{570nm, sample} - OD_{570nm, blank}}{OD_{570nm, control} - OD_{570nm, blank}} \times 100 \quad (25)$$

where $OD_{570nm, sample}$, $OD_{570nm, blank}$, and $OD_{570nm, control}$, are the optical densities of the sample, the blank, and the control, respectively.

3.3. Results and Discussion

3.3.1. Fabrication of PAM/Alginate hydrogels

As presented in **Figure 3.1**, the first network of PAM/Alginate hydrogel was developed via the free radical polymerization of AM with APS as the initiator and MBAA as the crosslinker, which produced transparent hydrogels. The second network was formed via the ionic crosslinking between alginate and calcium ion. After immersing in calcium chloride solution for 24 hours, the hydrogels turned into pale white (**Figure S3.1**).

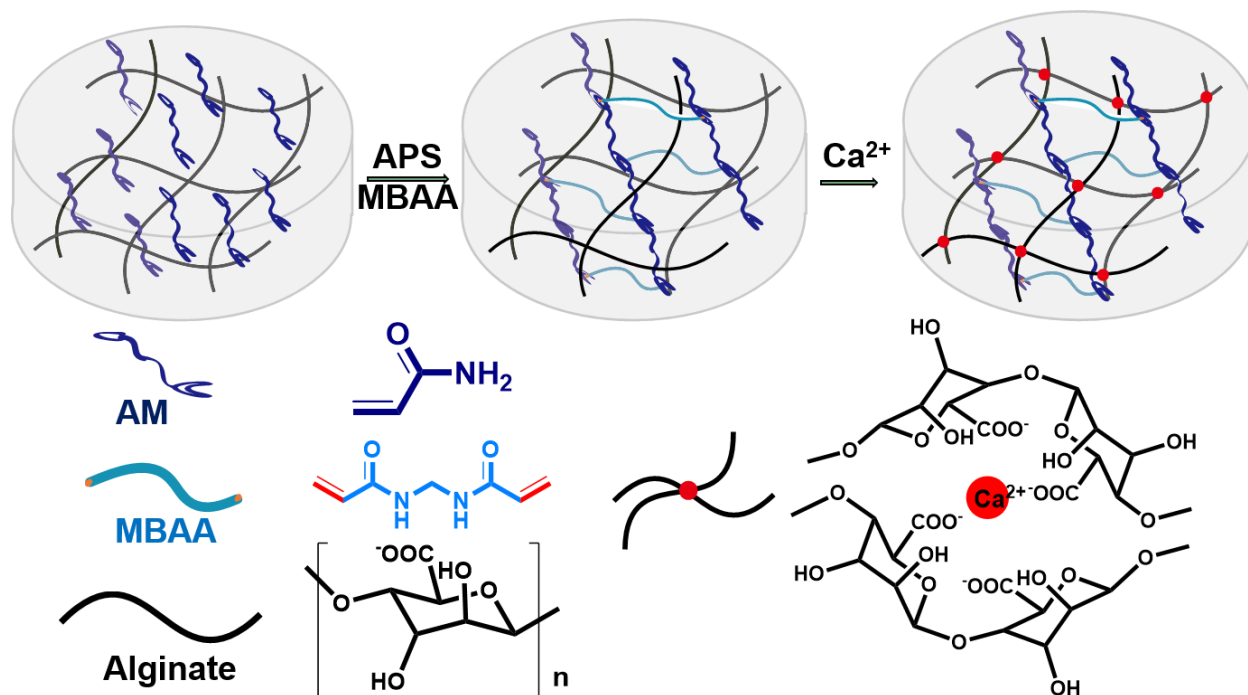


Figure 3.1 Schematic illustration of the gelation process of PAM/Alginate hydrogels

Figure 3.2A displays the FTIR spectra of alginate, acrylamide (AM), and H-2 (PAM/Alginate hydrogel). The absorption peak at 1022 cm^{-1} was attributed to the C-O stretching, shown in the spectra of both alginate and H-2, suggesting the presence of alginate in H-2. The absorption peaks at 1667 cm^{-1} and 1603 cm^{-1} corresponding to the C=O stretching, appeared in the spectrums of AM and H-2, indicating the existence of AM in H-2. Besides, the weak absorption peak at 2820 cm^{-1} , resulted from the C-H stretching of the alkene groups in AM and was absent in the spectrum of H-2, implying the polymerization of AM in the H-2. The surface morphology and microstructure of H-2 were characterized by FESEM. **Figure 3.2B** revealed the crosslinking network structure in H-2. Besides, the flake-like structure of hydrogel in **Figure 3.2B** could ascribe to the growth of the calcium chloride crystals along the pore wall of the hydrogel after freeze-drying [100, 101]. According to the calcium mapping in **Figure 3.2C** and **3.2D**, calcium ions were well

distributed in H-2, implying the uniform crosslinking of the alginate-calcium network. Summarized from the FTIR and SEM data, the PAM/Alginate hydrogel was successfully fabricated with covalently crosslinked PAM network and ionically crosslinked alginate-calcium network.

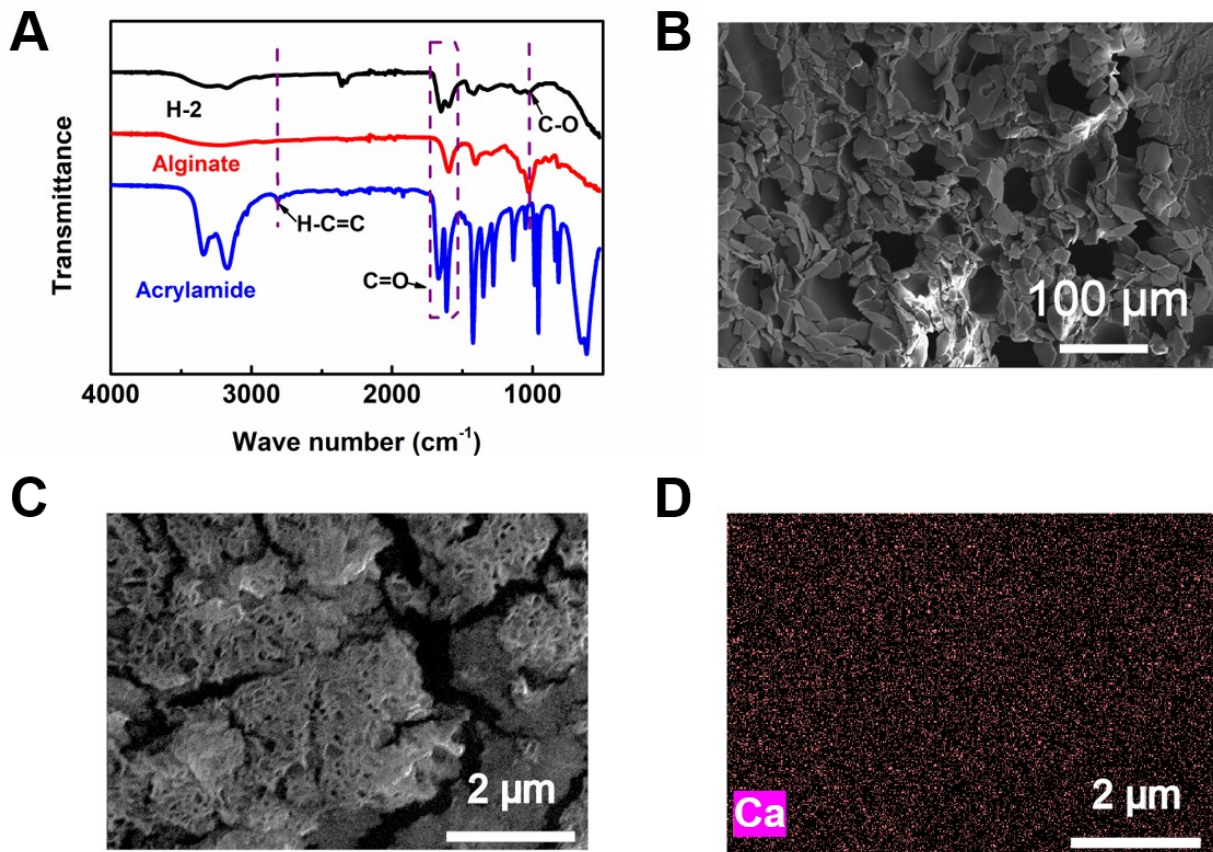


Figure 3.2 (A) The FTIR spectra of Acrylamide (AM), Alginate and H-2 (PAM/Alginate hydrogel). (B) The SEM image of H-2 (PAM/Alginate hydrogel). (C) The element mapping site of H-2. (D). The calcium element mapping in H-2.

The effect of alginate content (1, 1.5, 2, 2.5 and 3 w/v%) on the density, water percentage and equilibrium swelling ratio of PAM/Alginate hydrogel was studied. As the content of alginate

increased from 1 to 3 w/v%, the densities of PAM/Alginate hydrogels almost remained constant (**Figure S3.2**). However, due to the increased alginate content, the water percentage of the as-prepared hydrogels had a slight decrease (**Figure 3.3A**). In comparison, the water percentage of AF was 96.4%, much higher than those of the as-prepared hydrogels. Furthermore, the equilibrium swelling ratio of the as-prepared hydrogels decreased with increasing alginate content (**Figure 3.3B**), which is attributed to their increased crosslinking density [102]. The as-prepared PAM/Alginate hydrogels could still maintain the original shape after being immersed in water for 48 h (**Figure S3.3**). In contrast, the equilibrium swelling ratio of AF could not be accurately measured as AF was fully dissolved in water due to its low stability (**Figure 3.3C**), which may pose potential risks in the intraoral ultrasound imaging.

To further demonstrate the better stability of the as-prepared PAM-Alginate hydrogels compared to AF, their degradation tests in water were conducted. As presented in **Figure 3.3D**, H-3 almost remained initial weight after immersing in water for 50 hours. Moreover, the relative weight of the as-prepared hydrogels decreased with the increasing alginate content from H-1 to H-3 due to the increasing crosslinker density. Comparatively, the relative weight of AF sharply increased at first and then gradually decreased because AF absorbed water and dissolved in the water. After immersing for 55 hours, AF could only retain approximately half its original weight. Therefore, better stability in water makes the as-prepared PAM/Alginate hydrogels potential candidates for couplants.

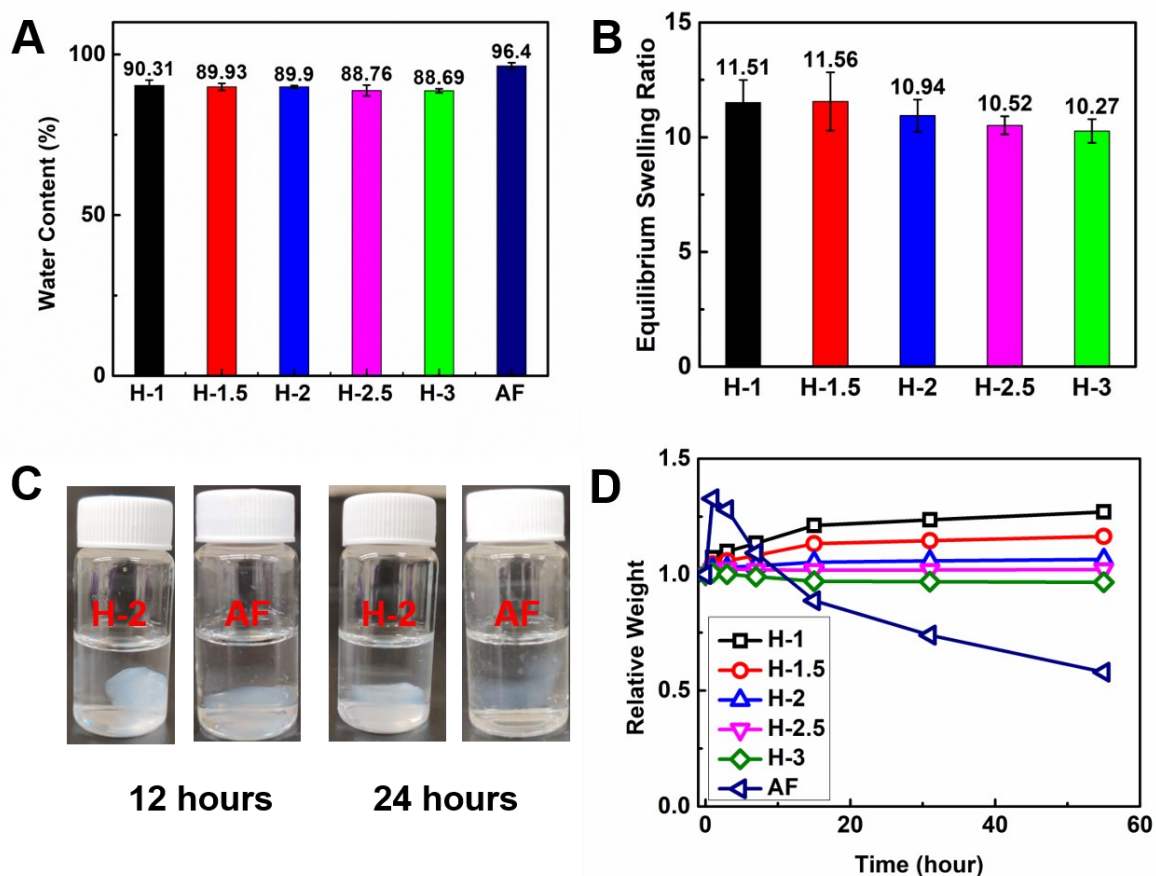


Figure 3.3 (A) The water content of the as-prepared PAM/Alginate hydrogels and AF. (B) The equilibrium swelling ratio of the as-prepared PAM/Alginate hydrogels. (C) Frozen-dry H-2 and AF swelling in deionized water for 12 hours and 24 hours respectively. (D) The relative weight of the as-prepared PAM/Alginate hydrogels and AF versus immersion time.

3.3.2. Mechanical properties

The mechanical properties of the as-prepared hydrogels and AF were characterized by uniaxial tensile tests. Compared to AF, the as-prepared hydrogels show desirable mechanical properties for intraoral ultrasound imaging. **Figure 3.4A** presents H-3 at the initial state (left) and after being stretched three times (right). **Figure 3.4B** shows the stress-strain curves of the as-

prepared hydrogels and AF. H-3 could be stretched to five times its initial length while AF could only be extended to three times its initial length. Moreover, the introduction of alginate can significantly improve the nominal tensile fracture stress of the hydrogels from 0.047 MPa (1 w/v % alginate, H-1) to 0.121 MPa (3 w/v % alginate, H-3). However, when samples were stretched, their cross-section area decreased, and the nominal tensile stress could not reflect the true tensile stress. Therefore, the true tensile stress of the as-prepared hydrogels was presented as a reference, which increased from 0.131 MPa to 0.700 MPa from H-1 to H-3 as well (**Figure 3.4C**). In comparison, the nominal and true fracture stresses of AF are 0.068 MPa and 0.351 MPa, respectively, which both fall between H-1.5 and H-2. It is noted that small steps could be occasionally observed in the stress-strain curve (e.g., H-2.5, **Fig 3.4B**), which was most likely caused by the possible stick-slip tearing behavior during the tensile test of double-network tough hydrogels as reported in previous studies [103-105].

Toughness quantifies the energy dissipated by unit volume material before rupture. The second network of the as-prepared hydrogels can dissipate energy by reversibly breaking the ionically crosslinked bonds between alginate and calcium ions. As the content of alginate increases, the amount of ionically crosslinked bonds per volume increases. It illustrates the rise in the toughness of the as-prepared hydrogels from 0.0628 MJ/m³ (H-1) to 0.4382 MJ/m³ (H-3) by employing the energy dissipation mechanism (**Figure 3.4D**). However, the toughness of AF is 0.1583 MJ/m³, which also falls between the toughness of H-1.5 and H-2.

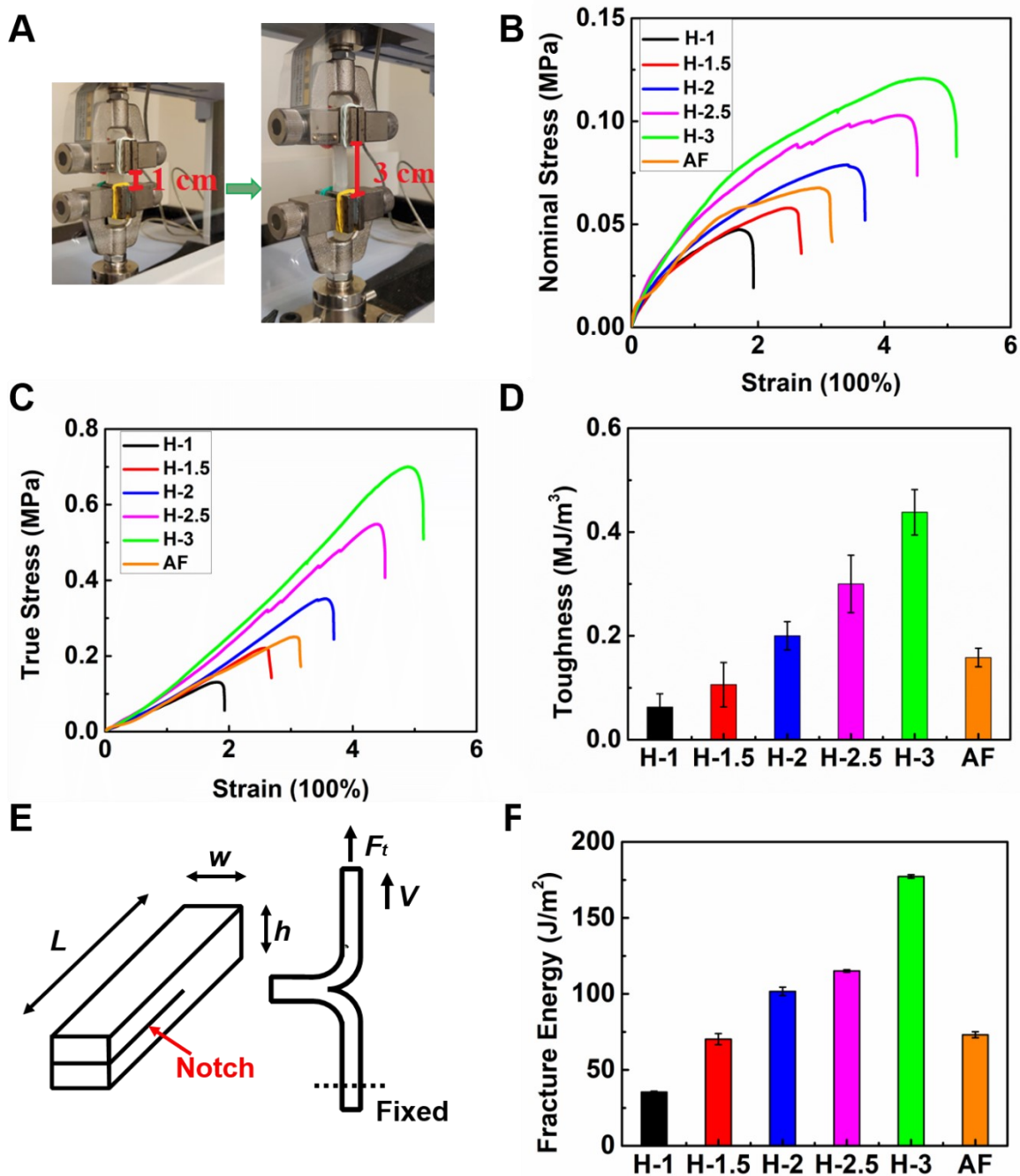


Figure 3.4 (A) H-3 at the initial and three times stretching states. (B) The nominal stress curves. (C) The true stress curves. (D) The toughness from the nominal stress curves. (E) The sample shape (Left, $L = 50$ mm, $w = 5$ mm, $h = 6.5$ mm, notch = 20 mm) and schematic illustration of the

tearing experiment (Right, F_t is the tearing force, and V is the pulling velocity). (F) The corresponding fracture energy.

As demonstrated in **Figure 3.4E**, the fracture energy of the as-prepared hydrogels and AF was characterized by the tearing test. As the amount of alginate increased, their fracture energy increased from 35 J/m^2 to 177 J/m^2 (**Figure 3.4F**), which is also ascribed to the energy dissipation mechanism of the second network. With the increase of alginate content, the crosslinked sites increase, and energy required to fracture increases. In comparison, AF only has fracture energy of 73 J/m^2 . Both the toughness and tearing tests show that the as-prepared hydrogels possess much better mechanical properties than AF. These superior mechanical properties are desirable for the hydrogels to be used intraorally so that they can conform to the contour and surface of the dental tissues without spontaneous rupture.

3.3.3. Frictional properties

In general, the frictional interaction between samples and substrates depends on the normal load, hydration, substrate, hydrogel structure, and sliding speed [65, 92, 93, 106-111]. Frictional properties of the as-prepared PAM/Alginate hydrogels and AF were characterized by the Nanotribometer via the ball-on-disc test with the titanium ball. **Figure 3.5A** illustrates that as the normal load increased, the friction force correspondingly increased. However, the coefficient of friction (CF) of the as-prepared hydrogels kept decreasing until the normal load increased to approximately 10 mN, and then their CF had a slight increase (**Figure 3.5B**). In comparison, the CF of AF almost remained constant under different normal loads. Under normal loads, the interstitial fluid is extruded from the porous structure to the conjunction, and the pressurization of interstitial fluid occurs to support a proportion of the applied loads, which reduces the coefficient

of friction as the lubricant. **Figure S3.4** presents the CF curves of H-2.5 vary under low (1 mN), medium (10 mN), and high (30 mN) normal loads. Under the low load, limited water was squeezed out to the conjunction. Without enough water as the lubricant, the coefficient of friction was relatively higher. However, the increase of normal load led to more water acting as the liquid lubricant, which elucidates the decrease in CF of the as-prepared PAM/Alginate hydrogels from low normal load to medium load. Based on the Stribeck Curve, the lubrication regimes of the as-prepared hydrogels from low load to medium load (**Figure 3.5B**) is the mixed lubrication of asperities and the liquid lubricant [106, 112-114]. When the normal load increased to the high load, the deformation of as-prepared hydrogels increased accordingly. The distortion of tough hydrogels took the dominant effect, which correspondingly led to an increase in their CF. Therefore, the lubrication regimes of the as-prepared hydrogels from medium load to high load are primarily the hydrodynamic lubrication [93, 115-117]. In comparison, the water content of AF was relatively high (96.4%), which makes the lubrication regime for AF all hydrodynamic lubrication. Therefore, the CF of AF did not change obviously under different normal loads (**Figure 3.5B**).

Besides, the CF of the as-prepared hydrogels is much higher than that of AF, which could be generated from the lower hydration level and metal complexation [118, 119]. Among the as-prepared hydrogels of different alginate contents, their CF reached the peak point at 2.5 w/v% alginate (H-2.5), which could be ascribed to the mutual interaction of polyacrylamide network and alginate-calcium network. Compared to AF and other as-prepared hydrogels, H-2.5 possesses a higher coefficient of friction, which can facilitate firm contact with tissues and transducers without slippage for the stable transmission of ultrasound.

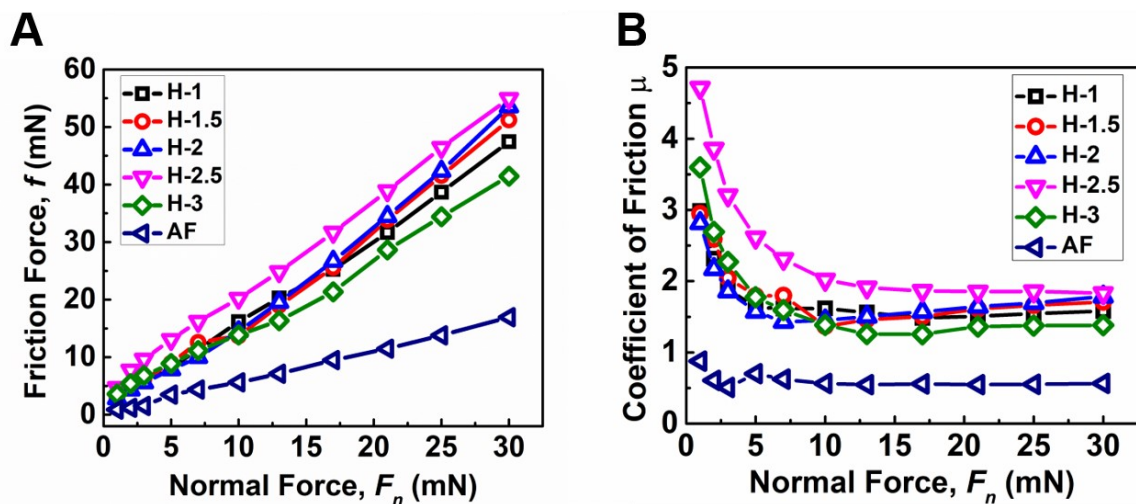


Figure 3.5 Frictional properties. (A) The dependences of the friction force on the normal force. (B) The dependences of the coefficient of friction (CF) on the normal force.

3.3.4. Ultrasonic properties

The transmission-through experiment was performed to measure the ultrasonic properties of the samples (Figure 3.6A), which were secured in place by the holder (Figure 3.6B). Figure 3.6C presents the typical responses of water and sample pulses. The phase velocities of ultrasound for the as-prepared hydrogels and AF do not depend on the frequency within the ± 6 dB frequency range, i.e., from 7.2 to 22.5 MHz (Figure 3.6D), which indicates there is no dispersion (slope = 0) (Table S3.1). The phase and group velocities of the as-prepared hydrogels are almost the same with an average of 1519 m/s. The velocities increase slightly from 1511 to 1525 m/s when the alginate content increases from 1 to 3 w/v% (Figure 3.6D). In comparison, AF has a velocity of 1600 m/s, about 5% faster than the average velocity (1519 m/s) of the as-prepared hydrogels. The hydrogels and AF all have velocities higher than water, which is 1480 m/s. The attenuation of the as-prepared hydrogels varies nonlinearly with frequency (Figure 3.6E). The increase in alginate content enhances the attenuation, for example, from 1.84 dB/cm to 3.50 dB/cm at 17 MHz as seen

in **Figure 3.6E** and **Table S3.1** with an average of 2.74 dB/cm. The attenuation of AF at 17 MHz is about 2.36 dB/cm within the ranges of the hydrogels. However, the mean value of the attenuation coefficients of the as-prepared hydrogels ($nBUA_{ave} = 0.20$ dB/cm·MHz) and AF ($nBUA_{AF} = 0.20$ dB/cm·MHz) are statistically equal, which implies their energy loss characteristics are very similar. The same is true for the density, which ranges from 1.01 to 1.03 g/cm³ (**Figure S3.2**).

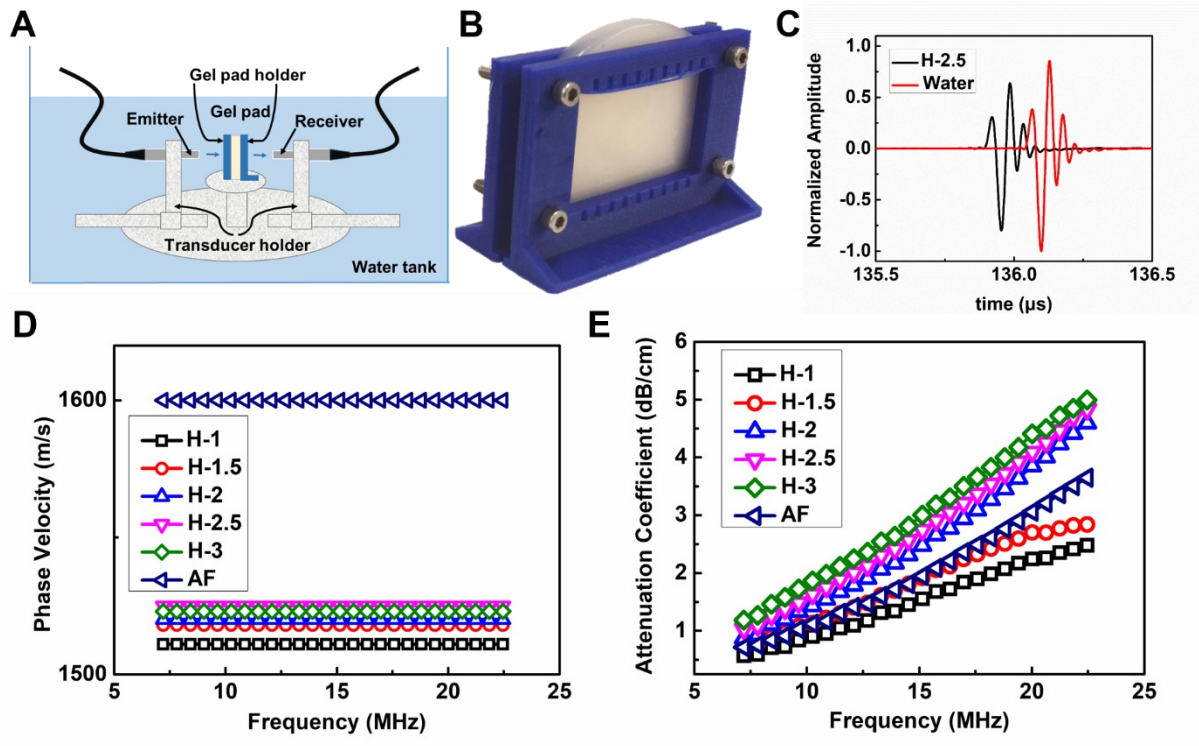


Figure 3.6 Ultrasonic characterization of potential couplants. (A) The transmission-through experimental setup. (B) A couplant mounted in a holder. (C) The reference pulse (Red, water) and sample pulse (Black, H-2.5). (D) The phase velocities versus frequency. (E) The attenuation coefficient versus frequency.

Figure 3.7 demonstrates the 20-MHz ultrasonography of a porcine tooth-periodontium complex using AF and H-2.5, respectively. The images clearly show part of the enamel, gingiva,

the alveolar bone, and cementum-enamel junction. The attenuation coefficient of H-2.5 is higher than AF, i.e., 3.21 dB/cm versus 2.36 dB/cm, indicating that the ultrasound experienced more energy absorption when going through the H-2.5 than AF. However, both gel pads provide ultrasound images of similar quality. All tissue boundaries are visibly identified. This is as expected as the strength of the echoes is governed by the reflection coefficients of the impedance contrast of the interfaces. The acoustic impedance, Z is defined by the product of density and velocity. In this case, the acoustic impedances of the H-2.5 and AF are very close in value, i.e., 1.54×10^6 rayls and 1.65×10^6 rayls respectively where $Z_{H-2.5}$ is approximately 93% of Z_{AF} .

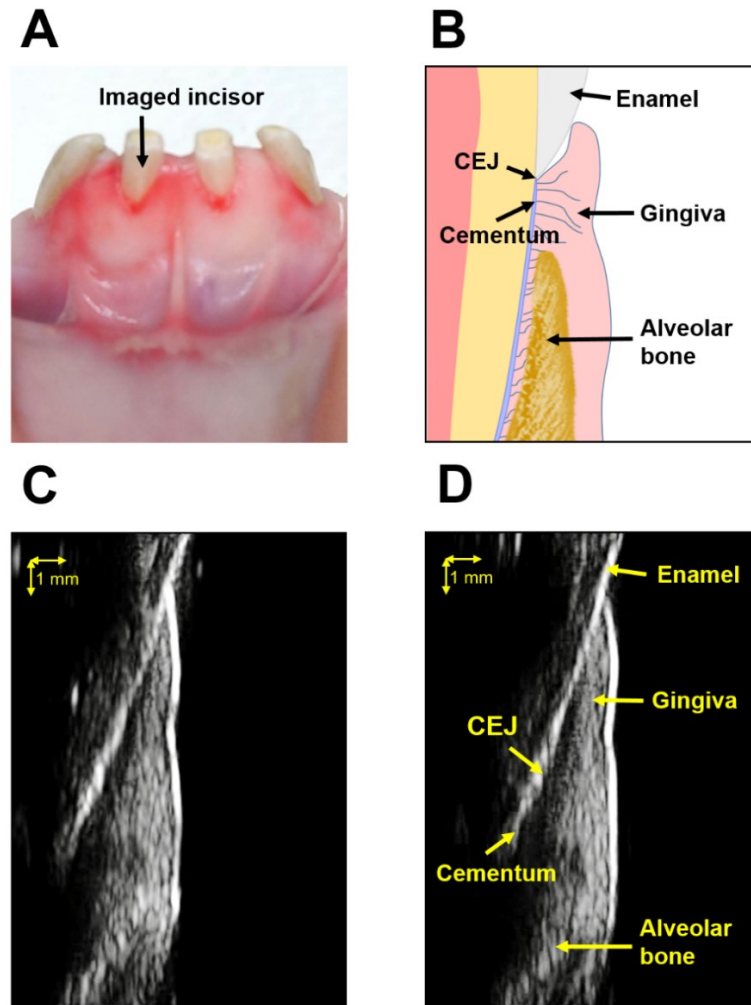


Figure 3.7 Ultrasonic imaging of the dento-periodontium: (A) The imaged incisor. (B) A schematic illustration of oral structure. (C) The ultrasound image with AF as the couplant. (D) The ultrasound image with H-2.5 as the couplant.

3.3.5. Biocompatibility

The biocompatibility of the as-prepared hydrogel (H-2.5) and AF were evaluated via using both cancer (HeLa) and fibroblast (MRC-5) cell lines with MTT assay. As shown in **Figure 3.8**, after 3 hours of cultivation in the extracts of H-2.5, the cell viability of over 95% was maintained

for both cancer cells and fibroblast cells, which elucidates that the hydrogel showed low cytotoxicity to both cells. Although acrylamide was reported to show potential cell cytotoxicity and cancer risk, many PAM-based hydrogels have been developed for biomedical applications. Due to the polymerization of acrylamide and interconnected polymer networks, PAM-based hydrogels show high biocompatibility [54]. Instead, AF showed lower biocompatibility for both HeLa and MRC-5 cells, which could be a concern for intraoral ultrasound imaging. Therefore, the developed hydrogels can serve as potential couplants for intraoral ultrasound imaging.

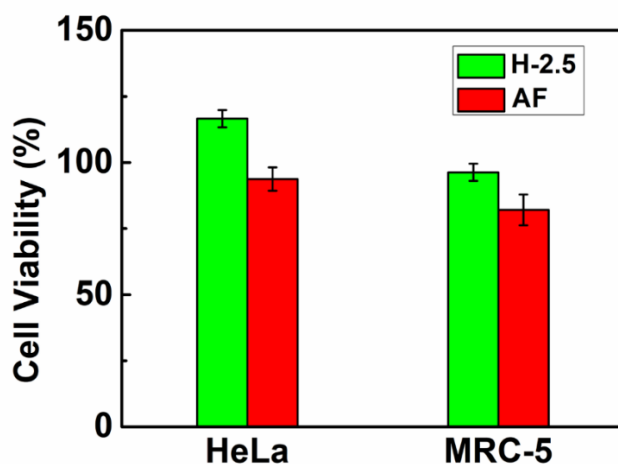


Figure 3.8 Cell viability of HeLa cancer cells and MRC-5 fibroblast cells after 3 hours incubation with the extracts.

3.4. Conclusions

PAM/Alginate tough hydrogels were explored as potential couplants for intraoral ultrasound imaging by a comprehensive comparison of their physical, mechanical, frictional, and ultrasound properties as well as biocompatibility to the commercial couplant (AF). When used as couplants

for porcine incisor, the as-developed PAM/Alginate hydrogels display as good ultrasound image quality as AF. However, compared to AF, the as-developed hydrogels have better stability in water, superior mechanical properties, and higher coefficients of friction. Additionally, the as-developed hydrogels show better biocompatibility to both cancer cells (Hela) and fibroblast cells (MRC-5) than AF. This work not only expands the application of tough hydrogels in the field of ultrasound imaging but also provides useful insights into the development of novel interfaces between human and medical devices for real-time health monitoring applications.

4. Mussel inspired adhesive double-network hydrogel for intraoral ultrasound imaging

4.2. Introduction

Ultrasound imaging has been widely applied to biomedical diagnosis, due to its portability, low cost, and low safety risks [4, 5, 8, 72]. Moreover, compared to quantitative computed tomography (QCT) and dual-energy X-ray absorptiometry, ultrasound imaging can image soft tissues with improved clarity [120-123]. Considering these benefits, ultrasound could be potentially used to image dento-periodontal tissues and diagnose periodontal diseases. For better image identification, gel-based couplants are often used between transducers and tissues to delay the ultrasound signals [1, 2, 124]. If applied intraorally, the couplants should possess good stability in water, excellent deformability to fit the contour of gums, as well as strong adhesiveness to both transducers and tissues to maintain functional coupling [125]. Nevertheless, commercially available couplants, such as Aquaflex (AF), are designed for external use and cannot fulfill these requirements. Hence, it is essential to develop a multifunctional biomaterial with the aforementioned properties for intraoral ultrasound imaging.

Due to the excellent biocompatibility and low cost, numerous poly(vinyl alcohol) (PVA)-based hydrogels have been widely utilized in biomedical applications [31, 126-130]. However, most PVA-based hydrogels could be easily ruptured and lose their functionalities when subjected to repeated compression or stretching [131, 132]. Hence, different PVA-based double-network (DN) hydrogels with improved mechanical properties have been extensively explored in different fields [133-135]. Among these, PVA/PAM (Poly(vinyl alcohol)/polyacrylamide) DN hydrogels

have been broadly studied in numerous biomedical applications [136-138]. The unique structure not only helps to maintain excellent stability in water but also allows mechanical energy to be dissipated for improved mechanical properties [139]. However, no attempt has been made to endow the PVA/PAM DN hydrogel with strong adhesive property, which limits their application in intraoral ultrasound imaging. Inspired by mussel adhesion mechanism, incorporating polydopamine (PDA) into the hydrogel network could achieve strong reversible adhesiveness to different substrates, which could ensure the functional coupling of tissue/couplant/transducer for stable ultrasound transmission [60-62, 74, 140-143].

Herein, we report a mussel-inspired PVA-PAM-PDA DN hydrogel as the potential couplant for intraoral ultrasound imaging. A series of hydrogels were synthesized with different PAM/PVA ratios and PDA content. A systematic comparison of physical, mechanical, adhesive, and ultrasound properties was conducted between PVA-PAM-PDA hydrogels and the commercial AF gel pad. The PVA-PAM-PDA hydrogel displays better stability in water, superior mechanical properties, and improved adhesive properties than AF. Besides, the PVA-PAM-PDA hydrogel has been successfully applied as the ultrasound couplant to image porcine mandibular incisor, which produces ultrasound images with the same quality as AF does. This work provides new insights into the development of novel hydrogel-based interfaces between human tissues and medical devices for health monitoring and disease diagnosis applications.

4.3. Materials and Methods

4.3.1. Materials

Acrylamide (AM, 99%), poly (vinyl alcohol) (PVA, Mw 89,000-98,000, 99+% hydrolyzed), ammonium persulfate (APS, 98%), N, N'-Methylenebisacrylamide (MBAA, 99.5%), N, N, N', N'-

Tetramethyl-ethylenediamine (TEMED, 99%), and dopamine hydrochloride (DA) were purchased from Sigma-Aldrich and used without further purification. All other reagents and solvents were used as received. Aquaflex ultrasound gel pad (AF) and Parker Aquasonic 100 ultrasound gel were purchased from Parker Laboratories Inc (USA).

4.3.2. Hydrogel preparation

PVA-PAM-PDA hydrogels were synthesized by the following procedures [40, 42, 43, 45, 144-146]. In brief, PVA was dissolved in 40 mL distilled water at 90 °C for half an hour. Then, DA was added to the PVA solution where pH was adjusted to 8 with 0.01M NaOH. The mixture was stirred for half an hour to induce the self-polymerization of DA. Next, AM, APS, MBAA, and TEMED were added into the mixture in an ice bath. After stirring for another half-hour, the mixture was transported into a glass petri dish and heated in an oven for 4 hours at 70 °C. Then it was subject to 12 hours of freezing at -10 °C, followed by 6 hours of thawing for two cycles. PVA-PAM hydrogels were also fabricated via the same procedure without the presence of DA. The detailed compositions of the hydrogels are listed in **Table 4.1**.

Hydrogels	AM (g)	PVA (g)	PAM/PVA Ratio	DA (g)	APS (g)	MBAA (g)	TEMED (μ L)	H ₂ O (mL)
Hd-0.5	2	4	0.5		0.200	0.012	16	
Hd-1	3	3	1	0.024	0.300	0.018	24	40
Hd-2	4	2	2		0.400	0.024	32	
H-0.5	2	4	0.5		0.020	0.012	16	
H-1	3	3	1	0	0.030	0.018	24	40
H-2	4	2	2		0.040	0.024	32	

Table 4.1 The compositions of the PVA-PAM-PDA (Hd) hydrogels and PVA-PAM (H) hydrogels (Hydrogels are denoted by their PAM/PVA ratios).

4.3.3. Characterization

Fourier transform infrared (FTIR) spectra of Hd-2, H-2, PVA, AM (acrylamide), and DA (dopamine hydrochloride) were measured with Nicolet iS50 FT-IR Spectrometer (ATR mode). In each case, the spectra measurement was performed between the wavenumber of 500 - 4000 cm^{-1} with the scan number of 32 and the resolution of 4 cm^{-1} . The microstructures of Hd-2 and H-2 were characterized by the field emission scanning electron microscopy (FESEM, Zeiss Sigma 300 vp). Samples were sectioned from hydrogels, lyophilized, and coated with a thin layer of gold. The water percentages of all the as-prepared hydrogels and AF were determined with their initial weights and their lyophilized weights. Their densities were measured by calculating their mass/volume ratios.

4.3.4. Swelling test

The swelling tests were conducted to characterize the equilibrium swelling ratio (ESR) of the as-prepared PVA-PAM-PDA and PVA-PAM hydrogels as well as AF. Briefly, the lyophilized samples were immersed into deionized water in sealed vials at room temperature. When reaching the pre-set time interval, samples were taken out from the vials and the superficial water was removed with a filter paper. Then, the samples were weighed. ESR was calculated by **equation 26**:

$$ESR = (W_t - W_{dry}) / W_{dry} \times 100\% \quad (26)$$

where W_{dry} and W_t were the lyophilized weight and the weight after swelling pre-set times, respectively.

4.3.5. Mechanical tests

The tensile strength of samples was measured by an AGS-X universal tensile test machine (Shimadzu, Japan) with a loading cell of 50 N [147]. Samples were cut into a cuboid of 60 mm × 5 mm × 4 mm. Each test was conducted with a crosshead speed of 10 mm/min. The strain was calculated by the extended gauge length divided by the original gauge length while the tensile stress was calculated by the applied force divided by the initial cross-section area [64]. Besides, the toughness (U) of PVA-PAM-PDA hydrogels was determined by the area under the tensile stress-strain curve (**equation 27**):

$$U = \int_0^{\varepsilon_f} S d\varepsilon_t \quad (27)$$

where ε_t is the tensile strain, ε_f is the tensile strain upon failure, and S is the tensile stress. Young's modulus was assessed from their tensile stress/strain ratios in the linear region. Moreover, the loading-unloading cyclic tensile tests were performed to Hd-2, H-2, and AF with their maximum strains as 300%, 300%, and 150% respectively.

Besides, the compressive tests were conducted with the same AGS-X universal test machine under the compression mode with a crosshead speed of 5 mm/min. The cylinder shape samples were prepared in vials with a diameter of 22.8 mm and a height of 11 mm. 5 cycles of loading-unloading compressive tests were conducted to each sample at the maximum strain of 70% to evaluate their recoverability after compression [42]. Each consequent cycle was conducted after a recovery period of 2 min. The compression strain (ε_c) was calculated as the deformed height (h)

divided by the initial height (h_0) of the samples (**equation 28**) while the compression stress (σ) was obtained with the compression load (F_c) divided by the initial cross-section area (A_0) of the samples (**equation 29**):

$$\varepsilon_c = h / h_0 \quad (28)$$

$$\sigma = F_c / A_0 \quad (29)$$

The maximum compression strength was defined as the stress when the compression strain reached 70%.

To further evaluate their mechanical properties, the dynamic rheology test of the samples was performed on an AR-G2 stress-controlled rheometer (TA Instruments) with a 20 mm diameter parallel-plate configuration and 50 μm gap at 25 °C [33, 66, 81, 148-153]. Dynamic frequency sweeps were performed at 1.0% strain amplitude with angular velocities ranging from 0.1 to 100 rad/s. Strain amplitude sweeps were performed at an angular frequency of 10 rad/s with the strain from 0.01% to 1000% to determine the linear viscoelasticity region.

4.3.6. Adhesion test

Following the tensile adhesion test methods, the AGS-X universal test machine was used to measure the adhesion strength of samples [42, 154-156]. The samples were placed on the surface of substrates with a bonding area of 10 mm \times 10 mm. Substrates were compressed together with a force of 20 N for 30 s and pulled to failure with a crosshead speed of 5 mm/min. The adhesion strength was calculated by the maximum force upon detachment normalized by the initial bonding area. Stainless steel, glass, and porcine skin were chosen as substrates, mimicking the adhesion to

the metal transducer, teeth, and soft tissues. The repeating adhesion of Hd-2 was measured by repeating the adhesion–strip process for 15 times.

4.3.7. Ultrasound characterization

Ultrasound characterization of the as-prepared hydrogels was performed by the immersion transmission-through technique with AF as the reference [10, 67, 125]. The experimental setup consisted of a piece of hydrogel mounted on a gel pad holder placed between the two coaxially mounted transducers. The transducers used were a pair of 6.35-mm-diameter 20-MHz unfocused transducers (Olympus V317-N-SU, Waltham, MA), separated by 20 cm with the samples placed at 14 cm away from the emitter, a bit farther than the near field distance. Care was taken to ensure the ultrasound beam was perpendicular to the surface of the samples. Five measurements were taken for each sample at five different regions of interest (ROI), shifted 5 mm apart from each other in a direction perpendicular to the beam. A pulse-receiver (Olympus 5800, Panametrics, Waltham, MA) excited the emitter and the transmitted signal was recorded by an oscilloscope (LeCroy WaveSuffer 422, LeCroy, Chestnut Ridge, NY). The recorded signals were averaged over 256 times to increase the signal-to-noise ratio.

A reference signal (water pulse) without the sample in the beam path and a sample pulse were measured. The velocity of ultrasound in the hydrogels can be determined by the group velocity (V , **equation 30**) in the time domain or the phase velocity ($c(\omega)$, **equation 31**) in the frequency domain[9, 10]:

$$V = h(h/V_{water} - \Delta t)^{-1} \quad (30)$$

$$c(\omega) = \omega h(\omega h/V_{water} - \Delta \varphi)^{-1} \quad (31)$$

where Δt is the delay time between the arrival times of the envelope peaks of the signals, h is the sample thickness, V_{water} , is 1480 m/s as measured from the water pulse, ω is the angular frequency, and $\Delta\varphi$ is the unwrapped phase difference between the water and sample spectra. Finally, the slope of the linear least-squares regression line fitted to the phase velocity versus frequency data determines the dispersion normally within the frequency range bounded between ± 6 dB.

The attenuation coefficient, α (in dB/cm) dictates the collective energy loss due to scattering, absorption, and transmission, as per **equation 32**,

$$\alpha(\omega) = 20h^{-1} \log_{10} \left[A_{ref}(\omega) / A_{sample}(\omega) \right] \quad (32)$$

where $A_{ref}(\omega)$ and $A_{sample}(\omega)$ are the amplitude spectra of the water and sample signals. The transmission loss caused by the water-hydrogel interfaces was not considered. The normalized broadband ultrasound attenuation (nBUA) in dB/MHz/cm is obtained by normalizing α by the relevant frequency band.

4.3.8. Ultrasound imaging

A porcine center incisor was scanned using a SonixTablet portable medical ultrasonic phased array system (Analogic, Vancouver, Canada) operating at 20 MHz with a frame rate of 29 Hz [2, 125]. The transducer was placed on the tooth and gingiva on the labial side with the transducer's long axis aligned with the long axis of the tooth. A piece of about 5-mm thick gel pad (H-2, Hd-2, or AF) was used as couplants between the transducer and the dental tissues with ultrasound gel (Parker Aquasonic 100, Parker Laboratories Inc., USA) to fill in any void between the transducer, gel pad, and the porcine tissues, ensuring the good transmission of ultrasound energy through the gap to the target.

4.4. Results and Discussion

4.4.1. Fabrication and characterization of the PVA-PAM-PDA hydrogels

The fabrication of the PVA-PAM-PDA hydrogels was achieved by incorporating PDA into the PVA-PAM double-networks, as presented in **Figure 4.1**. First, the PVA-PDA complex can be formed through the noncovalent interactions (e.g. hydrogen bonding) between PDA and PVA during the self-polymerization of DA. After the polymerization of AM in the PVA-PDA mixture, the 1st chemically crosslinked PAM network was formed. The obtained hydrogels were subjected to two cycles of the freeze-thaw process to induce the crystallization of PVA, forming the 2nd physically crosslinked PVA network and the final PVA-PAM-PDA hydrogels (**Figure S4.1**).

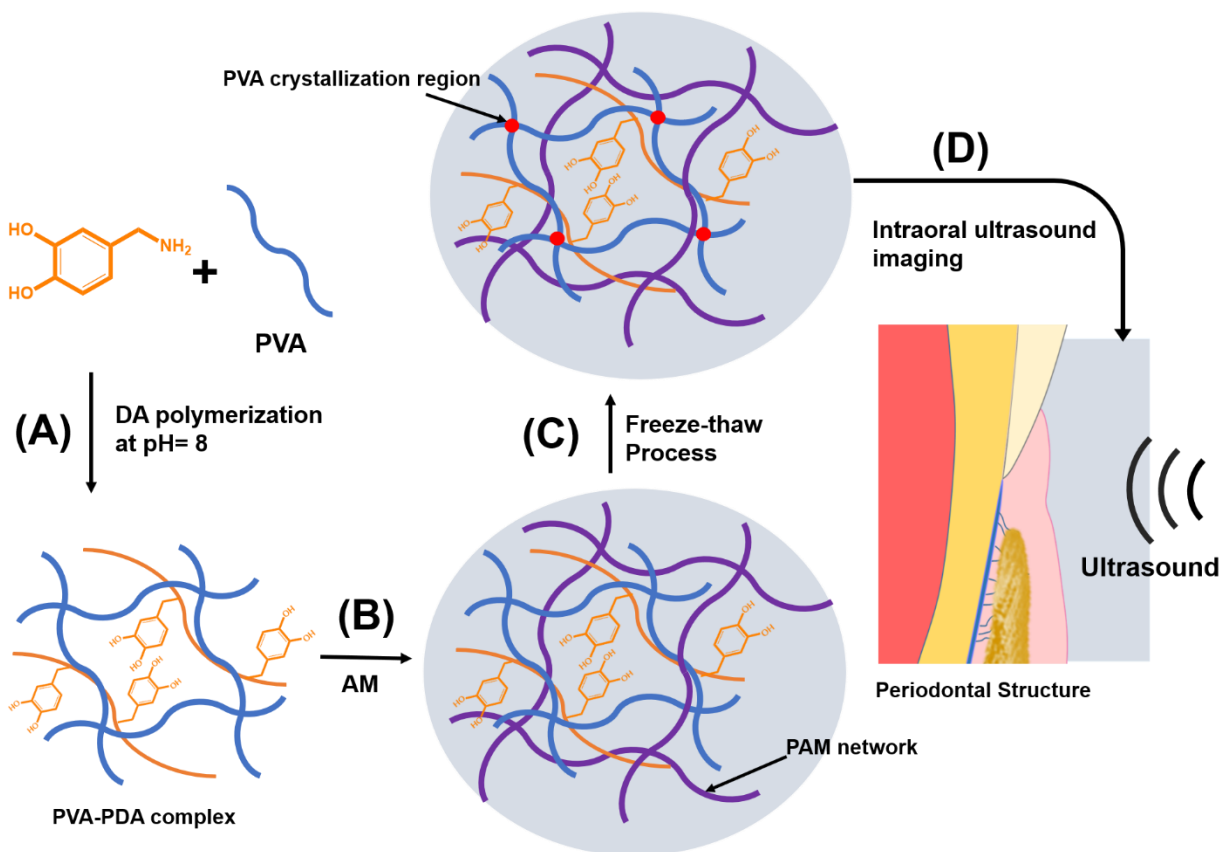


Figure 4.1 Schematic illustration of the fabrication of PVA-PAM-PDA hydrogels. (A) The formation of the PVA-PDA complex. (B) The formation of 1st chemically crosslinked PAM network in the PVA-PDA mixture. (C) The formation of 2nd physically crosslinked PVA network. (D) The PVA-PAM-PDA hydrogel was applied as the couplant for intraoral ultrasound imaging.

Figure 4.2A presents the FTIR spectra of DA, Hd-2, H-2, PVA, and AM. The weak absorption peak at 2930 cm^{-1} and the strong absorption peak at 1074 cm^{-1} in Hd-2, H-2, and PVA were ascribed to the intramolecular bonded O-H stretching and the C-O stretching respectively, indicating the presence of PVA in Hd-2 and H-2. Besides, the absorption peaks at 1667 cm^{-1} and 1605 cm^{-1} corresponding to the C=O stretching, appeared in the spectra of Hd-2, H-2, and AM, suggesting the existence of AM in Hd-2 and H-2. However, the weak absorption peak at 2820 cm^{-1} resulted from the C-H stretching of the alkene groups in AM and disappeared in the spectra of Hd-2 and H-2, implying the polymerization of acrylamide in Hd-2 and H-2. Due to the low content of DA, there is no clear difference between the absorption peaks of Hd-2 and H-2. The morphology of Hd-2 and H-2 was characterized by scanning electron microscope (SEM) after lyophilization and presented in **Figure 4.2B** and **4.2C**. The pores of H-2 distribute relatively uniformly while the pores of Hd-2 are heterogeneously scattered with sizes from 2-20 μm , indicating the interweaved three-dimensional structures of Hd-2 due to the incorporation of PDA [157].

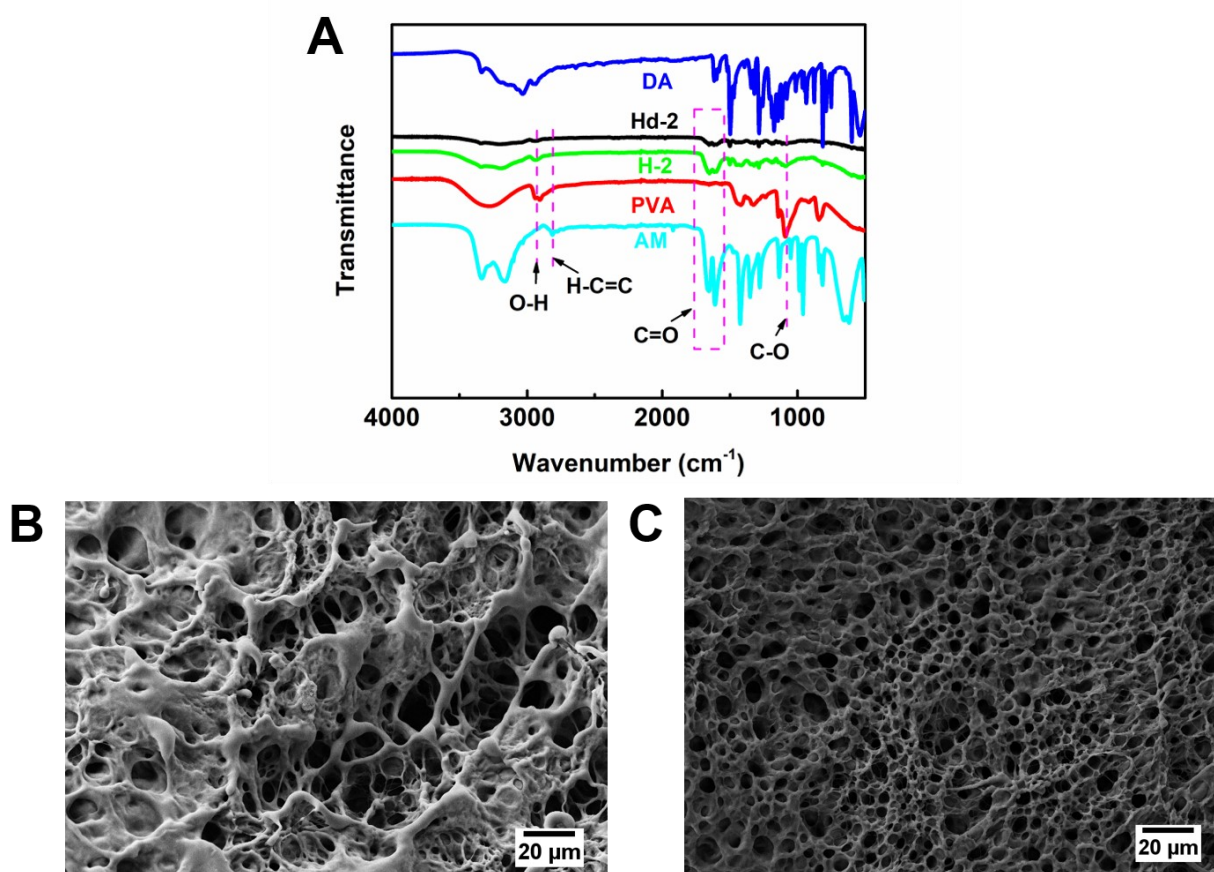


Figure 4.2 (A) The FTIR spectra of DA (dopamine hydrochloride), Hd-2, H-2, PVA, and AM (acrylamide). (B) The SEM image of Hd-2 (PVA-PAM-PDA hydrogel). (C) The SEM image of H-2 (PVA-PAM hydrogel).

The density, water percentage, and stability in water of the couplants may impact their ultrasound imaging performance [1, 124]. Therefore, the effect of the PAM/PVA ratio and the PDA content on the density, water percentage, and stability in water of the as-prepared hydrogels was studied. The densities of all as-prepared hydrogels were almost the same (**Figure S4.2A**). Besides, as shown in **Figure 4.3A**, for both PVA-PAM-PDA hydrogels and PVA-PAM hydrogels, their water percentages almost remained the same at around 84%. In contrast, the water percentage

of AF was 96.4%, much higher than that of the as-prepared hydrogels. Moreover, the equilibrium swelling ratios (*ESR*) of both PVA-PAM-PDA hydrogels and PVA-PAM hydrogels increased with the increasing PAM/PVA ratio (**Figure 4.3B** and **S4.2B**), which could result from the increase of amide groups at higher PAM/PVA ratio that could enhance the hydration capacity of the hydrogels and lead to the increase of *ESR*. However, the *ESR* of AF could not be precisely measured as AF fully dissolved in water (**Figure S4.3**). In comparison, both PVA-PAM-PDA and PVA-PAM hydrogels could retain original shapes after immersing in water for 24 hours (**Figure S4.3**), which suggests PVA-PAM-PDA hydrogels possess better stability in water for intraoral ultrasound imaging.

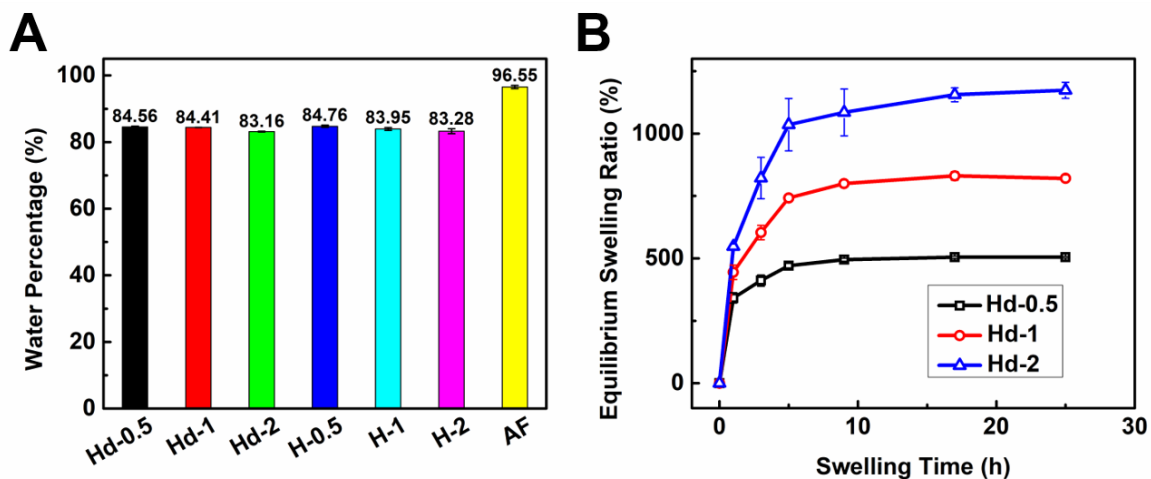


Figure 4.3 (A) The water percentage of the PVA-PAM-PDA hydrogels, PVA-PAM hydrogels, and AF. (B) The equilibrium swelling ratio of PVA-PAM-PDA hydrogels at different time intervals.

4.4.2. Mechanical Properties

Compared with AF, both PVA-PAM-PDA hydrogels and PVA-PAM hydrogels possess better stretchability (**Figure 4.4A** and **S4.4A**). As PAM/PVA ratio increased, the stretchability of both

PVA-PAM hydrogels and PVA-PAM-PDA hydrogels increased, which is due to the higher stretch limit of the PAM network [40]. Moreover, the increase of PAM/PVA ratio also led to an increase in the toughness of both PVA-PAM-PDA hydrogels and PVA-PAM hydrogels while resulted in the decrease in Young's modulus (**Figure 4.4B** and **S4.4B**). The increase of toughness could be ascribed to the enhanced energy dissipation through the rupture of more hydrogen bonds within the PVA/PAM network with the higher PAM/PVA ratio. The decrease in Young's modulus is attributed to the increasing amount of soft and ductile component in the system (i.e. PAM). Besides, the fatigue resistance properties of Hd-2, H-2, and AF were evaluated via five successive loading-unloading tensile tests. Both Hd-2 and H-2 exhibited superior recovery after stretching with almost no strength loss (**Figure 4.4C**, **S4.4C**, and **S4.5**). In comparison, the maximum strengths of AF at the strain of 150% were gradually compromised after each cycle (**Figure 4.4D**), suggesting the poor recovery of AF after stretching.

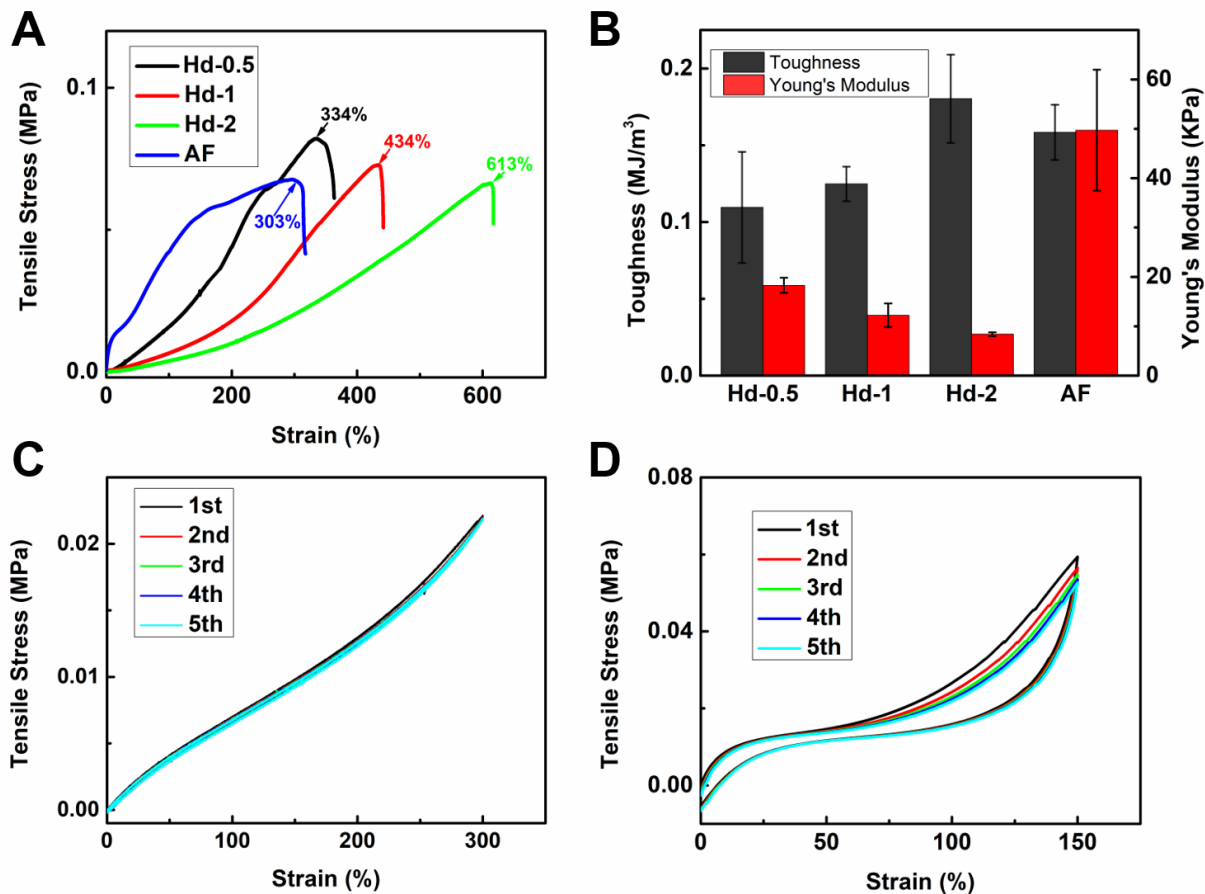


Figure 4.4 (A) The stress-strain curves of the PVA-PAM-PDA hydrogels and AF. (B) The toughness and Young's modulus of the PVA-PAM-PDA hydrogels and AF. Successive loading-unloading tensile test cycles of (C) Hd-2 and (D) AF.

Compression measurements with 5 loading-unloading cycles were also conducted to evaluate the compression-recover properties of AF and the PVA-PAM-PDA hydrogels. As shown in **Figure 4.5A**, AF could not recover to the initial state after the first cycle of compression. The maximum compression strength of AF successively decreased after each cycle (**Figure 4.5B**). In comparison, Hd-2 could fully recover after being compressed to the same strain of 70%. Besides, the maximum compression strength of the first cycle for the PVA-PAM-PDA hydrogels decreased from 441 KPa

to 42.8 KPa (**Figure 4.5C-E**) as the PAM/PVA ratio increased from 0.5 to 2, which suggests decreasing the stiffness of the hydrogel could lower the compression resistance of the PAM-PVA-PDA hydrogels as well as reduce their maximum compression strength. Similar results were also found in PAM-PVA hydrogels (**Figure S4.6**).

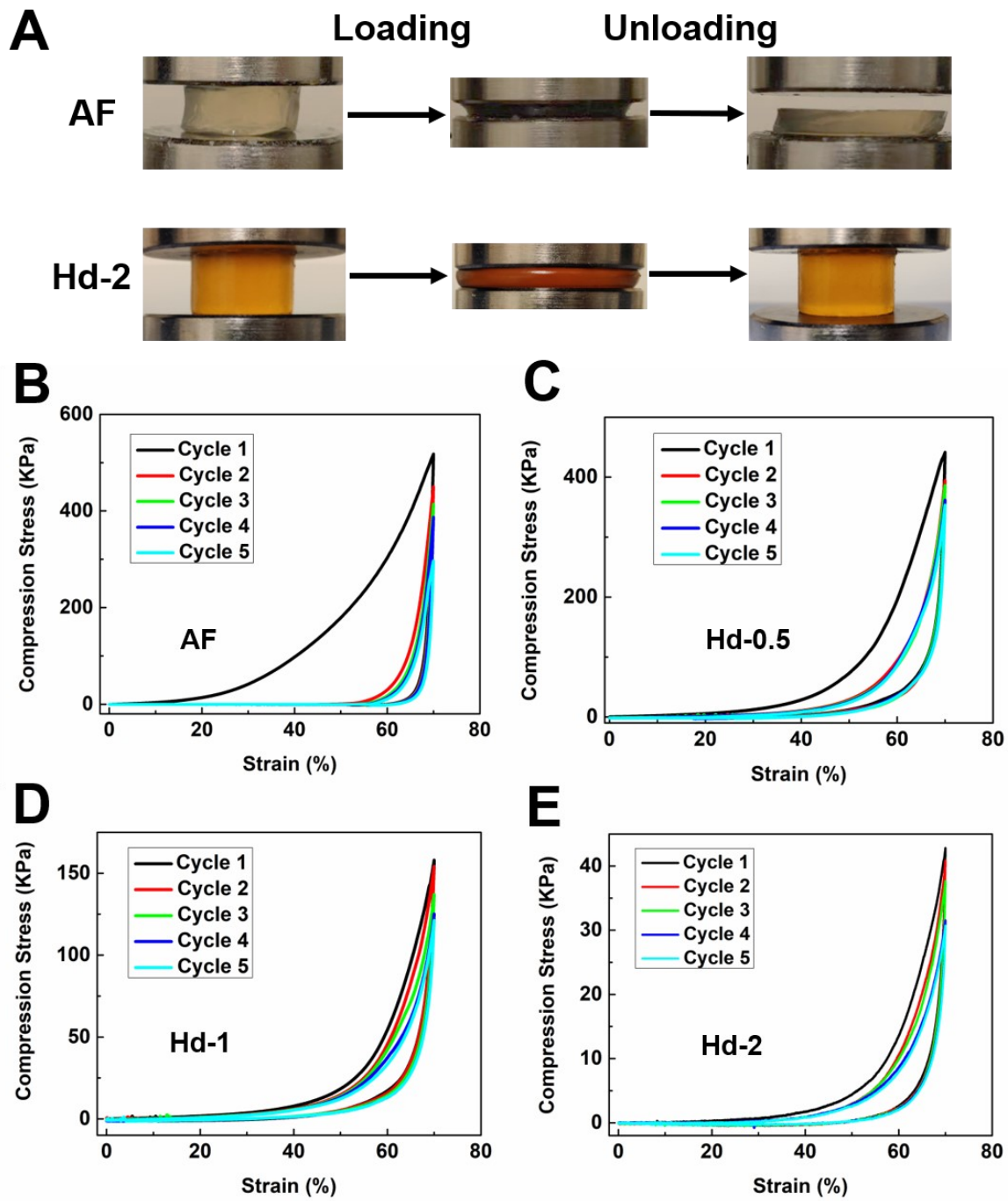


Figure 4.5 (A) Images of AF (upper) and Hd-2 (lower) undergoing compression testing to 70% strain. Cyclic loading-unloading curves: (B) AF. (C) Hd-0.5. (D) Hd-1. (E) Hd-2.

The mechanical properties of the PVA-PAM-PDA hydrogels and AF were further investigated using a rheometer [158]. In frequency sweeps, both PVA-PAM-PDA hydrogels and AF displayed dominant elastic solid behavior with the storage modulus (G') higher than the loss modulus (G'') over the entire angular frequency range (**Figure S4.7A** and **S4.7B**). In the PVA-PAM-PDA hydrogels, the increase of the PAM/PVA ratio led to the decrease of their viscoelastic modulus, suggesting the decrease of the stiffness of the hydrogels, which is consistent with Young's modulus results from the tensile tests. Besides, the strain sweep tests showed the linear viscoelastic region of the hydrogels and measured the critical strain for hydrogel failure (**Figure S4.7C** and **S4.7D**). Their strain sweeps present that each curve of storage modulus showed a constant region followed by a subsequent decrease while PVA-PAM-PDA hydrogels possessed high critical strains. As the PAM/PVA ratio increased, the critical strains of PVA-PAM-PDA hydrogels were elevated, which is consistent with the elongation results from the tensile tests.

Summarized from the mechanical tests, the increase of the PAM/PVA ratio enhances the stretchability and the toughness of PVA-PAM-PDA hydrogels and PVA-PAM hydrogels while reducing their maximum compression strength. Overall, the PVA-PAM-PDA hydrogel exhibits better stretchability and superior reversible recovery from deformation than AF, which could fulfill the requirements for intraoral ultrasound imaging.

4.4.3. Adhesion ability

Hd-2 exhibited strong adhesiveness to different substrates, as shown by its firm adhesion to the glass petri dish, skin tissues, metal, and bending arms (**Figure 4.6A**). The adhesion properties of the PVA-PAM-PDA hydrogels, PVA-PAM hydrogels, and AF were quantitatively measured by the tensile adhesion test methods (**Figure 4.6B**). It is noted that Hd-2 possesses much stronger

adhesion to all three substrates than the other hydrogels (**Figure 4.6C**). The strong adhesion of Hd-2 results from the synergy of two effects: 1) the strong interfacial bonds formed between the catechol groups and different substrates through various intermolecular interactions (e.g. hydrogen bonding, metal coordination, π - π stacking, etc.) [159-162]; 2) the relatively tough hydrogel matrix can dissipate energy effectively when the interface is stressed [163-165]. It is also noted that the adhesion of Hd-2 to porcine skin was much higher than its adhesion to glass and metal, which is ascribed to the increased number of hydrogen bonds formed between the catechol groups in Hd-2 and amide groups and carbonyl groups of porcine skin [45].

Apart from the relatively higher adhesion, Hd-2 presented repeatable adhesion to glass, metal, and porcine skin, mimicking the adhesion to teeth, the metal transducer, and oral tissues, which was illustrated with the adhesion–strip test over 15 cycles. There was almost no loss in its adhesion strengths to all three substrates (glass, metal, and porcine skin), and its adhesion strengths to their surfaces were respectively maintained at approximately 3.5 KPa, 2.6 KPa, and 10.5 KPa over the 15 cycles (**Figure 4.6D**). The combination of the relatively outstanding strength and repeatability of adhesiveness makes Hd-2 possess strong affinities to oral tissues, transducers, and teeth to maintain functional coupling for intraoral ultrasound imaging.

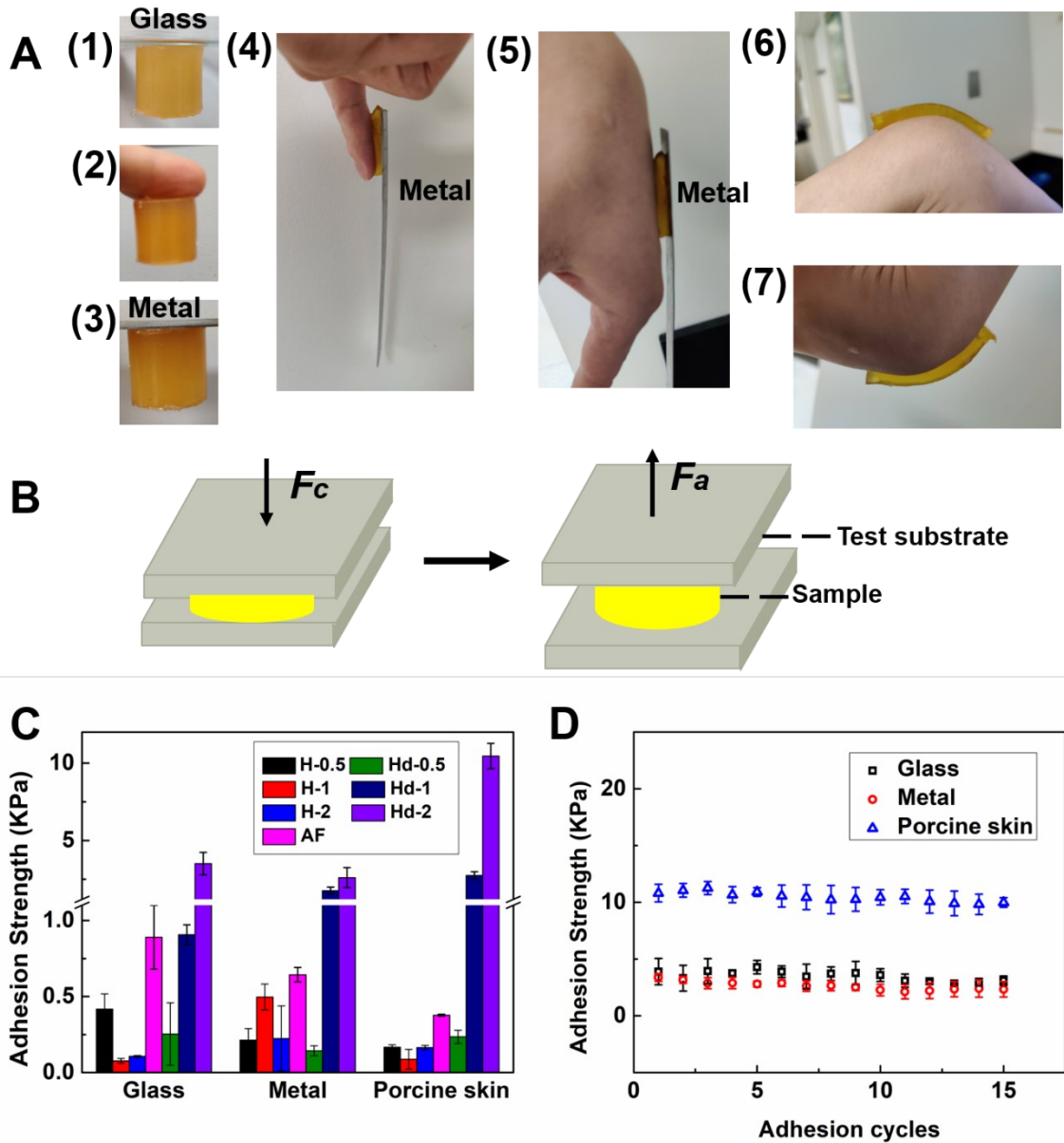


Figure 4.6 (A) The photos of Hd-2 adhered to different substrates: (1) glass, (2) skin, (3) metal, (4) finger and metal at two sides, (5) the back of hand and metal at two sides, (6) bending arm upward, and (7) bending arm downward. (B) Schematic illustration of the tensile adhesion test process (Left: attachment, F_c , Compression force; Right: detachment, F_a , Adhesion force). (C) The adhesion strength of samples to glass, metal, and porcine skin. (D) Repeatable adhesion

behavior of Hd-2 (PVA-PAM-PDA hydrogel) to different substrates (glass, metal, and porcine skin).

4.4.4. Ultrasound properties

The ultrasonic properties of the samples were measured by the transmission-through experiment (**Figure 4.7A**). **Figure 4.7B** presents the typical responses of reference (water) and sample pulses. The sample pulse arrived earlier than the reference pulse since all the velocities of the hydrogels and AF are higher than water velocity, which is 1480 m/s. The average phase velocities and standard deviations of the PVA-PAM hydrogels (1541 ± 5 m/s) and PVA-PAM-PDA hydrogels (1547 ± 5 m/s) are almost the same (**Figure 4.7C**, **S4.8A**, and **Table S4.1**). In comparison, AF has a velocity of 1592 m/s, about 3% faster than the average velocity of the hydrogels. The ultrasonic phase velocities of the hydrogels and AF are independent of the frequency from 11.7 to 24.4 MHz, within the ± 6 dB frequency range (**Figure 4.7C** and **S4.8A**) while the ultrasound attenuation varies nonlinearly with frequency (**Figure 4.7D** and **S4.8B**). **Table S4.1** shows that at 19.5 MHz, the average attenuation of the PVA-PAM hydrogels is 3.34 dB/cm, smaller than that of the PVA-PAM-PDA hydrogels (4.04 dB/cm) but higher than that of AF (2.86 dB/cm). The increase in PAM/PVA ratio enhances the attenuation, e.g., from 3.05 dB/cm to 3.52 dB/cm and from 3.71 dB/cm to 4.31 dB/cm for the PVA-PAM hydrogels and PVA-PAM-PDA hydrogels, respectively. The mean nBUA values of the PVA-PAM hydrogels and PVA-PAM-PDA hydrogels are 0.30 dB/cm·MHz and 0.34 dB/cm·MHz respectively, higher than that of AF (0.22 dB/cm·MHz).

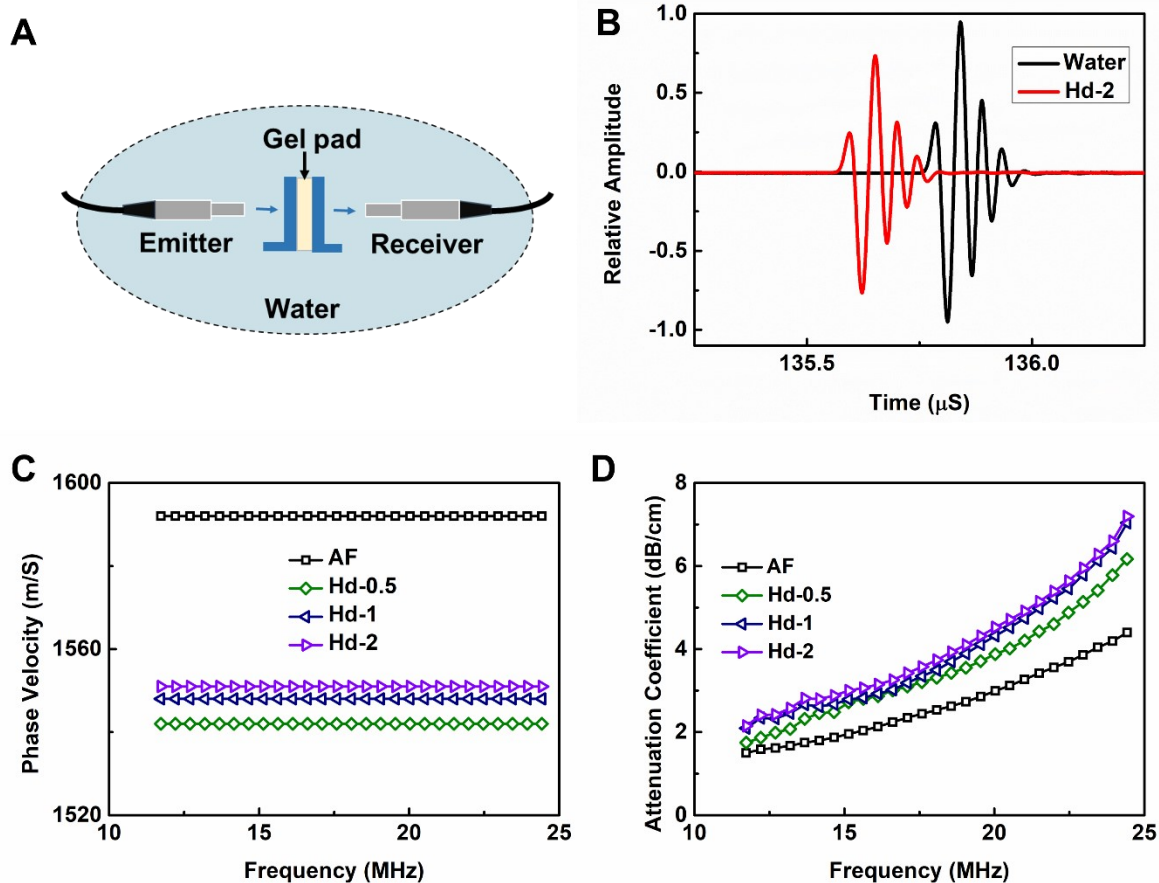


Figure 4.7 Ultrasound characterization of the potential couplants. (A) The transmission-through experimental setup. (B) The reference pulse (Black, water) and sample pulse (Red, Hd-2). (C) The phase velocities versus frequency. (D) The attenuation coefficient versus frequency.

4.4.5. Ultrasound imaging

Ultrasound scanning of a porcine incisor was schematically illustrated in **Figure 4.8A** with the recorded images using AF (**Figure 4.8B**), H-2 (**Figure 4.8C**), and Hd-2 (**Figure 4.8D**) respectively. The enamel, gingiva, alveolar bone, and cementum-enamel junction can be seen from the images. Even though the attenuation coefficients of the H-2 and Hd-2 hydrogels are much higher than the AF. However, both H-2 and Hd-2 hydrogels provide good and sharp ultrasound

images with clear tissue boundaries. The reflection coefficient or the strength of the echoes is affected by the impedance contrast of the interfaces. The H-2 and Hd-2 hydrogels have the acoustic impedance (product of density and velocity) values of 1.62×10^6 rayls and 1.61×10^6 rayls, respectively, very close to the acoustic impedance of AF (1.64×10^6 rayls). While both types of hydrogel provide similar ultrasound characteristics and image quality, Hd-2 is preferable as it has a much better adhesive property, which will prevent slipping during ultrasound imaging.

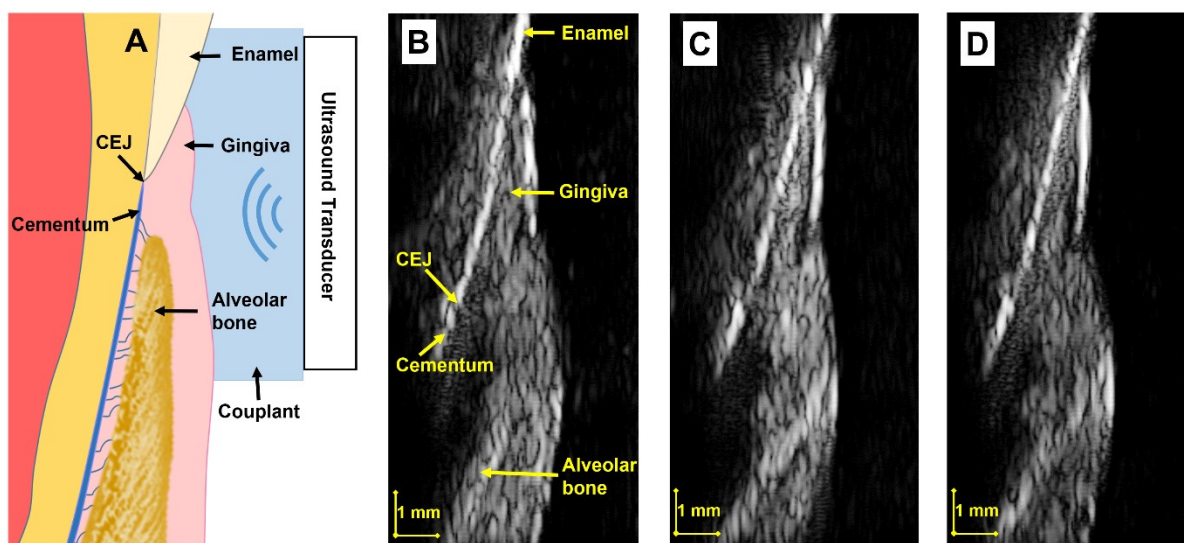


Figure 4.8 Ultrasound scan of a porcine incisor: (A) A schematic illustration of the ultrasound scan of the tooth-periodontium structure where the couplant sits between the transducer and the tissues. (B) The ultrasound image with AF as the couplant. (C) The ultrasound image with H-2 as the couplant. (D) The ultrasound image with Hd-2 as the couplant.

4.5. Conclusions

The mussel-inspired PVA-PAM-PDA hydrogels were fabricated and explored as potential couplants for intraoral ultrasound imaging. Comprehensive characterization and comparison of

their physical, mechanical, adhesive, and ultrasound properties were conducted between PVA-PAM-PDA DN hydrogels and the commercial AF. The increase of the PAM/PVA ratio enhances their stretchability and toughness while the incorporation of PDA into the hydrogel network could further facilitate their adhesiveness to various substrates. The as-prepared PVA-PAM-PDA hydrogel possesses better stability in water, superior mechanical property, and repeatable strong adhesiveness than commercially available couplants (such as AF). Moreover, when applied as couplants to image porcine incisor, the as-prepared hydrogel produces a similar quality of ultrasound images as AF does. Considering all these features, the PVA-PAM-PDA hydrogels could serve as an excellent couplant candidate for intraoral ultrasound imaging. This work provides novel insights into the development of multifunctional hydrogel-based interfaces between human tissues and medical devices for health monitoring and disease diagnosis applications.

5. Conclusions and Future Work

5.2. Major Conclusions and Contributions

In this thesis work, two types of double-network hydrogels are explored as the potential couplants for intraoral ultrasound imaging via a systematic comparison of the above-mentioned properties to commercially available gel pad (AF). It expands the application of these two DN hydrogels to intraoral ultrasound imaging and provides insights into the development of multifunctional hydrogel-based interfaces between human and medical devices for health monitoring and disease diagnosis applications. The major conclusions and original contributions are listed in the following:

(1) PAM/Alginate DN hydrogels were prepared and explored for the intraoral ultrasound imaging. When used as couplants for porcine incisor imaging, the PAM/Alginate hydrogels display as good ultrasound image quality as AF. Besides, compared to AF, the as-developed hydrogels have better stability in water, superior mechanical properties, and higher coefficients of friction. Additionally, the as-developed hydrogels show better biocompatibility to both cancer cells (Hela) and fibroblast cells (MRC-5) than AF. With these features, PAM/Alginate hydrogels could act as ideal candidates for couplants.

(2) PVA-PAM-PDA DN hydrogels were fabricated and explored as potential couplants for intraoral ultrasound imaging. A comprehensive comparison of the physical, mechanical, adhesive, and ultrasound properties was conducted between PVA-PAM-PDA hydrogels and commercial AF. The as-prepared PVA-PAM-PDA hydrogel possesses better stability in water, superior stretchability and excellent recovery from deformation, and strong and repeatable adhesion than commercially available couplant (such as AF). When applied as couplants to image porcine incisor,

the as-prepared hydrogel produced the same quality of ultrasound images as AF did. Considering all these features, PVA-PAM-PDA hydrogels could serve as an excellent couplant candidate for intraoral ultrasound imaging.

5.3. Future Work

In this study, we have explored the application of PAM/Alginate DN hydrogels and PVA-PAM-PDA DN hydrogels for intraoral ultrasound imaging by a comprehensive comparison of the properties to AF and pave the way for intraoral ultrasound imaging. However, there are still challenges regarding clinic applications, and some recommendations are presented.

- (1) Currently, these two hydrogels are fabricated in the lab scale. Further industrial process and fabrication methods need to be explored to manufacture these two hydrogels on a large scale for potential intraoral diagnosis applications.
- (2) The PAM/Alginate hydrogels have been explored as potential couplants via a variation of Alginate contents. Further researches on the effect of PAM content on the PAM/Alginate hydrogels could be investigated to find the PAM/Alginate hydrogel with better performance for intraoral ultrasound applications.
- (3) The as-prepared PVA-PAM-PDA hydrogel, with good stability in water, excellent mechanical properties, and enhanced adhesion, could act as the potential couplants for intraoral ultrasound imaging. However, the impact of PDA contents should also be further explored for the intraoral application of PVA-PAM-PDA hydrogels.

Bibliography

- [1] K.C.T. Nguyen, L.H. Le, N.R. Kaipatur, P.W. Major, Imaging the cemento-enamel junction using a 20-MHz ultrasonic transducer, *Ultrasound in medicine & biology* 42(1) (2016) 333-338.
- [2] K.C.T. Nguyen, L.H. Le, N.R. Kaipatur, R. Zheng, E.H. Lou, P.W. Major, High-resolution ultrasonic imaging of dento-periodontal tissues using a multi-element phased array system, *Annals of biomedical engineering* 44(10) (2016) 2874-2886.
- [3] D. Aiger, D. Cohen-Or, Real-time ultrasound imaging simulation, *Real-Time Imaging* 4(4) (1998) 263-274.
- [4] W.S. Chen, T.J. Matula, L.A. Crum, The disappearance of ultrasound contrast bubbles: observations of bubble dissolution and cavitation nucleation, *Ultrasound in medicine & biology* 28(6) (2002) 793-803.
- [5] H. Li, L.H. Le, M.D. Sacchi, E.H. Lou, Ultrasound imaging of long bone fractures and healing with the split-step Fourier imaging method, *Ultrasound in medicine & biology* 39(8) (2013) 1482-1490.
- [6] N. Bom, H. Ten Hoff, C. Lancee, W. Gussenhoven, J. Bosch, Early and recent intraluminal ultrasound devices, *Intravascular ultrasound*, Springer 1989, pp. 79-88.
- [7] T.L. Szabo, *Diagnostic ultrasound imaging: inside out*, Academic Press 2004.
- [8] K.K. Shung, Diagnostic ultrasound: Past, present, and future, *J Med Biol Eng* 31(6) (2011) 371-374.
- [9] L.H. Le, An investigation of pulse-timing techniques for broadband ultrasonic velocity determination in cancellous bone: a simulation study, *Physics in Medicine & Biology* 43(8) (1998) 2295-2308.
- [10] C. Zhang, L.H. Le, R. Zheng, D. Ta, E. Lou, Measurements of ultrasonic phase velocities and attenuation of slow waves in cellular aluminum foams as cancellous bone-mimicking phantoms, *The Journal of the Acoustical Society of America* 129(5) (2011) 3317-3326.
- [11] K.Y. Lee, D.J. Mooney, Hydrogels for tissue engineering, *Chemical reviews* 101(7) (2001) 1869-1880.
- [12] S.D. Bruck, Aspects of three types of hydrogels for biomedical applications, *Journal of biomedical materials research* 7(5) (1973) 387-404.
- [13] A. Singh, P.K. Sharma, V.K. Garg, G. Garg, Hydrogels: A review, *Int J Pharm Sci Rev Res* 4(2) (2010) 016.
- [14] E.M. Ahmed, Hydrogel: Preparation, characterization, and applications: A review, *Journal of advanced research* 6(2) (2015) 105-121.
- [15] A.K. Saxena, Synthetic biodegradable hydrogel (PleuraSeal) sealant for sealing of lung tissue after thoracoscopic resection, *The Journal of thoracic and cardiovascular surgery* 139(2) (2010) 496-497.

- [16] M.R. Guilherme, F.A. Aouada, A.R. Fajardo, A.F. Martins, A.T. Paulino, M.F. Davi, A.F. Rubira, E.C. Muniz, Superabsorbent hydrogels based on polysaccharides for application in agriculture as soil conditioner and nutrient carrier: A review, *European Polymer Journal* 72 (2015) 365-385.
- [17] X. Sun, G. Zhang, Q. Shi, B. Tang, Z. Wu, Preparation and characterization of water-swelling natural rubbers, *J Appl Polym Sci* 86 (2002) 3212-717.
- [18] K.N. Plunkett, J.S. Moore, Patterned Dual pH-Responsive Core– Shell Hydrogels with Controllable Swelling Kinetics and Volumes, *Langmuir* 20(16) (2004) 6535-6537.
- [19] S. Kaihara, S. Matsumura, J.P. Fisher, Synthesis and characterization of cyclic acetal based degradable hydrogels, *European Journal of Pharmaceutics and Biopharmaceutics* 68(1) (2008) 67-73.
- [20] D.F. Stamatialis, B.J. Papenburg, M. Girones, S. Saiful, S.N. Bettahalli, S. Schmitmeier, M. Wessling, Medical applications of membranes: drug delivery, artificial organs and tissue engineering, *Journal of Membrane Science* 308(1-2) (2008) 1-34.
- [21] E. Caló, V.V. Khutoryanskiy, Biomedical applications of hydrogels: A review of patents and commercial products, *European Polymer Journal* 65 (2015) 252-267.
- [22] D.L. Elbert, Liquid–liquid two-phase systems for the production of porous hydrogels and hydrogel microspheres for biomedical applications: a tutorial review, *Acta biomaterialia* 7(1) (2011) 31-56.
- [23] S. Van Vlierberghe, P. Dubruel, E. Schacht, Biopolymer-based hydrogels as scaffolds for tissue engineering applications: a review, *Biomacromolecules* 12(5) (2011) 1387-1408.
- [24] F. Onofri, Development of an extracellular matrix hydrogel for intestine tissue engineering, (2016).
- [25] M.W. Tibbitt, K.S. Anseth, Hydrogels as extracellular matrix mimics for 3D cell culture, *Biotechnology and bioengineering* 103(4) (2009) 655-663.
- [26] J.M. Saul, D.F. Williams, Hydrogels in regenerative medicine, *Handbook of Polymer Applications in Medicine and Medical Devices*, Elsevier 2011, pp. 279-302.
- [27] P. Sikareepaisan, U. Ruktanonchai, P. Supaphol, Preparation and characterization of asiaticoside-loaded alginate films and their potential for use as effectual wound dressings, *Carbohydrate Polymers* 83(4) (2011) 1457-1469.
- [28] M. Hamidi, A. Azadi, P. Rafiei, Hydrogel nanoparticles in drug delivery, *Advanced drug delivery reviews* 60(15) (2008) 1638-1649.
- [29] R. Ghadi, A. Jain, W. Khan, A. Domb, Microparticulate polymers and hydrogels for wound healing, *Wound Healing Biomaterials*, Elsevier 2016, pp. 203-225.
- [30] B.D. Ratner, A.S. Hoffman, Synthetic hydrogels for biomedical applications, *Hydrogels for medical and related applications* 31 (1976) 1-36.
- [31] W. Wang, R. Narain, H. Zeng, Rational design of self-healing tough hydrogels: a mini review, *Frontiers in Chemistry* 6 (2018) 497.

- [32] S. Naficy, H.R. Brown, J.M. Razal, G.M. Spinks, P.G. Whitten, Progress toward robust polymer hydrogels, *Australian Journal of Chemistry* 64(8) (2011) 1007-1025.
- [33] Y. Chen, W. Wang, D. Wu, M. Nagao, D.G. Hall, T. Thundat, R. Narain, Injectable self-healing zwitterionic hydrogels based on dynamic benzoxaborole–sugar interactions with tunable mechanical properties, *Biomacromolecules* 19(2) (2018) 596-605.
- [34] J.P. Gong, Y. Katsuyama, T. Kurokawa, Y. Osada, Double-network hydrogels with extremely high mechanical strength, *Advanced materials* 15(14) (2003) 1155-1158.
- [35] T. Nonoyama, J.P. Gong, Double-network hydrogel and its potential biomedical application: A review, *Proceedings of the Institution of Mechanical Engineers, Part H: Journal of Engineering in Medicine* 229(12) (2015) 853-863.
- [36] A.M. Costa, J.F. Mano, Extremely strong and tough hydrogels as prospective candidates for tissue repair—A review, *European Polymer Journal* 72 (2015) 344-364.
- [37] T. Sakai, T. Matsunaga, Y. Yamamoto, C. Ito, R. Yoshida, S. Suzuki, N. Sasaki, M. Shibayama, U.-i. Chung, Design and fabrication of a high-strength hydrogel with ideally homogeneous network structure from tetrahedron-like macromonomers, *Macromolecules* 41(14) (2008) 5379-5384.
- [38] J.Y. Sun, X. Zhao, W.R. Illeperuma, O. Chaudhuri, K.H. Oh, D.J. Mooney, J.J. Vlassak, Z. Suo, Highly stretchable and tough hydrogels, *Nature* 489(7414) (2012) 133-136.
- [39] J. Li, W.R. Illeperuma, Z. Suo, J.J. Vlassak, Hybrid hydrogels with extremely high stiffness and toughness, *ACS Macro Letters* 3(6) (2014) 520-523.
- [40] K. Ou, X. Dong, C. Qin, X. Ji, J. He, Properties and toughening mechanisms of PVA/PAM double-network hydrogels prepared by freeze-thawing and anneal-swelling, *Materials Science and Engineering: C* 77 (2017) 1017-1026.
- [41] K. Haraguchi, T. Takehisa, Nanocomposite hydrogels: A unique organic–inorganic network structure with extraordinary mechanical, optical, and swelling/de-swelling properties, *Advanced materials* 14(16) (2002) 1120-1124.
- [42] L. Han, X. Lu, K. Liu, K. Wang, L. Fang, L.T. Weng, H. Zhang, Y. Tang, F. Ren, C. Zhao, Mussel-inspired adhesive and tough hydrogel based on nanoclay confined dopamine polymerization, *ACS nano* 11(3) (2017) 2561-2574.
- [43] L. Han, X. Lu, M. Wang, D. Gan, W. Deng, K. Wang, L. Fang, K. Liu, C.W. Chan, Y. Tang, A mussel-inspired conductive, self-adhesive, and self-healable tough hydrogel as cell stimulators and implantable bioelectronics, *Small* 13(2) (2017) 1601916.
- [44] L. Han, J. Xu, X. Lu, D. Gan, Z. Wang, K. Wang, H. Zhang, H. Yuan, J. Weng, Biohybrid methacrylated gelatin/polyacrylamide hydrogels for cartilage repair, *Journal of Materials Chemistry B* 5(4) (2017) 731-741.
- [45] L. Han, L. Yan, K. Wang, L. Fang, H. Zhang, Y. Tang, Y. Ding, L.T. Weng, J. Xu, J. Weng, Tough, self-healable and tissue-adhesive hydrogel with tunable multifunctionality, *NPG Asia Materials* 9(4) (2017) e372.
- [46] C.W. Peak, J.J. Wilker, G. Schmidt, A review on tough and sticky hydrogels, *Colloid and Polymer Science* 291(9) (2013) 2031-2047.

- [47] A.E. Barkdoll, D.C. England, Contact lens having a hard center and soft, tough periphery, Google Patents, 1976.
- [48] R. Steckler, Disposable, hydrogel soft contact lenses, Google Patents, 1984.
- [49] A.E. Barkdoll, Soft, tough low refractive index contact lenses, Google Patents, 1976.
- [50] C. Azuma, K. Yasuda, Y. Tanabe, H. Taniguro, F. Kanaya, A. Nakayama, Y.M. Chen, J.P. Gong, Y. Osada, Biodegradation of high-toughness double network hydrogels as potential materials for artificial cartilage, *Journal of Biomedical Materials Research Part A: An Official Journal of The Society for Biomaterials, The Japanese Society for Biomaterials, and The Australian Society for Biomaterials and the Korean Society for Biomaterials* 81(2) (2007) 373-380.
- [51] K. Arakaki, N. Kitamura, H. Fujiki, T. Kurokawa, M. Iwamoto, M. Ueno, F. Kanaya, Y. Osada, J.P. Gong, K. Yasuda, Artificial cartilage made from a novel double-network hydrogel: In vivo effects on the normal cartilage and ex vivo evaluation of the friction property, *Journal of Biomedical Materials Research Part A: An Official Journal of The Society for Biomaterials, The Japanese Society for Biomaterials, and The Australian Society for Biomaterials and the Korean Society for Biomaterials* 93(3) (2010) 1160-1168.
- [52] J.A. Rowley, G. Madlambayan, D.J. Mooney, Alginate hydrogels as synthetic extracellular matrix materials, *Biomaterials* 20(1) (1999) 45-53.
- [53] W.H. Tan, S. Takeuchi, Monodisperse alginate hydrogel microbeads for cell encapsulation, *Advanced materials* 19(18) (2007) 2696-2701.
- [54] M.V. Risbud, R.R. Bhonde, Polyacrylamide-chitosan hydrogels: in vitro biocompatibility and sustained antibiotic release studies, *Drug Delivery* 7(2) (2000) 69-75.
- [55] M.C. Darnell, J.Y. Sun, M. Mehta, C. Johnson, P.R. Arany, Z. Suo, D.J. Mooney, Performance and biocompatibility of extremely tough alginate/polyacrylamide hydrogels, *Biomaterials* 34(33) (2013) 8042-8048.
- [56] B.I. Pavlyk, Biocompatible hydrogel, Google Patents, 1998.
- [57] M.I. Baker, S.P. Walsh, Z. Schwartz, B.D. Boyan, A review of polyvinyl alcohol and its uses in cartilage and orthopedic applications, *Journal of Biomedical Materials Research Part B: Applied Biomaterials* 100(5) (2012) 1451-1457.
- [58] M. Kita, Y. Ogura, Y. Honda, S.-H. Hyon, W.-I. Cha, Y. Ikada, Evaluation of polyvinyl alcohol hydrogel as a soft contact lens material, *Graefes archive for clinical and experimental ophthalmology* 228(6) (1990) 533-537.
- [59] J.D. Nelson, R.L. Farris, Sodium hyaluronate and polyvinyl alcohol artificial tear preparations: a comparison in patients with keratoconjunctivitis sicca, *Archives of ophthalmology* 106(4) (1988) 484-487.
- [60] L. Li, W. Smitthipong, H. Zeng, Mussel-inspired hydrogels for biomedical and environmental applications, *Polymer Chemistry* 6(3) (2015) 353-358.
- [61] L. Li, B. Yan, J. Yang, L. Chen, H. Zeng, Novel mussel-inspired injectable self-healing hydrogel with anti-biofouling property, *Advanced Materials* 27(7) (2015) 1294-1299.

- [62] L. Li, H. Zeng, Marine mussel adhesion and bio-inspired wet adhesives, *Biotribology* 5 (2016) 44-51.
- [63] Y. Tanaka, R. Kuwabara, Y.H. Na, T. Kurokawa, J.P. Gong, Y. Osada, Determination of fracture energy of high strength double network hydrogels, *The Journal of Physical Chemistry B* 109(23) (2005) 11559-11562.
- [64] J. Chen, Q. Peng, T. Thundat, H. Zeng, Stretchable, Injectable and Self-Healing Conductive Hydrogel Enabled by Multiple Hydrogen Bonding toward Wearable Electronics, *Chemistry of Materials* 31(12) (2019) 4553-4563.
- [65] J. Gong, M. Higa, Y. Iwasaki, Y. Katsuyama, Y. Osada, Friction of gels, *The Journal of Physical Chemistry B* 101(28) (1997) 5487-5489.
- [66] W. Wang, L. Xiang, L. Gong, W. Hu, W. Huang, Y. Chen, A.B. Asha, S. Srinivas, L. Chen, R. Narain, H. Zeng, Injectable, Self-Healing Hydrogel with Tunable Optical, Mechanical, and Antimicrobial Properties, *Chemistry of Materials* 31(7) (2019) 2366-2376.
- [67] Q. Ji, L.H. Le, L. Filipow, S. Jackson, Ultrasonic wave propagation in water-saturated aluminum foams, *Ultrasonics* 36(6) (1998) 759-765.
- [68] K.-C.T. Nguyen, L.H. Le, N.R. Kaipatur, R. Zheng, E.H. Lou, P.W. Major, High-resolution ultrasonic imaging of dento-periodontal tissues using a multi-element phased array system, *Annals of biomedical engineering* 44(10) (2016) 2874-2886.
- [69] A. Fenster, D.B. Downey, H.N. Cardinal, Three-dimensional ultrasound imaging, *Physics in medicine & biology* 46(5) (2001) R67.
- [70] K.K. Shung, *Diagnostic ultrasound: Imaging and blood flow measurements*, CRC press 2015.
- [71] J.A. Jensen, S.I. Nikolov, K.L. Gammelmark, M.H. Pedersen, Synthetic aperture ultrasound imaging, *Ultrasonics* 44 (2006) e5-e15.
- [72] W. Chen, L.H. Le, E.H. Lou, Ultrasound imaging of spinal vertebrae to study scoliosis, *Open Journal of Acoustics* 2(3) (2012) 95-103.
- [73] B. Klucinec, The effectiveness of the Aquaflex gel pad in the transmission of acoustic energy, *Journal of athletic training* 31(4) (1996) 313.
- [74] L. Li, B. Yan, J. Yang, W. Huang, L. Chen, H. Zeng, Injectable self-healing hydrogel with antimicrobial and antifouling properties, *ACS applied materials & interfaces* 9(11) (2017) 9221-9225.
- [75] B. Yan, J. Huang, L. Han, L. Gong, L. Li, J.N. Israelachvili, H. Zeng, Duplicating dynamic strain-stiffening behavior and nanomechanics of biological tissues in a synthetic self-healing flexible network hydrogel, *ACS nano* 11(11) (2017) 11074-11081.
- [76] C. Zhang, M.H. Hsieh, S.Y. Wu, S.H. Li, J. Wu, S.M. Liu, H.J. Wei, R.D. Weisel, H.W. Sung, R.K. Li, A self-doping conductive polymer hydrogel that can restore electrical impulse propagation at myocardial infarct to prevent cardiac arrhythmia and preserve ventricular function, *Biomaterials* 231 (2020) 119672.
- [77] D. Ramnath, Y. Sun, R.D. Weisel, R.K. Li, Conductive Biomaterial Polypyrrole-Chitosan Hydrogel Can Influence Our Resistant Fibrotic Scar Tissue Model to Perform Electrically Like Healthy Heart Tissue, *Circulation* 138(Suppl_1) (2018) A12268-A12268.

- [78] B. Yan, L. Han, H. Xiao, J. Zhang, J. Huang, W. Hu, Y. Gu, Q. Liu, H. Zeng, Rapid Dewatering and Consolidation of Concentrated Colloidal Suspensions: Mature Fine Tailings via Self-Healing Composite Hydrogel, *ACS applied materials & interfaces* 11(24) (2019) 21610-21618.
- [79] P. Sun, S. Ren, F. Liu, A. Wu, N. Sun, L. Shi, L. Zheng, Smart low molecular weight hydrogels with dynamic covalent skeletons, *Soft matter* 14(32) (2018) 6678-6683.
- [80] H. Xu, Y. Tan, W. Rao, D. Wang, S. Xu, W. Liao, Y.Z. Wang, Ultra-strong mechanical property and force-driven malleability of water-poor hydrogels, *Journal of colloid and interface science* 542 (2019) 281-288.
- [81] Y. Chen, D. Diaz-Dussan, D. Wu, W. Wang, Y.Y. Peng, A.B. Asha, D.G. Hall, K. Ishihara, R. Narain, Bioinspired self-healing hydrogel based on benzoxaborole-catechol dynamic covalent chemistry for 3D cell encapsulation, *ACS Macro Letters* 7(8) (2018) 904-908.
- [82] O. Maan, P. Song, N. Chen, Q. Lu, An In Situ Procedure for the Preparation of Zeolitic Imidazolate Framework - 8 Polyacrylamide Hydrogel for Adsorption of Aqueous Pollutants, *Advanced Materials Interfaces* 6(10) (2019) 1801895.
- [83] O. Maan, P. Song, N. Chen, Q. Lu, Metal-Organic Frameworks: An In Situ Procedure for the Preparation of Zeolitic Imidazolate Framework-8 Polyacrylamide Hydrogel for Adsorption of Aqueous Pollutants (*Adv. Mater. Interfaces* 10/2019), *Advanced Materials Interfaces* 6(10) (2019) 1970062.
- [84] P. Sun, F. Lu, A. Wu, Y. Yin, L. Shi, L. Zheng, Construction of pH - Responsive Supramolecular Assemblies Based on Dynamic Covalent Bonds for Tunable Drug Release, *Journal of Surfactants and Detergents* 21(4) (2018) 593-600.
- [85] X. Li, H. Qin, X. Zhang, Z. Guo, Triple-network hydrogels with high strength, low friction and self-healing by chemical-physical crosslinking, *Journal of colloid and interface science* 556 (2019) 549-556.
- [86] R. Liu, S. Liang, X.Z. Tang, D. Yan, X. Li, Z.Z. Yu, Tough and highly stretchable graphene oxide/polyacrylamide nanocomposite hydrogels, *Journal of Materials Chemistry* 22(28) (2012) 14160-14167.
- [87] C.H. Yang, M.X. Wang, H. Haider, J.H. Yang, J.Y. Sun, Y.M. Chen, J. Zhou, Z. Suo, Strengthening alginate/polyacrylamide hydrogels using various multivalent cations, *ACS applied materials & interfaces* 5(21) (2013) 10418-10422.
- [88] I. Jeon, J. Cui, W.R. Illeperuma, J. Aizenberg, J.J. Vlassak, Extremely stretchable and fast self-healing hydrogels, *Advanced Materials* 28(23) (2016) 4678-4683.
- [89] P. Lin, S. Ma, X. Wang, F. Zhou, Molecularly engineered dual-crosslinked hydrogel with ultrahigh mechanical strength, toughness, and good self-recovery, *Advanced Materials* 27(12) (2015) 2054-2059.
- [90] N.A. Peppas, Tear propagation resistance of semicrystalline polymeric networks, *Polymer* 18(4) (1977) 403-407.

- [91] Y. Tanaka, K. Fukao, Y. Miyamoto, Fracture energy of gels, *The European Physical Journal E* 3(4) (2000) 395-401.
- [92] M.E. Freeman, M.J. Furey, B.J. Love, J.M. Hampton, Friction, wear, and lubrication of hydrogels as synthetic articular cartilage, *Wear* 241(2) (2000) 129-135.
- [93] J.P. Gong, Friction and lubrication of hydrogels—its richness and complexity, *Soft matter* 2(7) (2006) 544-552.
- [94] A.V. Stanishevsky, S. Holliday, Mechanical properties of sol–gel calcium titanate bioceramic coatings on titanium, *Surface and Coatings Technology* 202(4-7) (2007) 1236-1241.
- [95] K. Mamada, H. Kosukegawa, V. Fridrici, P. Kapsa, M. Ohta, Friction properties of PVA-H/steel ball contact under water lubrication conditions, *Tribology International* 44(7-8) (2011) 757-763.
- [96] W. Smitthipong, M. Nardin, J. Schultz, K. Suchiva, Adhesion and self-adhesion of rubbers, crosslinked by electron beam irradiation, *International journal of adhesion and adhesives* 27(5) (2007) 352-357.
- [97] K.A. Wear, The dependencies of phase velocity and dispersion on volume fraction in cancellous-bone-mimicking phantoms, *The Journal of the Acoustical Society of America* 125(2) (2009) 1197-1201.
- [98] J.P. Draye, B. Delaey, A. Van de Voorde, A. Van Den Bulcke, B. De Reu, E. Schacht, In vitro and in vivo biocompatibility of dextran dialdehyde cross-linked gelatin hydrogel films, *Biomaterials* 19(18) (1998) 1677-1687.
- [99] M. Cheng, Y. Wang, L. Yu, H. Su, W. Han, Z. Lin, J. Li, H. Hao, C. Tong, X. Li, Macroscopic supramolecular assembly to fabricate 3D ordered structures: Towards potential tissue scaffolds with targeted modification, *Advanced Functional Materials* 25(44) (2015) 6851-6857.
- [100] X. Li, Q. Shen, Y. Su, F. Tian, Y. Zhao, D. Wang, Structure– function relationship of calcium alginate hydrogels: a novel crystal-forming engineering, *Crystal Growth and Design* 9(8) (2009) 3470-3476.
- [101] Y. Jin, B. Kundu, Y. Cai, S.C. Kundu, J. Yao, Bio-inspired mineralization of hydroxyapatite in 3D silk fibroin hydrogel for bone tissue engineering, *Colloids and surfaces B: biointerfaces* 134 (2015) 339-345.
- [102] C. Gao, M. Liu, J. Chen, X. Zhang, Preparation and controlled degradation of oxidized sodium alginate hydrogel, *Polymer degradation and stability* 94(9) (2009) 1405-1410.
- [103] H. Zeng, *Polymer adhesion, friction, and lubrication*, John Wiley & Sons 2013.
- [104] S. Liang, J. Hu, Z.L. Wu, T. Kurokawa, J.P. Gong, Toughness Enhancement and Stick–Slip Tearing of Double-Network Hydrogels in Poly (ethylene glycol) Solution, *Macromolecules* 45(11) (2012) 4758-4763.
- [105] S.Y. Zheng, H. Ding, J. Qian, J. Yin, Z.L. Wu, Y. Song, Q. Zheng, Metal-coordination complexes mediated physical hydrogels with high toughness, stick–slip tearing behavior, and good processability, *Macromolecules* 49(24) (2016) 9637-9646.

- [106] D. Baykal, R. Underwood, K. Mansmann, M. Marcolongo, S. Kurtz, Evaluation of friction properties of hydrogels based on a biphasic cartilage model, *Journal of the mechanical behavior of biomedical materials* 28 (2013) 263-273.
- [107] X. Li, C. Wu, Q. Yang, S. Long, C. Wu, Low-velocity super-lubrication of sodium-alginate/polyacrylamide ionic-covalent hybrid double-network hydrogels, *Soft matter* 11(15) (2015) 3022-3033.
- [108] R. Ma, D. Xiong, F. Miao, J. Zhang, Y. Peng, Friction properties of novel PVP/PVA blend hydrogels as artificial cartilage, *Journal of Biomedical Materials Research* 93(3) (2010) 1016-1019.
- [109] M. Samsom, M. Korogiannaki, L.N. Subbaraman, H. Sheardown, T.A. Schmidt, Hyaluronan incorporation into model contact lens hydrogels as a built-in lubricant: Effect of hydrogel composition and proteoglycan 4 as a lubricant in solution, *Journal of Biomedical Materials Research Part B: Applied Biomaterials* 106(5) (2018) 1818-1826.
- [110] M. Samsom, Y. Iwabuchi, H. Sheardown, T.A. Schmidt, Proteoglycan 4 and hyaluronan as boundary lubricants for model contact lens hydrogels, *Journal of Biomedical Materials Research Part B: Applied Biomaterials* 106(3) (2018) 1329-1338.
- [111] H. Li, Y.S. Choi, M.W. Rutland, R. Atkin, Nanotribology of hydrogels with similar stiffness but different polymer and crosslinker concentrations, *Journal of Colloid and Interface Science* 563 (2020) 347-353.
- [112] Y. Ishikawa, K.i. Hiratsuka, T. Sasada, Role of water in the lubrication of hydrogel, *Wear* 261(5-6) (2006) 500-504.
- [113] Y. Shi, D. Xiong, Microstructure and friction properties of PVA/PVP hydrogels for articular cartilage repair as function of polymerization degree and polymer concentration, *Wear* 305(1-2) (2013) 280-285.
- [114] H. Kosukegawa, V. Fridrici, P. Kapsa, Y. Sutou, K. Adachi, M. Ohta, Friction properties of medical metallic alloys on soft tissue-mimicking poly (vinyl alcohol) hydrogel biomodel, *Tribology Letters* 51(3) (2013) 311-321.
- [115] A. Pitenis, J. Urueña, K. Schulze, R. Nixon, A.C. Dunn, B. Krick, W. Sawyer, T. Angelini, Polymer fluctuation lubrication in hydrogel gemini interfaces, *Soft Matter* 10(44) (2014) 8955-8962.
- [116] B.H. Thomas, J.C. Fryman, K. Liu, J. Mason, Hydrophilic-hydrophobic hydrogels for cartilage replacement, *Journal of the mechanical behavior of biomedical materials* 2(6) (2009) 588-595.
- [117] G.W. Greene, B. Zappone, O. Söderman, D. Topgaard, G. Rata, H. Zeng, J.N. Israelachvili, Anisotropic dynamic changes in the pore network structure, fluid diffusion and fluid flow in articular cartilage under compression, *Biomaterials* 31(12) (2010) 3117-3128.
- [118] C. Heinzmann, C. Weder, L.M. de Espinosa, Supramolecular polymer adhesives: advanced materials inspired by nature, *Chemical Society Reviews* 45(2) (2016) 342-358.
- [119] X. Liu, Q. Zhang, Z. Gao, R. Hou, G. Gao, Bioinspired adhesive hydrogel driven by adenine and thymine, *ACS applied materials & interfaces* 9(20) (2017) 17645-17652.

- [120] J. Kofler, H.K. Edinger, Diagnostic ultrasound imaging of soft tissues in the bovine distal limb, *Veterinary Radiology & Ultrasound* 36(3) (1995) 246-252.
- [121] J.M. Yang, C. Favazza, R. Chen, J. Yao, X. Cai, K. Maslov, Q. Zhou, K.K. Shung, L.V. Wang, Simultaneous functional photoacoustic and ultrasonic endoscopy of internal organs in vivo, *Nature medicine* 18(8) (2012) 1297-1302.
- [122] D.H. Howry, W.R. Bliss, Ultrasonic visualization of soft tissue structures of the body, *The Journal of laboratory and clinical medicine* 40(4) (1952) 579-592.
- [123] T.H. Shawker, B.C. Sonies, M. Stone, Soft tissue anatomy of the tongue and floor of the mouth: an ultrasound demonstration, *Brain and language* 21(2) (1984) 335-350.
- [124] K.C.T. Nguyen, C. Pacheco-Pereira, N.R. Kaipatur, J. Cheung, P.W. Major, L.H. Le, Comparison of ultrasound imaging and cone-beam computed tomography for examination of the alveolar bone level: A systematic review, *PloS one* 13(10) (2018) e0200596.
- [125] J. Yi, K.C.T. Nguyen, W. Wang, W. Yang, M. Pan, E. Lou, P.W. Major, L.H. Le, H. Zeng, Polyacrylamide/Alginate double-network tough hydrogels for intraoral ultrasound imaging, *Journal of Colloid and Interface Science* 578 (2020) 598-607.
- [126] A. Kumar, S.S. Han, PVA-based hydrogels for tissue engineering: A review, *International journal of polymeric materials and polymeric biomaterials* 66(4) (2017) 159-182.
- [127] M. Teodorescu, M. Bercea, S. Morariu, Biomaterials of Poly (vinyl alcohol) and Natural Polymers, *Polymer Reviews* 58(2) (2018) 247-287.
- [128] S. Jiang, S. Liu, W. Feng, PVA hydrogel properties for biomedical application, *Journal of the mechanical behavior of biomedical materials* 4(7) (2011) 1228-1233.
- [129] M. Gauthier, J. Luo, D. Calvet, C. Ni, X.X. Zhu, M. Garon, M. Buschmann, Degree of crosslinking and mechanical properties of crosslinked poly (vinyl alcohol) beads for use in solid-phase organic synthesis, *Polymer* 45(24) (2004) 8201-8210.
- [130] M.S. Kurtis, T.A. Schmidt, W.D. Bugbee, R.F. Loeser, R.L. Sah, Integrin - mediated adhesion of human articular chondrocytes to cartilage, *Arthritis & Rheumatism* 48(1) (2003) 110-118.
- [131] J.L. Holloway, A.M. Lowman, G.R. Palmese, The role of crystallization and phase separation in the formation of physically cross-linked PVA hydrogels, *Soft Matter* 9(3) (2013) 826-833.
- [132] J.A. Stammen, S. Williams, D.N. Ku, R.E. Guldberg, Mechanical properties of a novel PVA hydrogel in shear and unconfined compression, *Biomaterials* 22(8) (2001) 799-806.
- [133] W. Yao, C. Geng, D. Han, F. Chen, Q. Fu, Strong and conductive double-network graphene/PVA gel, *Rsc Advances* 4(74) (2014) 39588-39595.
- [134] Y. Zhang, L. Ye, M. Cui, B. Yang, J. Li, H. Sun, F. Yao, Physically crosslinked poly (vinyl alcohol)-carrageenan composite hydrogels: pore structure stability and cell adhesive ability, *Rsc Advances* 5(95) (2015) 78180-78191.
- [135] H. Bodugoz-Senturk, C.E. Macias, J.H. Kung, O.K. Muratoglu, Poly (vinyl alcohol)-acrylamide hydrogels as load-bearing cartilage substitute, *Biomaterials* 30(4) (2009) 589-596.

- [136] Q. Tang, X. Sun, Q. Li, J. Wu, J. Lin, Fabrication of a high-strength hydrogel with an interpenetrating network structure, *Colloids and Surfaces A: Physicochemical and Engineering Aspects* 346(1-3) (2009) 91-98.
- [137] G. Ge, Y. Zhang, J. Shao, W. Wang, W. Si, W. Huang, X. Dong, Stretchable, Transparent, and Self-Patterned Hydrogel-Based Pressure Sensor for Human Motions Detection, *Advanced Functional Materials* 28(32) (2018) 1802576.
- [138] M. Jaiswal, S. Lale, N.G. Ramesh, V. Koul, Synthesis and characterization of positively charged interpenetrating double-network hydrogel matrices for biomedical applications, *Reactive and Functional Polymers* 73(11) (2013) 1493-1499.
- [139] U. Fumio, Y. Hiroshi, N. Kumiko, N. Sachihiko, S. Kenji, M. Yasunori, Swelling and mechanical properties of poly (vinyl alcohol) hydrogels, *International journal of pharmaceutics* 58(2) (1990) 135-142.
- [140] J. Huang, X. Qiu, L. Xie, G.D. Jay, T.A. Schmidt, H. Zeng, Probing the molecular interactions and lubrication mechanisms of purified full-length recombinant human proteoglycan 4 (rhPRG4) and hyaluronic acid (HA), *Biomacromolecules* 20(2) (2019) 1056-1067.
- [141] M. Binazadeh, A. Faghihnejad, L.D. Unsworth, H. Zeng, Understanding the effect of secondary structure on molecular interactions of Poly-l-lysine with different substrates by SFA, *Biomacromolecules* 14(10) (2013) 3498-3508.
- [142] H.Y. Yoo, J. Huang, L. Li, M. Foo, H. Zeng, D.S. Hwang, Nanomechanical contribution of collagen and von Willebrand Factor A in marine underwater adhesion and its implication for collagen manipulation, *Biomacromolecules* 17(3) (2016) 946-953.
- [143] D.S. Park, S.C. Regmi, D.A. Svystonyuk, G. Teng, D. Belke, J. Turnbull, D.G. Guzzardi, S. Kang, M.K. Cowman, T.A. Schmidt, Human pericardial proteoglycan 4 (lubricin): Implications for postcardiotomy intrathoracic adhesion formation, *The Journal of thoracic and cardiovascular surgery* 156(4) (2018) 1598-1608. e1.
- [144] L. Han, M. Wang, P. Li, D. Gan, L. Yan, J. Xu, K. Wang, L. Fang, C.W. Chan, H. Zhang, Mussel-inspired tissue-adhesive hydrogel based on the polydopamine–chondroitin sulfate complex for growth-factor-free cartilage regeneration, *ACS applied materials & interfaces* 10(33) (2018) 28015-28026.
- [145] Z. Gong, G. Zhang, X. Zeng, J. Li, G. Li, W. Huang, R. Sun, C. Wong, High-strength, tough, fatigue resistant, and self-healing hydrogel based on dual physically cross-linked network, *ACS applied materials & interfaces* 8(36) (2016) 24030-24037.
- [146] A. Mihic, Z. Cui, J. Wu, G. Vlacic, Y. Miyagi, S.H. Li, S. Lu, H.W. Sung, R.D. Weisel, R.K. Li, A conductive polymer hydrogel supports cell electrical signaling and improves cardiac function after implantation into myocardial infarct, *Circulation* 132(8) (2015) 772-784.
- [147] J. Chen, J. Liu, T. Thundat, H. Zeng, Polypyrrole-Doped Conductive Supramolecular Elastomer with Stretchability, Rapid Self-Healing, and Adhesive Property for Flexible Electronic Sensors, *ACS applied materials & interfaces* 11(20) (2019) 18720-18729.
- [148] Y. Chen, W. Wang, D. Wu, H. Zeng, D.G. Hall, R. Narain, Multiresponsive and Self-Healing Hydrogel via Formation of Polymer–Nanogel Interfacial Dynamic Benzoxaborole Esters at Physiological pH, *ACS Applied Materials & Interfaces* 11(47) (2019) 44742-44750.

- [149] Y. Chen, Z. Tan, W. Wang, Y.Y. Peng, R. Narain, Injectable, self-healing, and multi-responsive hydrogels via dynamic covalent bond formation between benzoxaborole and hydroxyl groups, *Biomacromolecules* 20(2) (2018) 1028-1035.
- [150] Y.G. Jia, X.X. Zhu, Self-healing supramolecular hydrogel made of polymers bearing cholic acid and β -cyclodextrin pendants, *Chemistry of Materials* 27(1) (2015) 387-393.
- [151] H. Dong, M. Cheng, Y. Zhang, H. Wei, F. Shi, Extraordinary drag-reducing effect of a superhydrophobic coating on a macroscopic model ship at high speed, *Journal of Materials Chemistry A* 1(19) (2013) 5886-5891.
- [152] Y. Wang, L. Tang, J. Yu, Investigation on the assembled structure–property correlation of supramolecular hydrogel formed from low-molecular-weight gelator, *Journal of colloid and interface science* 319(1) (2008) 357-364.
- [153] M. Wu, J. Chen, W. Huang, B. Yan, Q. Peng, J. Liu, L. Chen, H. Zeng, Injectable and Self-Healing Nanocomposite Hydrogels with Ultrasensitive pH-Responsiveness and Tunable Mechanical Properties: Implications for Controlled Drug Delivery, *Biomacromolecules* 21(6) (2020) 2409-2420.
- [154] K. Kim, M. Shin, M.Y. Koh, J.H. Ryu, M.S. Lee, S. Hong, H. Lee, TAPE: A medical adhesive inspired by a ubiquitous compound in plants, *Advanced Functional Materials* 25(16) (2015) 2402-2410.
- [155] C.C. Berndt, Tensile adhesion testing methodology for thermally sprayed coatings, *Journal of materials engineering* 12(2) (1990) 151-158.
- [156] M. Cheng, M. Song, H. Dong, F. Shi, Surface adhesive forces: a metric describing the drag-reducing effects of superhydrophobic coatings, *Small* 11(14) (2015) 1665-1671.
- [157] M. Liao, P. Wan, J. Wen, M. Gong, X. Wu, Y. Wang, R. Shi, L. Zhang, Wearable, healable, and adhesive epidermal sensors assembled from mussel-inspired conductive hybrid hydrogel framework, *Advanced Functional Materials* 27(48) (2017) 1703852.
- [158] A.K. Gaharwar, C.P. Rivera, C.J. Wu, G. Schmidt, Transparent, elastomeric and tough hydrogels from poly (ethylene glycol) and silicate nanoparticles, *Acta biomaterialia* 7(12) (2011) 4139-4148.
- [159] Y. Ma, S. Ma, Y. Wu, X. Pei, S.N. Gorb, Z. Wang, W. Liu, F. Zhou, Remote control over underwater dynamic attachment/detachment and locomotion, *Advanced Materials* 30(30) (2018) 1801595.
- [160] A. Faghijnejad, K.E. Feldman, J. Yu, M.V. Tirrell, J.N. Israelachvili, C.J. Hawker, E.J. Kramer, H. Zeng, Adhesion and surface interactions of a self-healing polymer with multiple hydrogen-bonding groups, *Advanced Functional Materials* 24(16) (2014) 2322-2333.
- [161] J. Zhang, L. Xiang, B. Yan, H. Zeng, Nanomechanics of Anion– π Interaction in Aqueous Solution, *Journal of the American Chemical Society* 142(4) (2020) 1710-1714.
- [162] H. Zeng, D.S. Hwang, J.N. Israelachvili, J.H. Waite, Strong reversible Fe³⁺-mediated bridging between dopa-containing protein films in water, *Proceedings of the National Academy of Sciences* 107(29) (2010) 12850-12853.

- [163] P. Karami, C.I.S. Wyss, A. Khoushabi, A. Schmocker, M. Broome, C. Moser, P.-E. Bourban, D.P. Pioletti, Composite double-network hydrogels to improve adhesion on biological surfaces, *ACS applied materials & interfaces* 10(45) (2018) 38692-38699.
- [164] H. Yuk, T. Zhang, G.A. Parada, X. Liu, X. Zhao, Skin-inspired hydrogel–elastomer hybrids with robust interfaces and functional microstructures, *Nature communications* 7(1) (2016) 1-11.
- [165] J. Li, A. Celiz, J. Yang, Q. Yang, I. Wamala, W. Whyte, B. Seo, N. Vasilyev, J. Vlassak, Z. Suo, D. Mooney, Tough adhesives for diverse wet surfaces, *Science* 357(6349) (2017) 378-381.

Appendices

Appendix A Supporting Information for Chapter 3

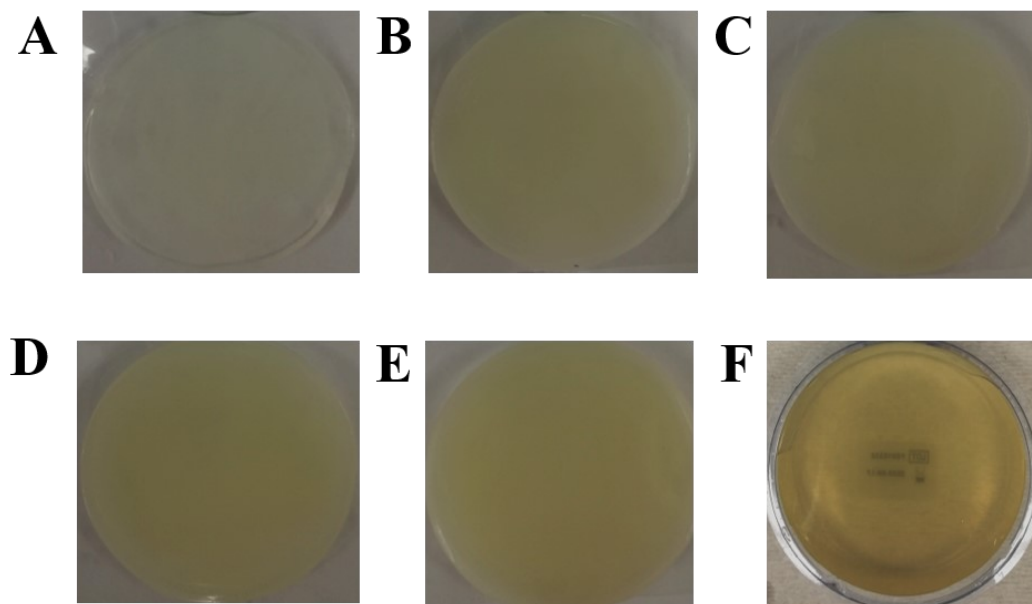


Figure S3.1 The pictures of the as-prepared PAM/Alginate hydrogels and commercial gel pad. (A)

H-1. (B) H-1.5. (C) H-2. (D) H-2.5. (E) H-3. (F) AF.

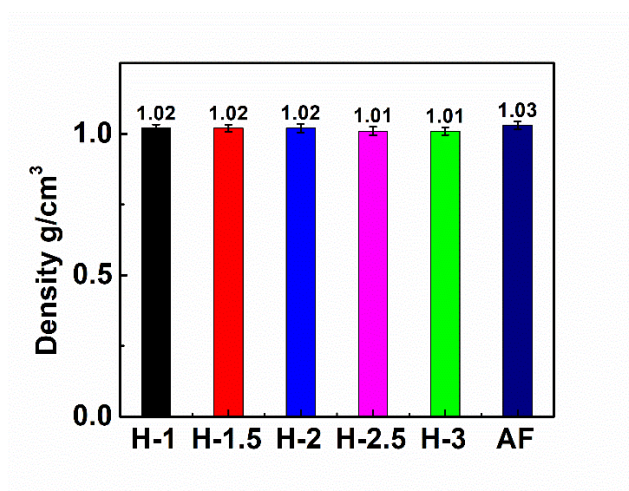


Figure S3.2 The densities of the as-prepared PAM/Alginate hydrogels and AF.

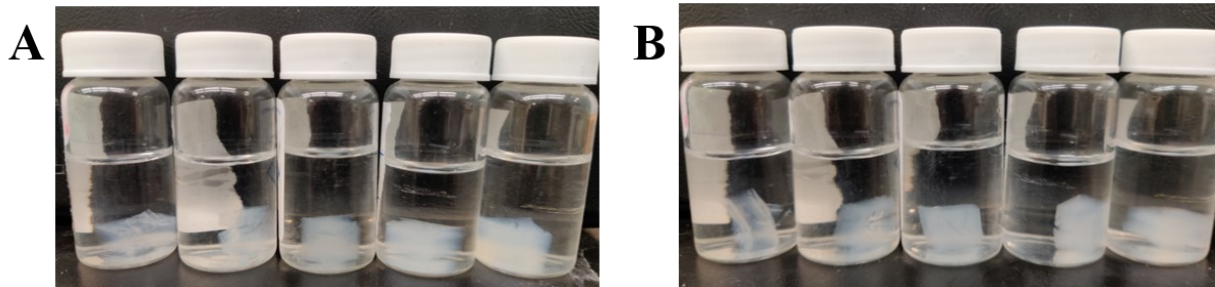


Figure S3.3 The as-prepared PAM/Alginate hydrogel samples (H-1 – H-3, from left to right) swelling in water. (A) After 12h. (B) After 48h.

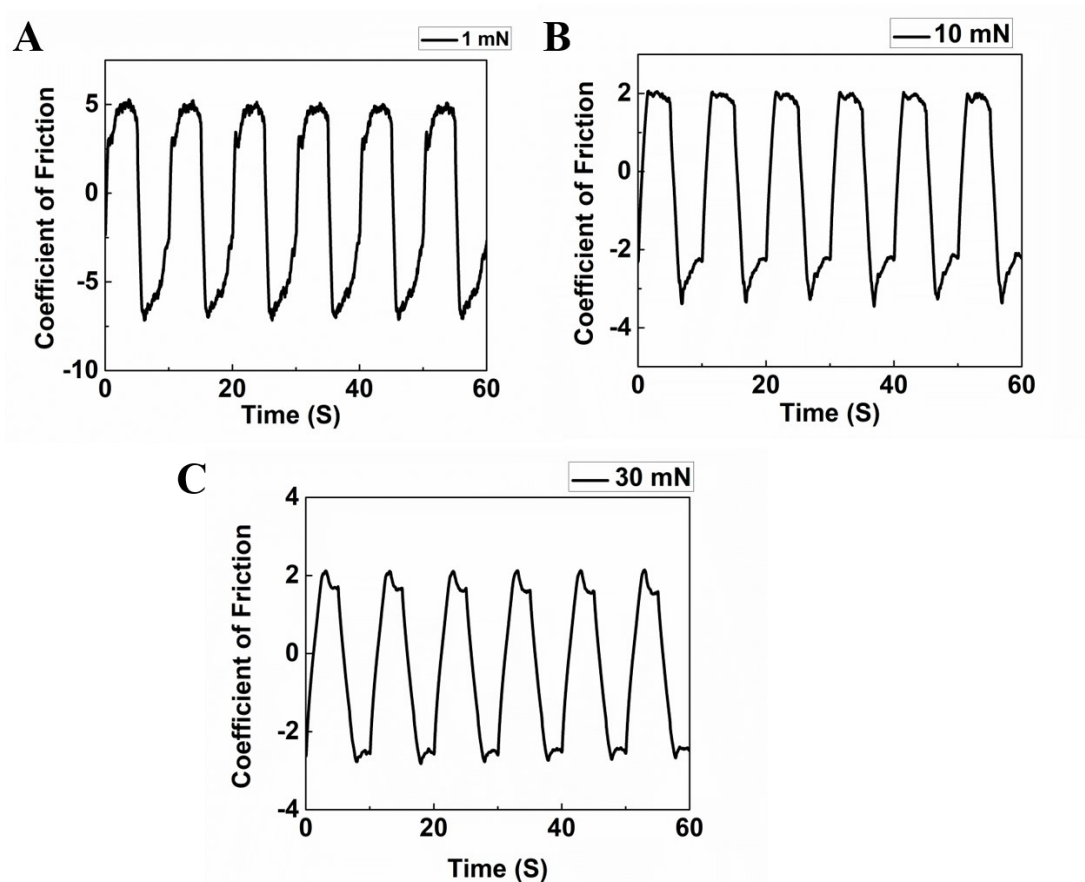


Figure S3.4 The friction coefficient curves of H-2.5 under different normal loads: (A) 1 mN (low load). (B) 10 mN (medium load). (C) 30 mN (high load).

Sample #	Nominal Frequency (MHz)	Group Velocity (m/s)	Dispersion (11.7 – 24.4 MHz)		α^\dagger (dB/cm)	nBUA (dB/cm·MHz)
			Slope (m/s·MHz)	Intercept (m/s)		
Aquaflex	20	1601 ± 1	0	1600 ± 1	2.36 ± 0.04	0.20 ± 0.01
H-1	20	1512 ± 2	0	1511 ± 1	1.84 ± 0.12	0.13 ± 0.02
H-1.5	20	1517 ± 1	0	1518 ± 1	2.25 ± 0.18	0.15 ± 0.04
H-2	20	1520 ± 1	0	1520 ± 2	2.94 ± 0.07	0.24 ± 0.01
H-2.5	20	1525 ± 1	0	1525 ± 1	3.21 ± 0.12	0.25 ± 0.02
H-3	20	1523 ± 2	0	1523 ± 2	3.50 ± 0.15	0.25 ± 0.03

Table S3.1 Group velocities, dispersion, and nBUA of hydrogels. ([†] The attenuation coefficients, α are determined at 17 MHz, the dominant frequencies of the spectra.)

Appendix B Supporting Information for Chapter 4

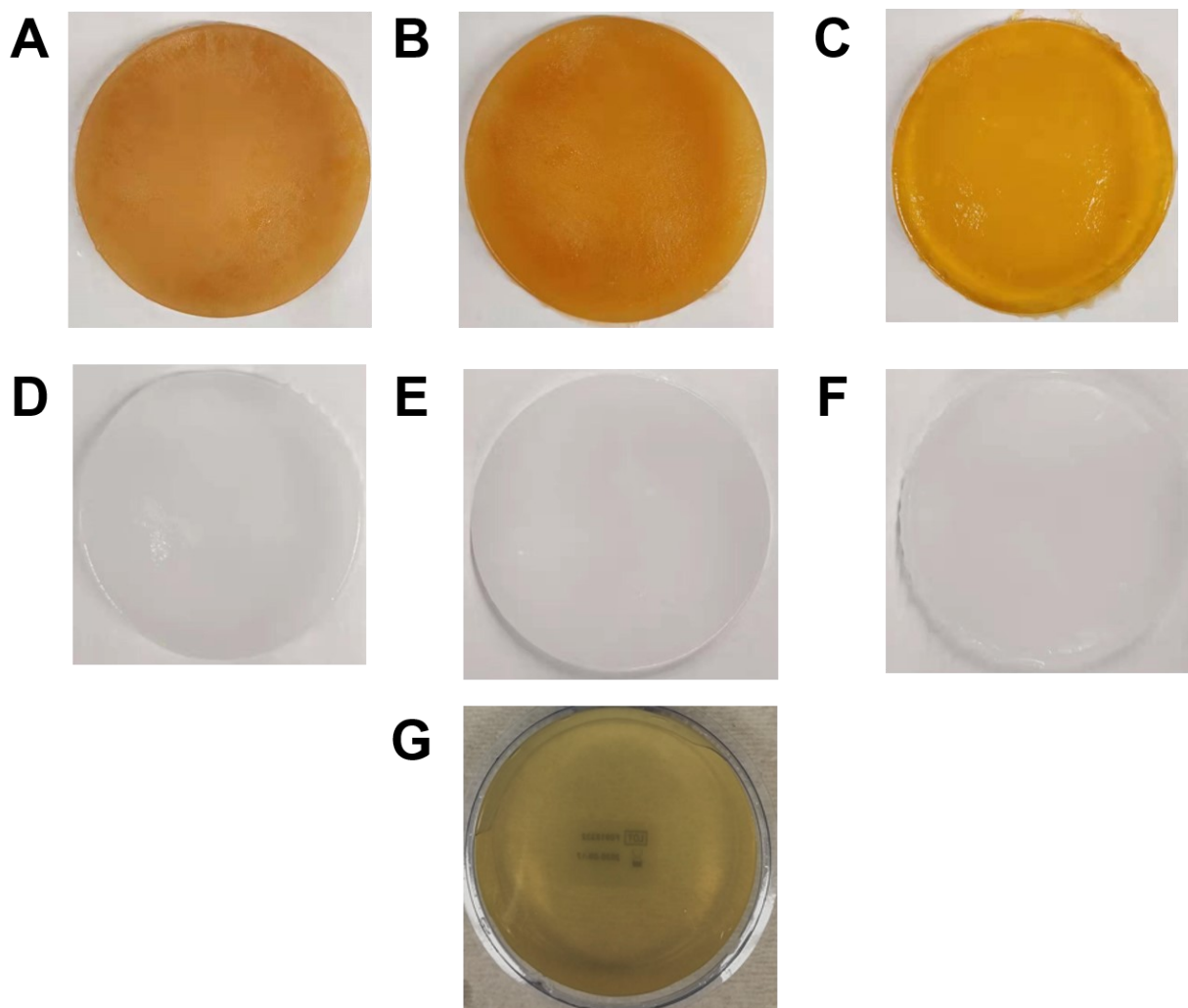


Figure S4.1 The pictures of the as-prepared PVA-PAM-PDA hydrogels, PVA-PAM hydrogels, and commercial gel pad: (A) Hd-0.5. (B) Hd-1. (C) Hd-2. (D) H-0.5. (E) H-1. (F) H-2. (G) AF (Aquaflex ultrasound gel pad).

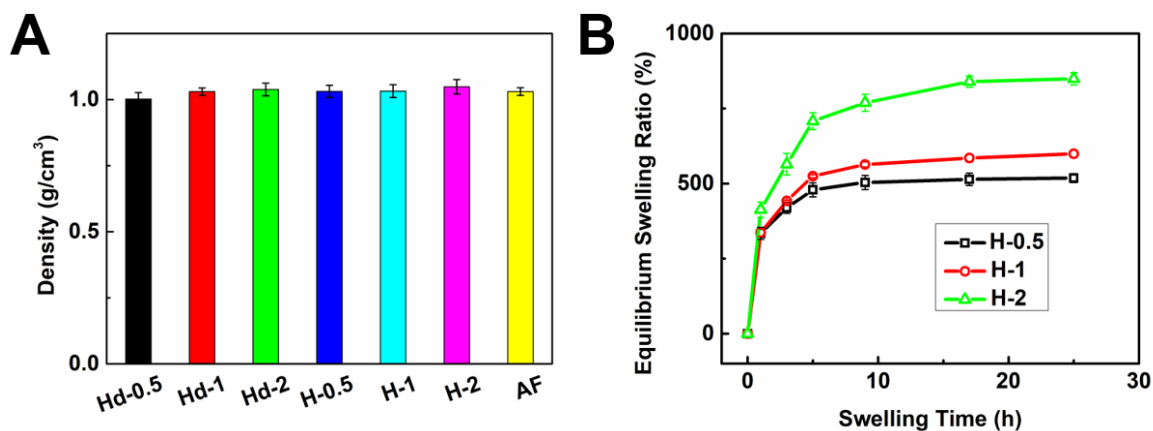


Figure S4.2 (A) The densities of the as-prepared PVA-PAM-PDA hydrogels, PVA-PAM hydrogels, and AF. (B) The equilibrium swelling ratio of PVA-PAM hydrogels at different time intervals.

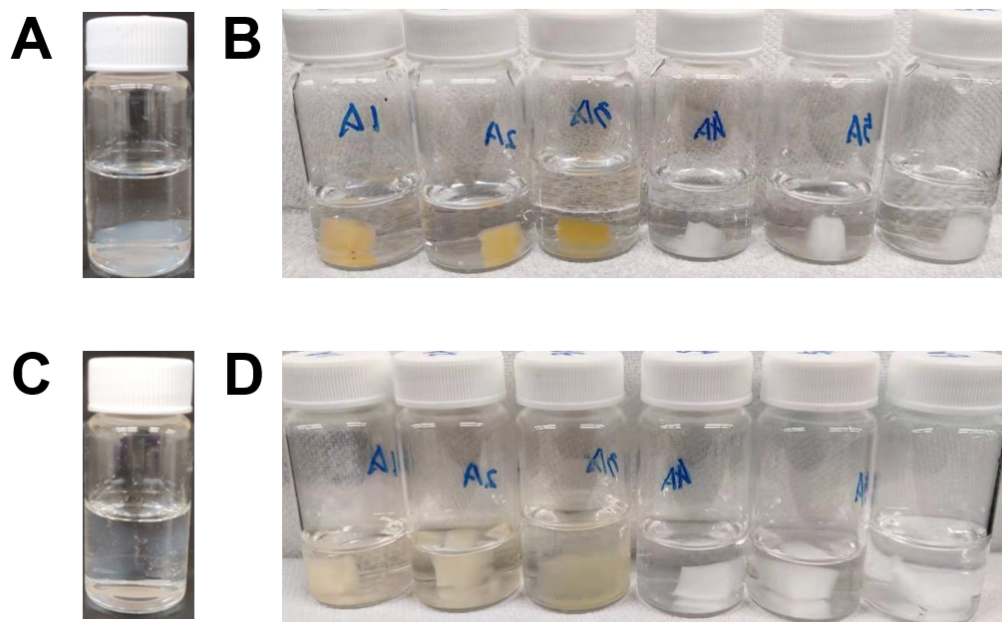


Figure S4.3 Frozen-dry AF and the as-prepared hydrogels immersed in distilled water. 12 h: (A) AF, (B) Hd-0.5, Hd-1, Hd-2, H-0.5, H-1, and H-2 (from left to right) ; 24 h: (C) AF, (D) Hd-0.5, Hd-1, Hd-2, H-0.5, H-1, and H-2 (from left to right).

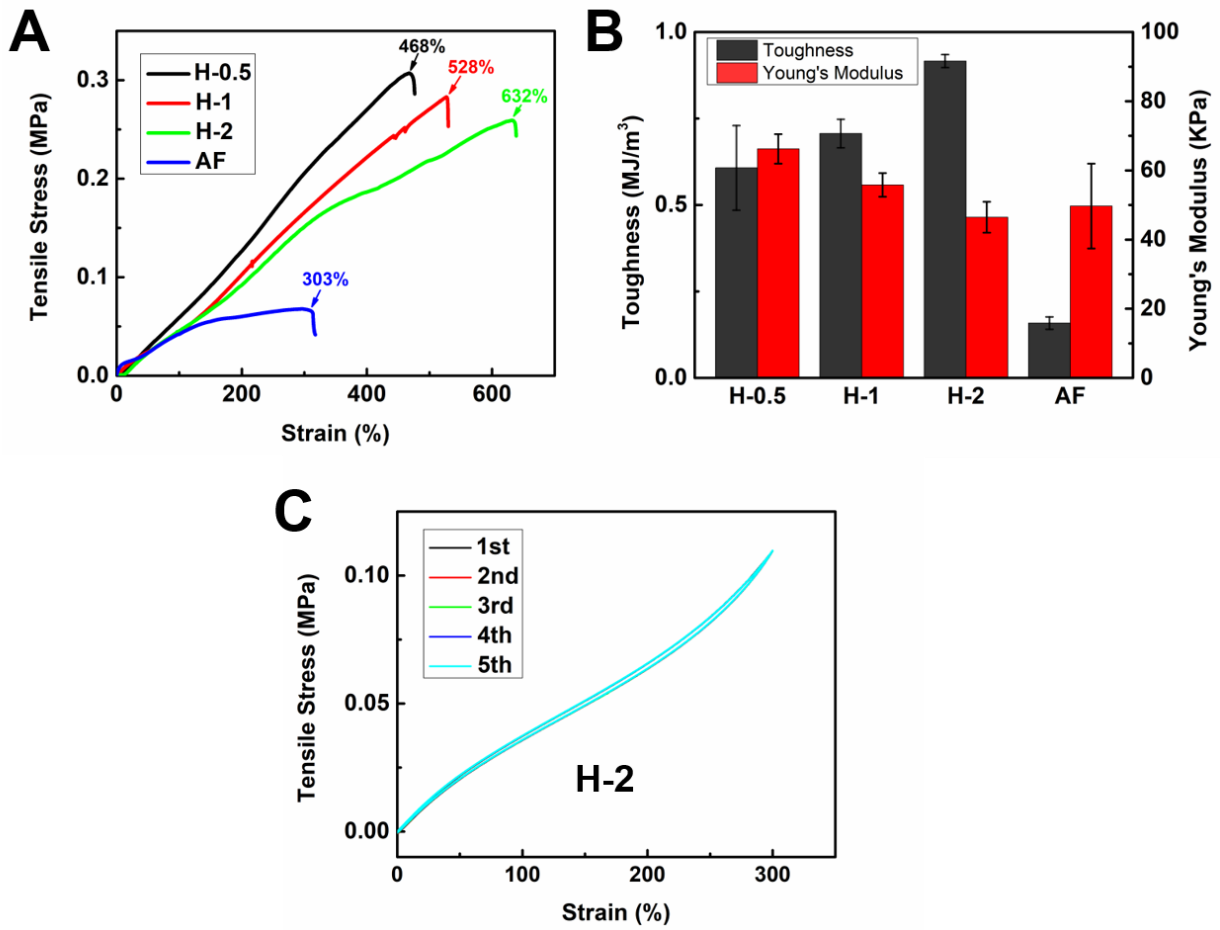


Figure S4.4 (A) The stress-strain curves of the PVA-PAM hydrogels and AF. (B) The toughness and Young's modulus of the PVA-PAM hydrogels and AF. (C) The successive loading-unloading tensile test cycles of H-2.

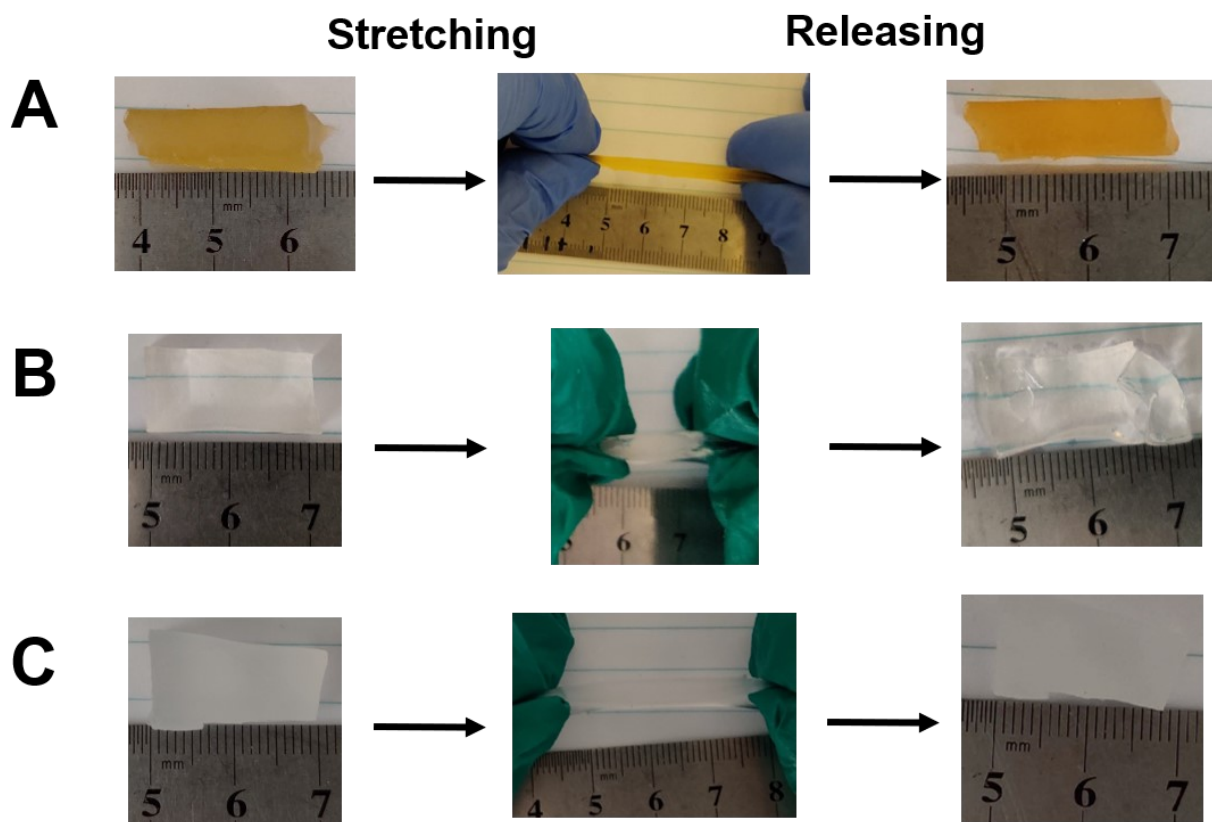


Figure S4.5 Images of the samples undergoing the stretching-releasing process. (A) Hd-2. (B) AF. (C) H-2.

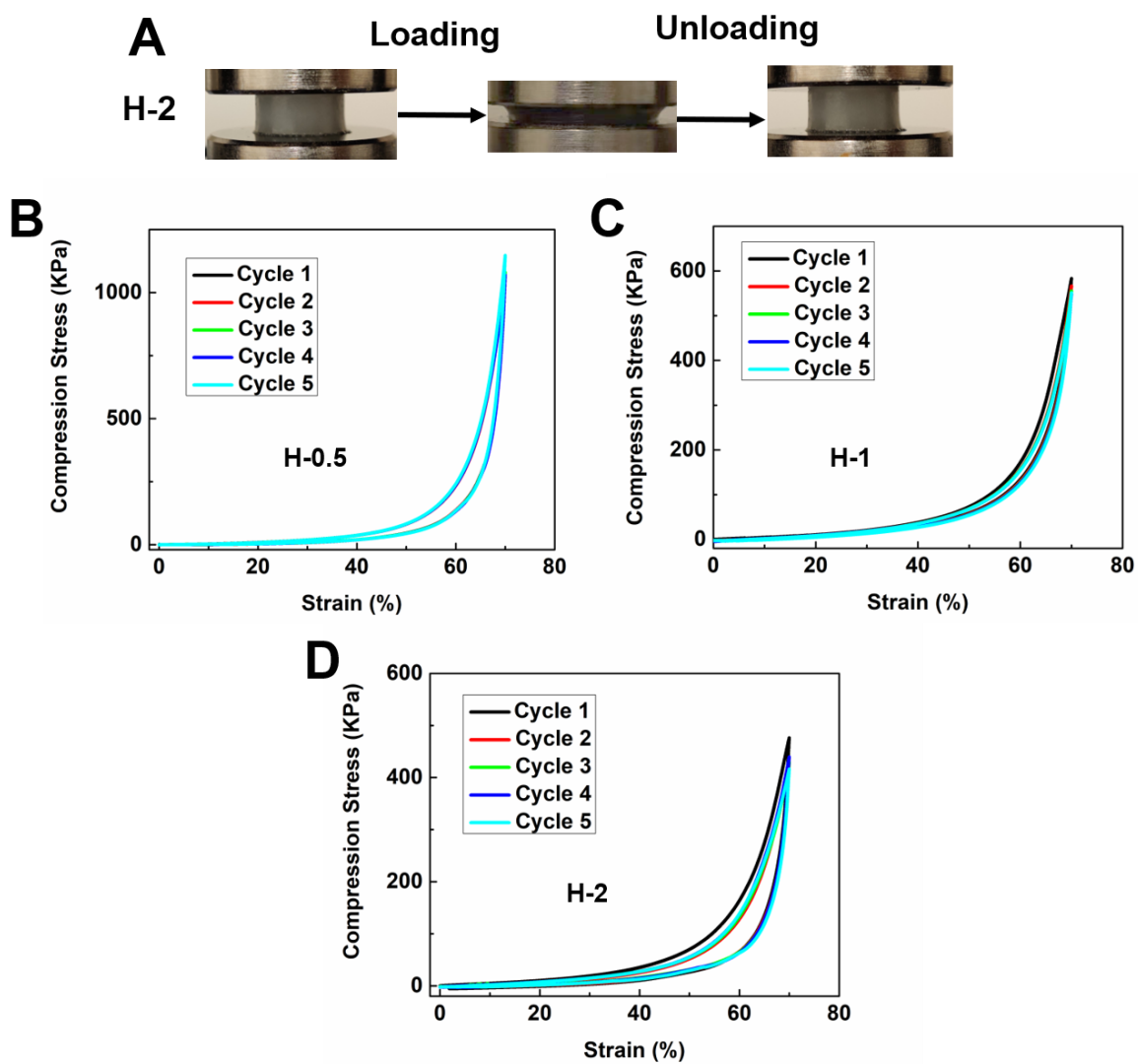


Figure S4.6 (A) Images of Hd-2 undergoing compression testing to 70% strain. The cyclic loading-unloading curves of PVA-PAM hydrogels: (B) H-0.5, (C) H-1, (D) H-2.

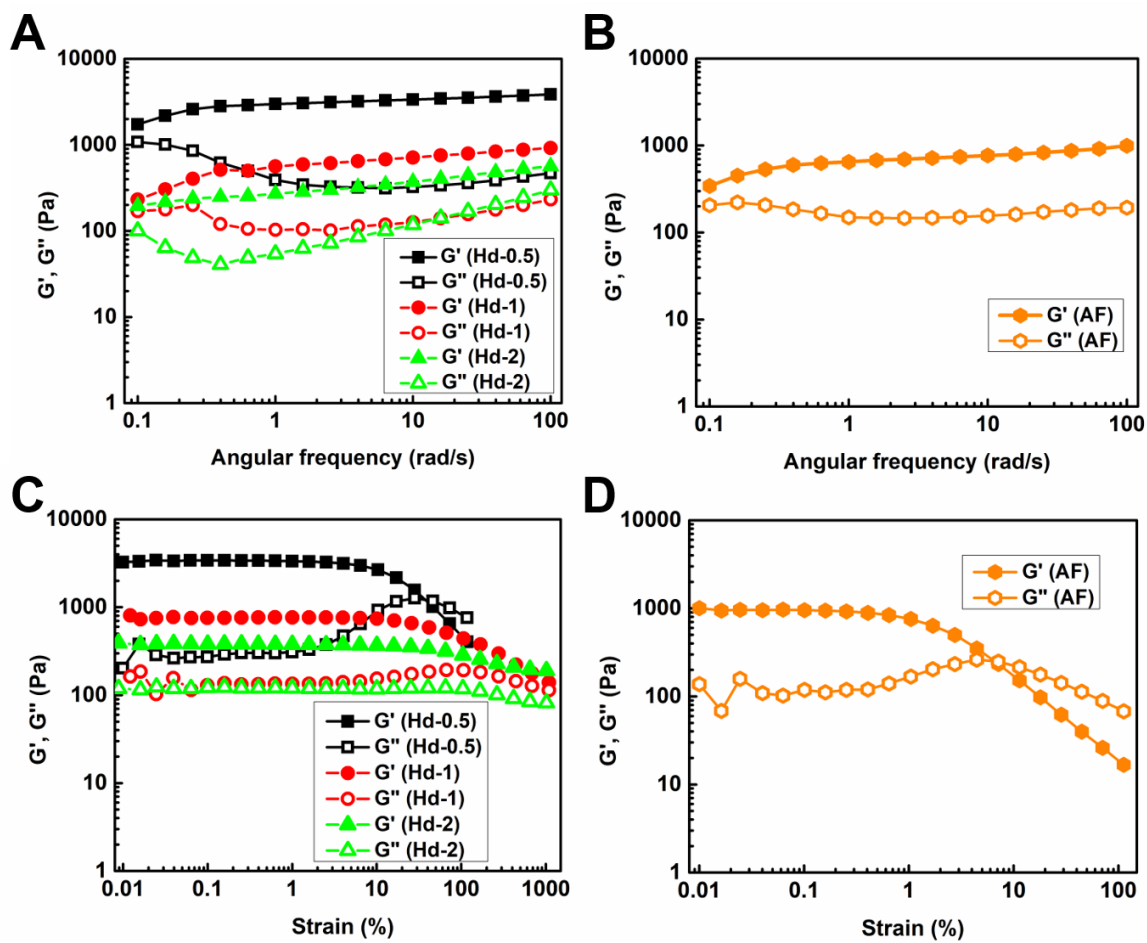


Figure S4.7 Dynamic rheology of the samples on frequency: (A) PVA-PAM-PDA hydrogels, (B) AF. Dynamic rheology of the samples on strain: (C) PVA-PAM-PDA hydrogels, (D) AF.

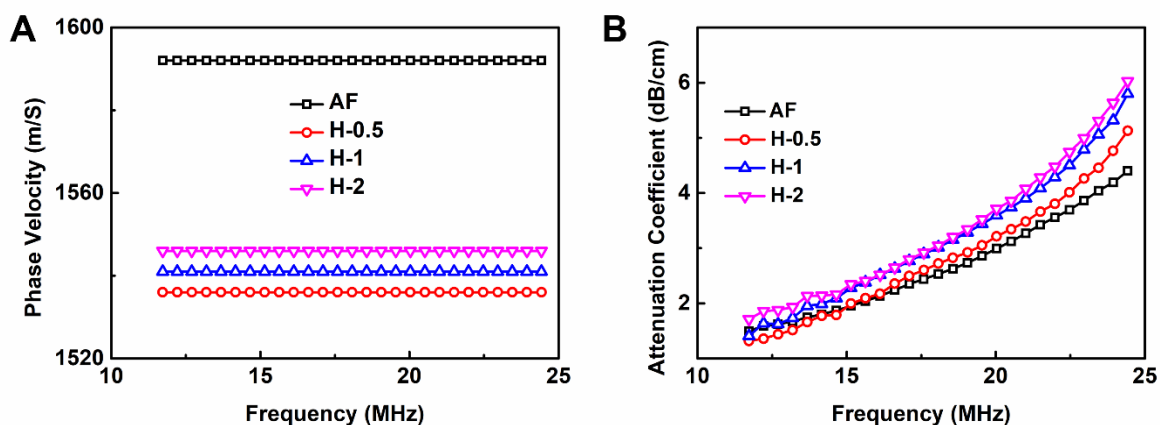


Figure S4.8 (A) The phase velocities of PVA-PAM hydrogels and AF versus frequency. (B) The attenuation coefficient of PVA-PAM hydrogel and AF versus frequency.

Sample #	Nominal Frequency (MHz)	Group Velocity (m/s)	Dispersion (11.7 – 24.4 MHz)		α^\dagger (dB/cm)	nBUA (dB/cm·MHz)
			Slope (m/s·MHz)	Intercept (m/s)		
Aquaflex	20	1593 ± 1	0	1592 ± 1	2.86 ± 0.09	0.22 ± 0.01
H-0.5	20	1537 ± 2	0	1536 ± 1	3.05 ± 0.20	0.28 ± 0.02
H-1	20	1542 ± 1	0	1541 ± 1	3.44 ± 0.15	0.31 ± 0.01
H-2	20	1546 ± 1	0	1546 ± 1	3.52 ± 0.14	0.32 ± 0.01
Hd-0.5	20	1542 ± 2	0	1542 ± 1	3.71 ± 0.19	0.31 ± 0.02
Hd-1	20	1548 ± 1	0	1548 ± 1	4.11 ± 0.18	0.35 ± 0.01
Hd-2	20	1551 ± 1	0	1551 ± 1	4.31 ± 0.19	0.36 ± 0.01

Table S4.1 Group velocities, dispersion, and nBUA of AF and the as-prepared hydrogels. († The attenuation coefficients, α are determined at 19.5 MHz, the dominant frequencies of the spectra.)